TTP-22-006, P3H-22-013

NLO results with operator mixing for fully heavy tetraquarks in QCD sum rules

Ren-Hua Wu[1],* Yu-Sheng Zuo[1],† Chen-Yu Wang[2],‡ Ce Meng[1],§ Yan-Qing Ma[1,3,4],¶ and Kuang-Ta Chao[1,3,4]**
[1] *School of Physics and State Key Laboratory of Nuclear Physics and Technology, Peking University, Beijing 100871, China*
[2] *Institute for Theoretical Particle Physics, KIT, Karlsruhe, Germany*
[3] *Center for High Energy Physics, Peking University, Beijing 100871, China*
[4] *Collaborative Innovation Center of Quantum Matter, Beijing 100871, China*

(Dated: January 28, 2022)

We study the mass spectra of $\bar{Q}Q\bar{Q}Q$ ($Q = c, b$) systems in QCD sum rules with the complete next-to-leading order (NLO) contribution to the pertabative QCD part of the correlation functions. Instead of meson-meson or diquark-diquark currents, we use diagonalized currents under operator renormalization. Numerical results show that the NLO corrections are very important for the $\bar{Q}Q\bar{Q}Q$ system, because they not only give significant contributions but also reduce parameter dependence and makes Borel platform more distinct, especially for the $\bar{b}b\bar{b}b$ in the $\overline{\text{MS}}$ scheme. We find that the operator mixing induced by NLO corrections is crucial to understand the color structure of the states. We use currents that have good perturbative convergence in our phenomenological analysis. We get three $J^{PC} = 0^{++}$ states, with masses $6.35^{+0.20}_{-0.17}$ GeV, $6.56^{+0.18}_{-0.20}$ GeV and $6.95^{+0.21}_{-0.31}$ GeV, respectively. The first two seem to agree with the broad structure around $6.2 \sim 6.8$ GeV measured by the LHCb collaboration in the $J/\psi J/\psi$ spectrum, and the third seems to agree with the narrow resonance $X(6900)$. For the 2^{++} states we find one with mass $7.03^{+0.22}_{-0.26}$ GeV, which is also close to that of $X(6900)$, and another one around 7.3 GeV but with larger uncertainties.

I. INTRODUCTION

In recent years, a large number of new hadronic states containing heavy quarks (the charm quark c or bottom quark b) have been observed at hadron colliders and e^+e^- colliders [1]. They are expected to be candidates of tetraquark states, pentaquark states, and baryons which contain two heavy quarks [2–4]. These findings have opened up a new stage for the study of hadron physics and QCD. Lately, the LHCb collaboration has discovered a narrow resonance X(6900) and a broad struction around $6.2 \sim 6.8$ GeV in the double-J/ψ spectrum [5], where the X(6900) may be a $\bar{c}c\bar{c}c$ resonance.

Fully heavy tetraquark $\bar{Q}Q\bar{Q}Q$ system is a good platform for studying QCD and exotic states because the system has a strong symmetry in structure and avoids pollution from light quarks. Since 1975, there have been many theoretical studies of full heavy tetraquark system using potential models [6–22], QCD Sum Rules [23–29] and other techniques [30–33]. But it is still under debate whether there exist compact bound states below di-heavy-quarkonium threshold, e.g. di-η_c, di-J/ψ, di-η_b, di-$\Upsilon(1S)$ and so on. Some works imply that there is no stable state below the corresponding threshold [8, 16, 18, 20, 21, 34–36], while some other works have opposite conclusion [11, 13, 14, 16, 17, 19, 30, 37–43]. Moreover, there are different interpretations of the nature of X(6900) state, e.g. tetraquark [21, 22, 27, 33, 35, 36, 44–50], gluonic tetracharm [51], or coupled channel effect [31, 32, 52]. Therefore, further study of $\bar{Q}Q\bar{Q}Q$ system is still needed.

The QCD Sum Rule [53, 54] approach is a powerful tool to study hadronic properties [55–58]. Currently, there have been many leading order (LO) in α_s calculations of the $\bar{Q}Q\bar{Q}Q$ system [23–26, 28, 29], which however results in different conclusions. The importance of purely perturbative part, denoted as C_1, at the next-to-leading order (NLO) in α_s has been emphasized in many works, e.g. for the proton [59, 60], singly heavy baryons [61], the doubly heavy baryon Ξ_{cc}^{++} [62], and fully heavy baryons Ω_{ccc}^{++} and Ω_{bbb}^{-} [63]. Our previous work on Ω_{QQQ} ($Q = c, b$) [63] shows that the NLO contribution of fully heavy quark system can not only lead to a large correction, but also reduce parameters dependence, which makes the Borel platform more distinct. Especially for Ω_{bbb} in the $\overline{\text{MS}}$ scheme, the platform appears only at NLO but not at LO. Therefore, it is reasonable to expect that the NLO corrections are also sizable and important for the $\bar{Q}Q\bar{Q}Q$ system.

Partial NLO contributions of C_1 for the $\bar{Q}Q\bar{Q}Q$ system, originated from the so-called factorized diagrams, have been considered in Ref. [27]. However, to further reduce theoritical uncertainties, it is necessary to perform a complete NLO corrections to C_1, which will be presented in this paper. The rest of the paper is organized as the following. In

* renhuawu@pku.edu.cn
† 1801210125@pku.edu.cn
‡ chen-yu.wang@kit.edu
§ mengce75@pku.edu.cn
¶ yqma@pku.edu.cn
** ktchao@pku.edu.cn

Sec. II, sum rules for calculation of the mass of $\bar{Q}Q\bar{Q}Q$ are given. In Sec. III, we present our methods to calculate perturbative coefficients. Phenomenology results and discussions are given in Sec. V. Some details of our calculations and results are given in Apps. A, B and C.

II. QCD SUM RULE

In this section, we briefly review the framework of the QCD sum rules used to calculate the mass of the tetraquark ground state. See Ref. [55] for more details. We start with a two-point correlation function

$$\Pi(q^2) = i\int \mathrm{d}^D x e^{iq\cdot x}\langle\Omega|T[J(x)J^\dagger(0)]|\Omega\rangle, \tag{1}$$

where D denotes the spacetime dimension, Ω denotes the QCD vacuum and J is the (pseudo-)scalar tetraquark current to be defined later.

On the one hand, the correlation function $\Pi(q^2)$ can be related to the phenomenological spectrum by the Källén-Lehmann representation [55],

$$\Pi(q^2) = \int \mathrm{d}s \frac{\rho(s)}{s-q^2-i\epsilon}\,, \tag{2}$$

where $\rho(s)$ denotes the physical spectrum density. Taking the narrow resonance approximation for the physical ground state, one can parametrize the spectrum density as a pole plus a continuum part

$$\rho(s) = \lambda_H \delta(s-M_H^2) + \rho_{\mathrm{cont}}(s)\theta(s-s_h)\,, \tag{3}$$

where M_H and λ_H denote the mass of the ground state and pole residue, respectively. $\rho_{\mathrm{cont}}(s)$ denotes the continuum spectrum density, which could also contain information of higher resonances. s_h is the threshold of the continuum spectrum.

On the other hand, in the region where $-q^2 = Q^2 \gg \Lambda^2_{\mathrm{QCD}}$, one can calculate correlation function $\Pi(q^2)$ using the operator product expansion (OPE), which reads

$$\Pi(q^2) = C_1(q^2) + \sum_i C_i(q^2)\langle O_i\rangle\,, \tag{4}$$

where C_1 and C_i are perturbatively calculable Wilson coefficients, and $\langle O_i\rangle$ is a shorthand of the vacuum condensate $\langle\Omega|O_i|\Omega\rangle$, which is a nonperturbative but universal quantity. The relative importance of the vacuum condensate is power suppressed by the dimension of the operator O_i. In our calculations, we will only keep the relevant vacuum condensates up to dimension four, which gives the approximated expression of the OPE as

$$\Pi(q^2) = C_1(q^2) + C_{GG}(q^2)\langle g_s^2\hat{G}\hat{G}\rangle\,, \tag{5}$$

where $\langle g_s^2\hat{G}\hat{G}\rangle$ denotes the gluon-gluon (GG) condensate $\langle\Omega|g_s^2\hat{G}\hat{G}|\Omega\rangle$.

According to Eq. (2), one can relate the physical spectrum density to the imaginary part of $\Pi(q^2)$ in Eq. (5) using the dispersion relation, which gives

$$\begin{aligned}\Pi(q^2) &= \int \mathrm{d}s \frac{\rho(s)}{s-q^2-i\epsilon}\\ &= \frac{1}{\pi}\int_{s_{\mathrm{th}}}^{\infty}\mathrm{d}s\frac{\mathrm{Im}C_1(s)+\mathrm{Im}C_{GG}(s)\langle g_s^2\hat{G}\hat{G}\rangle}{s-q^2-i\epsilon}\,,\end{aligned} \tag{6}$$

where $s_{\mathrm{th}} = 16m_Q^2$ is the QCD threshold for the $\bar{Q}Q\bar{Q}Q$ system, and the integral in the second line has been assumed to be convergent. Then by employing the quark-hadron duality and Borel transformation [55], we obtain a sum rule for $\Pi(q^2)$,

$$\lambda_H e^{-\frac{M_H^2}{M_B^2}} = \int_{s_{\mathrm{th}}}^{s_0}\mathrm{d}s\frac{1}{\pi}\mathrm{Im}C_1(s)\,e^{-\frac{s}{M_B^2}} + \int_{s_{\mathrm{th}}}^{\infty}\mathrm{d}s\frac{1}{\pi}\mathrm{Im}C_{GG}(s)e^{-\frac{s}{M_B^2}}\langle g_s^2\hat{G}\hat{G}\rangle\,, \tag{7}$$

where s_0 is the threshold parameter and M_B is the Borel parameter. They are introduced into the formula due to the qurak-hadron duality and Borel transformation, respectively. By differentiating both sides of Eq. (7) with respect to $-\frac{1}{M_B^2}$, one can get

$$\lambda_H\ M_H^2\ e^{-\frac{M_H^2}{M_B^2}} = \int_{s_{\rm th}}^{s_0} {\rm d}s \frac{1}{\pi} {\rm Im} C_1(s)\, e^{-\frac{s}{M_B^2}} s + \int_{s_{\rm th}}^{\infty} {\rm d}s \frac{1}{\pi} {\rm Im} C_{GG}(s) e^{-\frac{s}{M_B^2}} s \langle g_s^2 \hat{G}\hat{G}\rangle \,. \tag{8}$$

Finally, one can solve M_H according to Eq. (7) and (8),

$$M_H^2 = \frac{\int_{s_{\rm th}}^{s_0} {\rm d}s\ s\ \rho_1(s)\ e^{-\frac{s}{M_B^2}} + \int_{s_{\rm th}}^{\infty} {\rm d}s\ s\ \rho_{GG}(s)\ e^{-\frac{s}{M_B^2}} \langle g_s^2 \hat{G}\hat{G}\rangle}{\int_{s_{\rm th}}^{s_0} {\rm d}s\ \rho_1(s)\ e^{-\frac{s}{M_B^2}} + \int_{s_{\rm th}}^{\infty} {\rm d}s\ \rho_{GG}(s)\ e^{-\frac{s}{M_B^2}} \langle g_s^2 \hat{G}\hat{G}\rangle} \,, \tag{9}$$

where $\rho_1 = \frac{1}{\pi}{\rm Im}C_1$ and $\rho_{GG} = \frac{1}{\pi}{\rm Im}C_{GG}$.

Similar to Eq. (1), for the (axial-)vector and tensor tetraquark currents J_μ and $J_{\mu\nu}$ (to be defined later), one can introduce two-point correlation functions as

$$\Pi_{\mu\nu}^{V(A)}(q^2) = i \int {\rm d}^D x e^{iq\cdot x} \langle \Omega | T[J_\mu(x) J_\nu^\dagger(0)] | \Omega \rangle \,, \tag{10}$$

$$\Pi_{\mu\nu,\rho\sigma}^{T}(q^2) = i \int {\rm d}^D x e^{iq\cdot x} \langle \Omega | T[J_{\mu\rho}(x) J_{\nu\sigma}^\dagger(0)] | \Omega \rangle \,. \tag{11}$$

For $J^P = 1^-$ vector particle and $J^P = 1^+$ axial vector particle, the correlation function $\Pi_{\mu\nu}^V$ and $\Pi_{\mu\nu}^A$ can be decomposed as

$$\begin{aligned} \Pi_{\mu\nu}^V(q^2) &= \left(-g_{\mu\nu} + \frac{q_\mu q_\nu}{q^2}\right) \Pi_1^V(q^2) + \frac{q_\mu q_\nu}{q^2} \Pi_2^V(q^2) \,, \\ \Pi_{\mu\nu}^A(q^2) &= \left(-g_{\mu\nu} + \frac{q_\mu q_\nu}{q^2}\right) \Pi_1^A(q^2) + \frac{q_\mu q_\nu}{q^2} \Pi_2^A(q^2) \,. \end{aligned} \tag{12}$$

While for $J^P = 2^+$ tensor particle, the correlation function $\Pi_{\mu\nu,\rho\sigma}^T$ can be decomposed as

$$\begin{aligned} \Pi_{\mu\nu,\rho\sigma}^T(q^2) = &\left(\frac{\theta_{\mu\rho}\theta_{\nu\sigma} + \theta_{\mu\sigma}\theta_{\nu\rho}}{2} - \frac{\theta_{\mu\nu}\theta_{\rho\sigma}}{D-1}\right) \Pi_1^T(q^2) + \frac{\theta_{\mu\rho}\omega_{\nu\sigma} + \theta_{\mu\sigma}\omega_{\nu\rho} + \omega_{\mu\rho}\theta_{\nu\sigma} + \omega_{\mu\sigma}\theta_{\nu\rho}}{2} \Pi_2^T(q^2) \\ &+ \frac{\theta_{\mu\nu}\theta_{\rho\sigma}}{D-1} \Pi_3^T(q^2) + \omega_{\mu\nu}\omega_{\rho\sigma} \Pi_4^T(q^2) + \frac{\theta_{\mu\nu}\omega_{\rho\sigma}}{\sqrt{D-1}} \Pi_5^T(q^2) + \frac{\omega_{\mu\nu}\theta_{\rho\sigma}}{\sqrt{D-1}} \Pi_6^T(q^2) \\ &+ \frac{\theta_{\mu\rho}\omega_{\nu\sigma} - \theta_{\mu\sigma}\omega_{\nu\rho} + \omega_{\mu\rho}\theta_{\nu\sigma} - \omega_{\mu\sigma}\theta_{\nu\rho}}{2} \Pi_7^T(q^2) + \frac{\theta_{\mu\rho}\theta_{\nu\sigma} - \theta_{\mu\sigma}\theta_{\nu\rho}}{2} \Pi_8^T(q^2) \\ &+ \frac{\theta_{\mu\rho}\omega_{\nu\sigma} - \theta_{\mu\sigma}\omega_{\nu\rho} - \omega_{\mu\rho}\theta_{\nu\sigma} + \omega_{\mu\sigma}\theta_{\nu\rho}}{2} \Pi_9^T(q^2) \\ &+ \frac{\theta_{\mu\rho}\omega_{\nu\sigma} + \theta_{\mu\sigma}\omega_{\nu\rho} - \omega_{\mu\rho}\theta_{\nu\sigma} - \omega_{\mu\sigma}\theta_{\nu\rho}}{2} \Pi_{10}^T(q^2) \,, \end{aligned} \tag{13}$$

where $\theta_{\mu\nu} = g_{\mu\nu} - \frac{q_\mu q_\nu}{q^2}$ and $\omega_{\mu\nu} = \frac{q_\mu q_\nu}{q^2}$. In this paper we use $\Pi_1^{V(A)}$ and Π_1^T to construct sum rules, as they project out the spin-1 and spin-2 degrees of freedom we are interested in. The calculation of the corresponding ground state masses is similar to that in Eq. (9).

III. CALCULATION OF C_1 AND C_{GG}

In QCD Sum Rules, there are two kinds of expansions: the OPE and the perturbative expansion in α_s. For the OPE, we only consider the most important contributions, the purely perturbative term C_1 and the GG condensate term $C_{GG}\langle g_s^2 \hat{G}\hat{G}\rangle$, because other higher dimensional operators are power suppressed in the OPE. According to Eq. (9), we need to calculate the imaginary parts of C_1 and C_{GG} perturbatively. We can expect that the LO contribution of C_1 is the dominant one, and the next important contribution can be the NLO corrections for C_1 or the LO contribution of C_{GG}. Therefore, the NLO corrections to C_1 need to be considered in the calculation in order to reduce theoretical

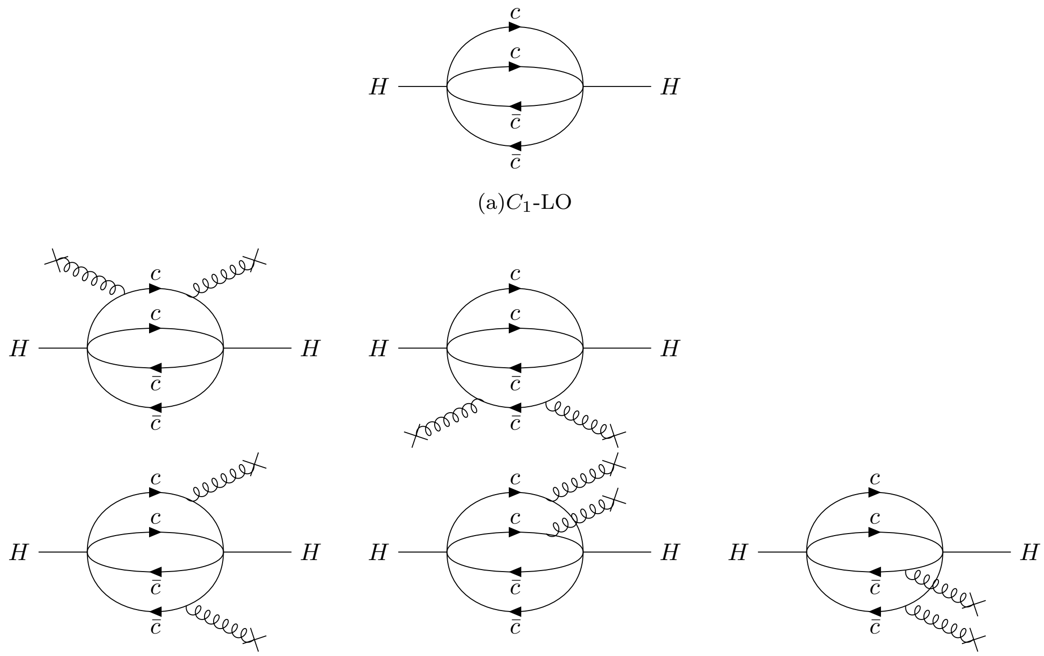

(a)C_1-LO

(b)C_{GG}-LO

FIG. 1. LO Feynman diagrams of C_1 and C_{GG}. H denotes the interpolating current.

uncertainties. For convenience, we will call the sum of the LO of C_1 and C_{GG} as the LO contribution and the NLO corrections to C_1 as the NLO contribution in the following.

We use `FeynArts` [64, 65] to generate Feynman diagrams and Feynman amplitudes of C_1 and C_{GG}. Some representative Feynman diagrams at the LO and the NLO are shown in Fig. 1 and Fig. 2, respectively.

The calculation procedure for C_1 and C_{GG} are summarized below:

- 1. We use `FeynCalc` [66, 67] to simplify spinor structures of Feynman amplitudes with the Naive-γ_5 scheme [68].

- 2. We use `Reduze` [69] to reduce all loop integrals to linear combinations of a set of simpler integrals,

  which are called master integrals (MIs).

- 3. We set up differential equations for MIs [70–73] and solve them numerically, with boundary conditions obtained via auxiliary mass flow [74]. MIs and thus C_1 and C_{GG} are expressed as general series expansion.

- 4. Renormalization. There are no infrared divergences in the NLO amplitude of C_1. After performing wave-function and mass renormalization of quarks (m_Q is renormalized in either the $\overline{\text{MS}}$ scheme or the on-shell scheme), the remaining ultraviolet divergences can be removed by the renomalization of the current operators. When there are more than one current operator share the same quantum number J^{PC}, they are usually mixed with each others under the renormalization. We get operator renormalization matrices for different J^{PC} in the $\overline{\text{MS}}$ scheme, which are shown explicitly in Appendix A.

Because the expressions of C_1 and C_{GG} are too complicated to be shown in the paper, we attach the imaginary part of C_1 and C_{GG}, which are the only needed information in phenomenological study, as ancillary files.

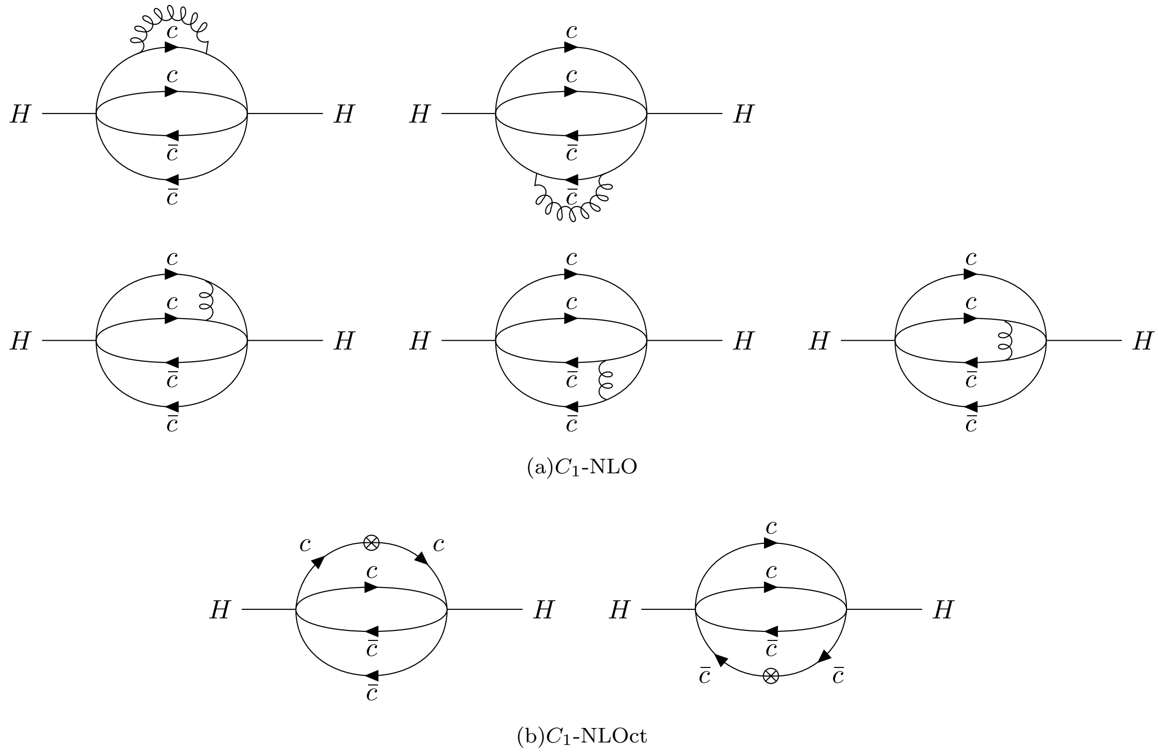

FIG. 2. NLO and counter term Feynman diagrams of C_1. H denotes the interpolating current.

IV. CURRENT OPERATORS

A. $J^P = 0^+$

For the $J^{PC} = 0^{++}$ scalar $\bar{Q}Q\bar{Q}Q$ system, there are five independent interpolating currents. The operator basis, in the color-singlet meson-meson type currents, can be chosen as

$$\begin{aligned}
J^{\text{M-M}}_{\text{S},1} &= (\bar{Q}_a\gamma^\mu Q_a)(\bar{Q}_b\gamma_\mu Q_b)\,, \\
J^{\text{M-M}}_{\text{S},2} &= (\bar{Q}_a\gamma^\mu\gamma^5 Q_a)(\bar{Q}_b\gamma_\mu\gamma^5 Q_b)\,, \\
J^{\text{M-M}}_{\text{S},3} &= (\bar{Q}_a Q_a)(\bar{Q}_b Q_b)\,, \\
J^{\text{M-M}}_{\text{S},4} &= (\bar{Q}_a i\gamma^5 Q_a)(\bar{Q}_b i\gamma^5 Q_b)\,, \\
J^{\text{M-M}}_{\text{S},5} &= (\bar{Q}_a\sigma^{\mu\nu} Q_a)(\bar{Q}_b\sigma_{\mu\nu} Q_b)\,,
\end{aligned} \tag{14}$$

where a and b represent color indices. Alternatively, one can choose the diquark-antidiquark type currents as the basis like those in Ref. [23], which are given by

$$\begin{aligned}
J^{\text{Di-Di}}_{\text{S},1} &= (Q_a^T\hat{C}\gamma^\mu Q_b)(\bar{Q}_a\gamma_\mu\hat{C}\bar{Q}_b^T)\,, \\
J^{\text{Di-Di}}_{\text{S},2} &= (Q_a^T\hat{C}\gamma^\mu\gamma^5 Q_b)(\bar{Q}_a\gamma_\mu\gamma^5\hat{C}\bar{Q}_b^T)\,, \\
J^{\text{Di-Di}}_{\text{S},3} &= (Q_a^T\hat{C} Q_b)(\bar{Q}_a\hat{C}\bar{Q}_b^T)\,, \\
J^{\text{Di-Di}}_{\text{S},4} &= (Q_a^T\hat{C}i\gamma^5 Q_b)(\bar{Q}_a i\gamma^5\hat{C}\bar{Q}_b^T)\,, \\
J^{\text{Di-Di}}_{\text{S},5} &= (Q_a^T\hat{C}\sigma^{\mu\nu} Q_b)(\bar{Q}_a\sigma_{\mu\nu}\hat{C}\bar{Q}_b^T)\,,
\end{aligned} \tag{15}$$

where $\hat{C}$ is the charge-conjugation matrix. The two types of bases can be associated with each other by the Fierz transformation in 4 dimension,

$$\vec{J}_{\rm S}^{\text{Di-Di}} = \frac{1}{8}\begin{pmatrix} 4 & -4 & 8 & 8 & 0 \\ -4 & 4 & 8 & 8 & 0 \\ 2 & 2 & -2 & 2 & 1 \\ 2 & 2 & 2 & -2 & -1 \\ 0 & 0 & 24 & -24 & 4 \end{pmatrix} \cdot \vec{J}_{\rm S}^{\text{M-M}} , \tag{16}$$

where we use the column vector $\vec{J}$ to represent the basis in Eq. (14) or (15).

A physical state can well be a mixture of all possible currents that share the same quantum numbers. The operator mixing has significant effects on the QCD sum rules calculations, say, for the heavy baryon spectrum [62]. However, there are no natural standards to pin down the mixing scheme only based on the LO calculation of C_1 and C_{GG}. Thanks to the NLO calculations, the currents are mixed with each others naturally under the renormalization. If one choose the basis which diagonalizes the anomalous dimension matrix, then the operators in the basis have universal anomalous dimensions, separately. Thus, inserting these operators into the calculations in QCD sum rules, the dependence on the renormalization scale μ tends to be cancelled out in the righthand side of Eq. (9), which is desirable since the left-hand side M_H^2 is a physical quantity.

For $J^{PC} = 0^{++}$ state, if we choose the currents in Eq. (14) as the operator basis, the operator anomalous dimension matrix $\mathcal{A}_{\rm S}^{\text{M-M}}$ is given by

$$\mathcal{A}_{\rm S}^{\text{M-M}} = \delta \begin{pmatrix} -6 & -2 & -12 & -12 & 0 \\ -2 & -6 & 12 & 12 & 0 \\ 0 & 0 & 26 & 6 & \frac{1}{3} \\ 0 & 0 & 6 & 26 & -\frac{1}{3} \\ 0 & 0 & -40 & 40 & -\frac{68}{3} \end{pmatrix} , \tag{17}$$

where $\delta = -\frac{\alpha_s}{16\pi}$. To diagonalize the matrix in Eq. (17), one needs the following transformation matrix

$$\mathcal{T}_{\rm S}^{\text{Dia}} = \begin{pmatrix} \frac{1}{2} & \frac{1}{2} & 0 & 0 & 0 \\ -\frac{1}{2} & \frac{1}{2} & -\frac{1}{3} & -\frac{1}{3} & 0 \\ 0 & 0 & \frac{1}{2} & \frac{1}{2} & 0 \\ 0 & 0 & -\frac{15}{\sqrt{241}} & \frac{15}{\sqrt{241}} & \frac{1}{2} - \frac{8}{\sqrt{241}} \\ 0 & 0 & \frac{15}{\sqrt{241}} & -\frac{15}{\sqrt{241}} & \frac{1}{2} + \frac{8}{\sqrt{241}} \end{pmatrix} . \tag{18}$$

So, we get the new basis

$$\vec{J}_{\rm S}^{\text{Dia}} = \mathcal{T}_{\rm S}^{\text{Dia}} \cdot \vec{J}_{\rm S}^{\text{M-M}} . \tag{19}$$

The anomalous dimension matrix of $\vec{J}_{\rm S}^{\text{Dia}}$ is diagonal, which is given by

$$\begin{aligned} \mathcal{A}_{\rm S}^{\text{Dia}} &= \mathcal{T}_{\rm S}^{\text{Dia}} \cdot \mathcal{A}_{\rm S}^{\text{M-M}} \cdot (\mathcal{T}_{\rm S}^{\text{Dia}})^{-1} \\ &= \frac{4}{3}\delta \begin{pmatrix} -6 & 0 & 0 & 0 & 0 \\ 0 & -3 & 0 & 0 & 0 \\ 0 & 0 & 24 & 0 & 0 \\ 0 & 0 & 0 & -1+\sqrt{241} & 0 \\ 0 & 0 & 0 & 0 & -1-\sqrt{241} \end{pmatrix} . \end{aligned} \tag{20}$$

Because the eigenvalues of anomalous dimension matrix do not degenerate, the transformation matrix $\mathcal{T}_{\rm S}^{\text{Dia}}$ is unique, and thus the basis $\vec{J}_{\rm S}^{\text{Dia}}$ in Eq. (19) is unique.

B. $J^P = 0^-$

For the $J^P = 0^-$ pseudoscalar system, there are three independent interpolating currents. The operator basis, in the color-singlet meson-meson type currents, can be chosen as

$$\begin{aligned} J_{\rm P,1}^{\text{M-M}} &= (\bar{Q}_a \gamma^\mu Q_a)(\bar{Q}_b \gamma_\mu \gamma^5 Q_b) , \\ J_{\rm P,2}^{\text{M-M}} &= (\bar{Q}_a Q_a)(\bar{Q}_b i\gamma^5 Q_b) , \\ J_{\rm P,3}^{\text{M-M}} &= (\bar{Q}_a \sigma^{\mu\nu} Q_a)(\bar{Q}_b \sigma_{\mu\nu} i\gamma^5 Q_b) , \end{aligned} \tag{21}$$

where $J^{\text{M-M}}_{\text{P},1}$ couples to the state with $J^{PC}=0^{--}$, while $J^{\text{M-M}}_{\text{P},2}$ and $J^{\text{M-M}}_{\text{P},3}$ couple to the state with $J^{PC}=0^{-+}$. Of course, one can choose the diquark-antidiquark type currents [23] as the basis, which are given by

$$\begin{aligned}
J^{\text{Di-Di}}_{\text{P},1} &= (Q_a^T\hat{C}Q_b)(\bar{Q}_a i\gamma^5\hat{C}\bar{Q}_b^T) - (Q_a^T\hat{C}i\gamma^5 Q_b)(\bar{Q}_a\hat{C}\bar{Q}_b^T)\,,\\
J^{\text{Di-Di}}_{\text{P},2} &= (Q_a^T\hat{C}Q_b)(\bar{Q}_a i\gamma^5\hat{C}\bar{Q}_b^T) + (Q_a^T\hat{C}i\gamma^5 Q_b)(\bar{Q}_a\hat{C}\bar{Q}_b^T)\,,\\
J^{\text{Di-Di}}_{\text{P},3} &= (Q_a^T\hat{C}\sigma^{\mu\nu}Q_b)(\bar{Q}_a\sigma_{\mu\nu}i\gamma^5\hat{C}\bar{Q}_b^T)\,,
\end{aligned} \tag{22}$$

where $J^{\text{Di-Di}}_{\text{P},1}$ couples to the state with $J^{PC}=0^{--}$, while $J^{\text{Di-Di}}_{\text{P},2}$ and $J^{\text{Di-Di}}_{\text{P},3}$ couple to the state with $J^{PC}=0^{-+}$. The two types bases can be associated with each other by the Fierz transformation in 4 dimension, which is given as

$$\vec{J}^{\text{Di-Di}}_{\text{P}} = \frac{1}{4}\begin{pmatrix} -4\,i & 0 & 0\\ 0 & -4 & 1\\ 0 & 24 & 2\end{pmatrix}\cdot\vec{J}^{\text{M-M}}_{\text{P}}\,. \tag{23}$$

Choosing the currents in Eq. (21) as the operator basis, one can get the anomalous dimension matrix

$$\mathcal{A}^{\text{M-M}}_{\text{P}} = \frac{\delta}{3}\begin{pmatrix} -24 & 0 & 0\\ 0 & 60 & 1\\ 0 & -240 & -68\end{pmatrix}\,. \tag{24}$$

To diagonalize the matrix in Eq. (24), one needs the transformation matrix

$$\mathcal{T}^{\text{Dia}}_{\text{P}} = \begin{pmatrix} 1 & 0 & 0\\ 0 & -\frac{30}{\sqrt{241}} & \frac{1}{2}-\frac{8}{\sqrt{241}}\\ 0 & \frac{30}{\sqrt{241}} & \frac{1}{2}+\frac{8}{\sqrt{241}}\end{pmatrix}\,. \tag{25}$$

And one can get a unique set of the diagonalized currents

$$\vec{J}^{\text{Dia}}_{\text{P}} = \mathcal{T}^{\text{Dia}}_{\text{P}}\cdot\vec{J}^{\text{M-M}}_{\text{P}}\,. \tag{26}$$

The anomalous dimension matrix of $\vec{J}^{\text{Dia}}_{\text{P}}$ is diagonal, which is given by

$$\begin{aligned}
\mathcal{A}^{\text{Dia}}_{\text{P}} &= \mathcal{T}^{\text{Dia}}_{\text{P}}\cdot\mathcal{A}^{\text{M-M}}_{\text{P}}\cdot(\mathcal{T}^{\text{Dia}}_{\text{P}})^{-1}\\
&= \frac{4}{3}\delta\begin{pmatrix} -6 & 0 & 0\\ 0 & -1+\sqrt{241} & 0\\ 0 & 0 & -1-\sqrt{241}\end{pmatrix}\,.
\end{aligned} \tag{27}$$

C. $J^P = 1^+$

For the $J^P=1^+$ axial vector system, there are four independent interpolating currents. The operator basis, in the color singlet meson-meson type currents, can be chosen as

$$\begin{aligned}
J^{\text{M-M}}_{\text{A},1} &= (\bar{Q}_aQ_a)(\bar{Q}_b\gamma^\mu\gamma^5Q_b)\,,\\
J^{\text{M-M}}_{\text{A},2} &= (\bar{Q}_a\sigma^{\mu\nu}i\gamma^5Q_a)(\bar{Q}_b\gamma_\nu Q_b)\,,\\
J^{\text{M-M}}_{\text{A},3} &= (\bar{Q}_a i\gamma^5Q_a)(\bar{Q}_b\gamma^\mu Q_b)\,,\\
J^{\text{M-M}}_{\text{A},4} &= (\bar{Q}_a\sigma^{\mu\nu}Q_a)(\bar{Q}_b\gamma_\nu\gamma^5 Q_b)\,,
\end{aligned} \tag{28}$$

where $J^{\text{M-M}}_{\text{A},1}$ and $J^{\text{M-M}}_{\text{A},2}$ couple to states with $J^{PC}=1^{++}$, while $J^{\text{M-M}}_{\text{A},3}$ and $J^{\text{M-M}}_{\text{A},4}$ couple to states with $J^{PC}=1^{+-}$. Alternatively, one can choose the diquark-antidiquark type currents [23] as the basis, which are given by

$$\begin{aligned}
J^{\text{Di-Di}}_{\text{A},1} &= (Q_a^T\hat{C}\gamma^\mu\gamma^5Q_b)(\bar{Q}_a\hat{C}\bar{Q}_b^T) + (Q_a^T\hat{C}Q_b)(\bar{Q}_a\gamma^\mu\gamma^5\hat{C}\bar{Q}_b^T)\,,\\
J^{\text{Di-Di}}_{\text{A},2} &= (Q_a^T\hat{C}\sigma^{\mu\nu}i\gamma^5Q_b)(\bar{Q}_a\gamma_\nu\hat{C}\bar{Q}_b^T) + (Q_a^T\hat{C}\gamma_\nu Q_b)(\bar{Q}_a\sigma^{\mu\nu}i\gamma^5\hat{C}\bar{Q}_b^T)\,,\\
J^{\text{Di-Di}}_{\text{A},3} &= (Q_a^T\hat{C}\gamma^\mu\gamma^5Q_b)(\bar{Q}_a\hat{C}\bar{Q}_b^T) - (Q_a^T\hat{C}Q_b)(\bar{Q}_a\gamma^\mu\gamma^5\hat{C}\bar{Q}_b^T)\,,\\
J^{\text{Di-Di}}_{\text{A},4} &= (Q_a^T\hat{C}\sigma^{\mu\nu}i\gamma^5Q_b)(\bar{Q}_a\gamma_\nu\hat{C}\bar{Q}_b^T) - (Q_a^T\hat{C}\gamma_\nu Q_b)(\bar{Q}_a\sigma^{\mu\nu}i\gamma^5\hat{C}\bar{Q}_b^T)\,,
\end{aligned} \tag{29}$$

where $J^{\text{Di-Di}}_{\text{A},1}$ and $J^{\text{Di-Di}}_{\text{A},2}$ couple to states with $J^{PC}=1^{++}$, while $J^{\text{Di-Di}}_{\text{A},3}$ and $J^{\text{Di-Di}}_{\text{A},4}$ couple to states with $J^{PC}=1^{+-}$. In the calculation, $J^{\text{Di-Di}}_{\text{A}}$ can be associated with $J^{\text{M-M}}_{\text{A}}$ by the Fierz transformation in 4 dimension.

$$\vec{J}^{\text{Di-Di}}_{\text{A}} = \begin{pmatrix} -1 & 1 & 0 & 0 \\ 3 & 1 & 0 & 0 \\ 0 & 0 & i & i \\ 0 & 0 & -3\,i & i \end{pmatrix} \cdot \vec{J}^{\text{M-M}}_{\text{A}} \,. \tag{30}$$

Choosing the currents in Eq. (28) as the operator basis, one can get the anomalous dimension matrix

$$\mathcal{A}^{\text{M-M}}_{\text{A}} = \frac{\delta}{3}\begin{pmatrix} 30 & 2 & 0 & 0 \\ -30 & -34 & 0 & 0 \\ 0 & 0 & 30 & -2 \\ 0 & 0 & 30 & -34 \end{pmatrix} . \tag{31}$$

To diagonalize the matrix in Eq. (31), one needs the transformation matrix

$$\mathcal{T}^{\text{Dia}}_{\text{A}} = \frac{1}{2\sqrt{241}}\begin{pmatrix} 15 & \sqrt{241}+16 & 0 & 0 \\ -15 & \sqrt{241}-16 & 0 & 0 \\ 0 & 0 & -15 & \sqrt{241}+16 \\ 0 & 0 & 15 & \sqrt{241}-16 \end{pmatrix} . \tag{32}$$

And one can get a unique set of the diagonalized currents

$$\vec{J}^{\text{Dia}}_{\text{A}} = \mathcal{T}^{\text{Dia}}_{\text{A}} \cdot \vec{J}^{\text{M-M}}_{\text{A}} \,. \tag{33}$$

The anomalous dimension matrix of $\vec{J}^{\text{Dia}}_{\text{A}}$ is diagonal, which is given by

$$\mathcal{A}^{\text{Dia}}_{\text{A}} = -\frac{2}{3}\delta\begin{pmatrix} 1+\sqrt{241} & 0 & 0 & 0 \\ 0 & 1-\sqrt{241} & 0 & 0 \\ 0 & 0 & 1+\sqrt{241} & 0 \\ 0 & 0 & 0 & 1-\sqrt{241} \end{pmatrix} . \tag{34}$$

D. $J^P = 1^-$

For the $J^P=1^-$ vector system, there are four independent interpolating currents. The operator basis, in the color singlet meson-meson type currents, can be chosen as

$$\begin{aligned} J^{\text{M-M}}_{\text{V},1} &= (\bar{Q}_a Q_a)(\bar{Q}_b \gamma^\mu Q_b)\,, \\ J^{\text{M-M}}_{\text{V},2} &= (\bar{Q}_a \sigma^{\mu\nu} i\gamma^5 Q_a)(\bar{Q}_b \gamma_\nu \gamma^5 Q_b)\,, \\ J^{\text{M-M}}_{\text{V},3} &= (\bar{Q}_a i\gamma^5 Q_a)(\bar{Q}_b \gamma^\mu \gamma^5 Q_b)\,, \\ J^{\text{M-M}}_{\text{V},4} &= (\bar{Q}_a \sigma^{\mu\nu} Q_a)(\bar{Q}_b \gamma_\nu Q_b)\,, \end{aligned} \tag{35}$$

where $J^{\text{M-M}}_{\text{V},1}$ and $J^{\text{M-M}}_{\text{V},2}$ couple to states with $J^{PC}=1^{--}$, while $J^{\text{M-M}}_{\text{V},3}$ and $J^{\text{M-M}}_{\text{V},4}$ couple to states with $J^{PC}=1^{-+}$. Of course, one can choose the diquark-antidiquark type currents [23] as the basis, which are given by

$$\begin{aligned} J^{\text{Di-Di}}_{\text{V},1} &= (Q_a^T \hat{C}\gamma^\mu\gamma^5 Q_b)(\bar{Q}_a i\gamma^5 \hat{C}\bar{Q}_b^T) - (Q_a^T \hat{C} i\gamma^5 Q_b)(\bar{Q}_a \gamma^\mu\gamma^5 \hat{C}\bar{Q}_b^T)\,, \\ J^{\text{Di-Di}}_{\text{V},2} &= (Q_a^T \hat{C}\sigma^{\mu\nu} Q_b)(\bar{Q}_a \gamma_\nu \hat{C}\bar{Q}_b^T) - (Q_a^T \hat{C}\gamma_\nu Q_b)(\bar{Q}_a \sigma^{\mu\nu} \hat{C}\bar{Q}_b^T)\,, \\ J^{\text{Di-Di}}_{\text{V},3} &= (Q_a^T \hat{C}\gamma^\mu\gamma^5 Q_b)(\bar{Q}_a i\gamma^5 \hat{C}\bar{Q}_b^T) + (Q_a^T \hat{C} i\gamma^5 Q_b)(\bar{Q}_a \gamma^\mu\gamma^5 \hat{C}\bar{Q}_b^T)\,, \\ J^{\text{Di-Di}}_{\text{V},4} &= (Q_a^T \hat{C}\sigma^{\mu\nu} Q_b)(\bar{Q}_a \gamma_\nu \hat{C}\bar{Q}_b^T) + (Q_a^T \hat{C}\gamma_\nu Q_b)(\bar{Q}_a \sigma^{\mu\nu} \hat{C}\bar{Q}_b^T)\,, \end{aligned} \tag{36}$$

where $J^{\text{Di-Di}}_{\text{V},1}$ and $J^{\text{Di-Di}}_{\text{V},2}$ couple to states with $J^{PC}=1^{--}$, while $J^{\text{Di-Di}}_{\text{V},3}$ and $J^{\text{Di-Di}}_{\text{V},4}$ couple to states with $J^{PC}=1^{-+}$.

In the calculation, $\vec{J}_{\rm V}^{\text{Di-Di}}$ can be associated with $\vec{J}_{\rm V}^{\text{M-M}}$ by Fierz Transformation in 4 dimension, which is given by

$$\vec{J}_{\rm V}^{\text{Di-Di}} = \begin{pmatrix} -i & i & 0 & 0 \\ -3\,i & -i & 0 & 0 \\ 0 & 0 & -1 & -1 \\ 0 & 0 & -3 & 1 \end{pmatrix} \cdot \vec{J}_{\rm V}^{\text{M-M}} \,. \tag{37}$$

If we choose the currents in Eq. (35) as the operator basis, the anomalous dimension matrix $\mathcal{A}_{\rm V}^{\text{M-M}}$ is the same as $\mathcal{A}_{\rm A}^{\text{M-M}}$ shown in Eq. (31). Thus, similarly with axial vector ($J^P = 1^+$) system, one can get a unique set of diagonalized currents

$$\begin{aligned} \vec{J}_{\rm V}^{\text{Di-Di}} &= \mathcal{T}_{\rm A}^{\text{Dia}} \cdot \vec{J}_{\rm V}^{\text{M-M}} \\ &= \frac{1}{2\sqrt{241}} \begin{pmatrix} 15 & \sqrt{241}+16 & 0 & 0 \\ -15 & \sqrt{241}-16 & 0 & 0 \\ 0 & 0 & -15 & \sqrt{241}+16 \\ 0 & 0 & 15 & \sqrt{241}-16 \end{pmatrix} \cdot \vec{J}_{\rm V}^{\text{M-M}} \,, \end{aligned} \tag{38}$$

which make the anomalous dimension matrix $\mathcal{A}_{\rm V}^{\text{M-M}}$ diagonal.

E. $J^P = 2^+$

For the $J^{PC} = 2^{++}$ tensor system, there are three independent interpolating currents. The operator basis, in the color-singlet meson-meson type currents, can be chosen as

$$\begin{aligned} J_{\rm T,1}^{\text{M-M}} &= (\bar{Q}_a \gamma^\mu Q_a)(\bar{Q}_b \gamma^\nu Q_b) \,, \\ J_{\rm T,2}^{\text{M-M}} &= (\bar{Q}_a \gamma^\mu \gamma^5 Q_a)(\bar{Q}_b \gamma^\nu \gamma^5 Q_b) \,, \\ J_{\rm T,3}^{\text{M-M}} &= (\bar{Q}_a \sigma^{\mu\alpha} Q_a)(\bar{Q}_b \sigma^{\nu\alpha} Q_b) \,. \end{aligned} \tag{39}$$

One could also construct the following operators

$$\begin{aligned} J_{\rm T,4}^{\text{M-M}} &= g^{\mu\nu} (\bar{Q}_a Q_a)(\bar{Q}_b Q_b) \,, \\ J_{\rm T,5}^{\text{M-M}} &= g^{\mu\nu} (\bar{Q}_a i\gamma^5 Q_a)(\bar{Q}_b i\gamma^5 Q_b) \,, \\ J_{\rm T,6}^{\text{M-M}} &= (\bar{Q}_a Q_a)(\bar{Q}_b \sigma^{\mu\nu} Q_b) \,, \end{aligned} \tag{40}$$

but they won't contribute to Π_1^T. This suggests that these operators can not correspond to a tensor particle and we discard them from our analysis.

Of course, one can choose the diquark-antidiquark type currents [23] as the basis, which are given by

$$\begin{aligned} J_{\rm T,1}^{\text{Di-Di}} &= (Q_a^T \hat{C} \gamma^\mu Q_b)(\bar{Q}_a \gamma^\nu \hat{C} \bar{Q}_b^T) + (Q_a^T \hat{C} \gamma^\nu Q_b)(\bar{Q}_a \gamma^\mu \hat{C} \bar{Q}_b^T) \,, \\ J_{\rm T,2}^{\text{Di-Di}} &= (Q_a^T \hat{C} \gamma^\mu \gamma^5 Q_b)(\bar{Q}_a \gamma^\nu \gamma^5 \hat{C} \bar{Q}_b^T) + (Q_a^T \hat{C} \gamma^\nu \gamma^5 Q_b)(\bar{Q}_a \gamma^\mu \gamma^5 \hat{C} \bar{Q}_b^T) \,, \\ J_{\rm T,3}^{\text{Di-Di}} &= (Q_a^T \hat{C} \sigma^{\mu\alpha} Q_b)(\bar{Q}_a \sigma^{\nu\alpha} \hat{C} \bar{Q}_b^T) + (Q_a^T \hat{C} \sigma^{\nu\alpha} Q_b)(\bar{Q}_a \sigma^{\mu\alpha} \hat{C} \bar{Q}_b^T) \,. \end{aligned} \tag{41}$$

In the calculation, $\vec{J}_{\rm T}^{\text{Di-Di}}$ can associate with $\vec{J}_{\rm T}^{\text{M-M}}$ by the Fierz Transformation in 4 dimension, which is given by

$$\vec{J}_{\rm T}^{\text{Di-Di}} = -\frac{1}{2} \begin{pmatrix} -1 & 1 & 1 \\ -1 & 1 & -1 \\ 2 & 2 & 0 \end{pmatrix} \cdot \vec{J}_{\rm T}^{\text{M-M}} \,. \tag{42}$$

Choosing the currents in Eq. (39) as the operator basis, one can get the anomalous dimension matrix

$$\mathcal{A}_{\rm T}^{\text{M-M}} = -\frac{2}{3} \delta \begin{pmatrix} 3 & 5 & 3 \\ 5 & 3 & -3 \\ 0 & 0 & 16 \end{pmatrix} \,. \tag{43}$$

To diagonalize the matrix in Eq. (43), one needs the transformation matrix

$$\mathcal{T}_{\mathrm{T}}^{\mathrm{Dia}} = \frac{1}{6}\begin{pmatrix} -3 & 3 & 1 \\ 3 & 3 & 0 \\ 0 & 0 & 6 \end{pmatrix} . \tag{44}$$

And one can get a unique set of the diagonalized currents

$$\vec{J}_{\mathrm{T}}^{\mathrm{Dia}} = \mathcal{T}_{\mathrm{T}}^{\mathrm{Dia}} \cdot \vec{J}_{\mathrm{T}}^{\mathrm{M\text{-}M}} . \tag{45}$$

The anomalous dimension matrix of $\vec{J}_{\mathrm{T}}^{\mathrm{Dia}}$ is diagonal, which is given by

$$\begin{aligned} \mathcal{A}_{\mathrm{T}}^{\mathrm{Dia}} &= \mathcal{T}_{\mathrm{T}}^{\mathrm{Dia}} \cdot \mathcal{A}_{\mathrm{T}}^{\mathrm{M\text{-}M}} \cdot (\mathcal{T}_{\mathrm{T}}^{\mathrm{Dia}})^{-1} \\ &= -\frac{4}{3}\delta \begin{pmatrix} -1 & 0 & 0 \\ 0 & 4 & 0 \\ 0 & 0 & 8 \end{pmatrix} . \end{aligned} \tag{46}$$

Thus, all diagonalized currents can be determined uniquely.

V. PHENOMENOLOGY

In our numerical analysis, we choose the following parameters [62, 75–78],

$$\begin{aligned} m_c^{\overline{\mathrm{MS}}}(m_c) &= 1.27 \pm 0.03 \ \mathrm{GeV} , \\ m_c^{\mathrm{OS}} &= 1.46 \pm 0.07 \ \mathrm{GeV}, \\ m_b^{\overline{\mathrm{MS}}}(m_b) &= 4.18 \pm 0.03 \ \mathrm{GeV} , \\ m_b^{\mathrm{OS}} &= 4.65 \pm 0.05 \ \mathrm{GeV} , \\ \langle g_s^2 \hat{G}\hat{G} \rangle &= 4\pi^2 (0.037 \pm 0.015) \ \mathrm{GeV}^4 , \\ \alpha_s(m_Z &= 91.1876 \ \mathrm{GeV}) = 0.1181 . \end{aligned} \tag{47}$$

It is worth emphasizing that $\alpha_s(\mu)$ and the heavy quark mass $m_Q^{\overline{\mathrm{MS}}}(\mu)$ are obtained through two-loop running. Note that we don't need to consider the running of $\langle g_s^2 \hat{G}\hat{G} \rangle$ for the LO GG condensate contribution, as its anomalous dimension vanishes up to this order. As a typical choice, we set $\mu = M_B$ in our phenomenological analysis [53, 79], but the renormalization scale dependence will also be discussed. On-Shell (OS) masses m_c^{OS} and m_b^{OS} are extracted from the QCD sum rules analysis of the J/ψ and $\Upsilon(1S)$ spectrum, respectively, in which the mass renormalization scheme and truncation order of α_s are the same as this paper.

According to Eq. (9), numerical result M_H also depends on the other two parameters: s_0 and M_B. However, the physical value of M_H should be independent of any artificial parameters. So a credible result should be obtained from an appropriate region where the dependence of s_0 and M_B is weak. On the other hand, the choice of M_B and s_0 should ensure the validity of the OPE and ground-state contribution dominance, which constrain the two parameters to be the so-called "Borel window". Within the Borel window, one should find the region, the so-called "Borel platform", in which M_H depends on s_0 and M_B weakly.

To search for the Borel window, we define the relative contributions of the condensate and continuum as

$$\begin{aligned} r_{GG} &= \frac{\langle g_s^2 \hat{G}\hat{G} \rangle \int_{s_{th}}^{\infty} \mathrm{d}s \ \rho_{GG}(s)\, e^{-\frac{s}{M_B^2}}}{\int_{s_{th}}^{\infty} \mathrm{d}s \ \rho_1(s)\, e^{-\frac{s}{M_B^2}}} , \\ r_{\mathrm{cont}} &= \frac{\int_{s_0}^{\infty} \mathrm{d}s \ \rho_1(s)\, e^{-\frac{s}{M_B^2}}}{\int_{s_{th}}^{\infty} \mathrm{d}s \ \rho_1(s)\, e^{-\frac{s}{M_B^2}}} , \end{aligned} \tag{48}$$

and impose the following constraints:

$$|r_{GG}| \leq 30\%, \qquad |r_{\mathrm{cont}}| \leq 30\% . \tag{49}$$

The two constraints guarantee the validity of OPE and the gound-state contribution dominance, respectively. In addition to the conditions given in Eq. (49), we also impose the following constrain on s_0:

$$s_0 < (M_H + 1 \text{ GeV})^2, \tag{50}$$

since, roughly speaking, s_0 denotes the energy scale where the continuum spectrum begins to contribute and that the binding energy in a pure heavy hadron is usually smaller than 1 GeV. To find the Borel platform, we search for the point where the parameter dependence of M_H is weakest within the Borel window. More explicitly, we choose the variables as $x = s_0$ and $y = M_B^2$ and define the function

$$\Delta(x, y) = \left(\frac{\partial M_H}{\partial x}\right)^2 + \left(\frac{\partial M_H}{\partial y}\right)^2 . \tag{51}$$

By minimizing the function $\Delta(x, y)$ within the Borel window and with the constrain Eq. (50), we get a point (x_0, y_0), which will be used to calculate the central value of M_H. To estimate errors of M_H, we vary the values of s_0 and M_B^2 around the point (x_0, y_0) up to 10% in magnitude. It should be emphasized that the central point (x_0, y_0) may lies on the margin of the Borel window in some cases. Therefore, the parameter space used to estimate errors of M_H may exceed the Borel window, and also, the upper and the lower errors are usually asymmetric.

A. Numerical results and discussions for the $\bar{c}c\bar{c}c$ system

Our main results are shown in Fig. 3, where the 19 diagonalized currents, which should be more reasonable to be used in the QCD sum rules, are clustered to different quantum numbers. We set $\mu = M_B$ and choose the $\overline{\text{MS}}$ renormalization scheme, and errors of M_H include only that originated from uncertainties of s_0 and M_B^2. As references, we also plot masses of the $X(6900)$ and two J/ψ's.

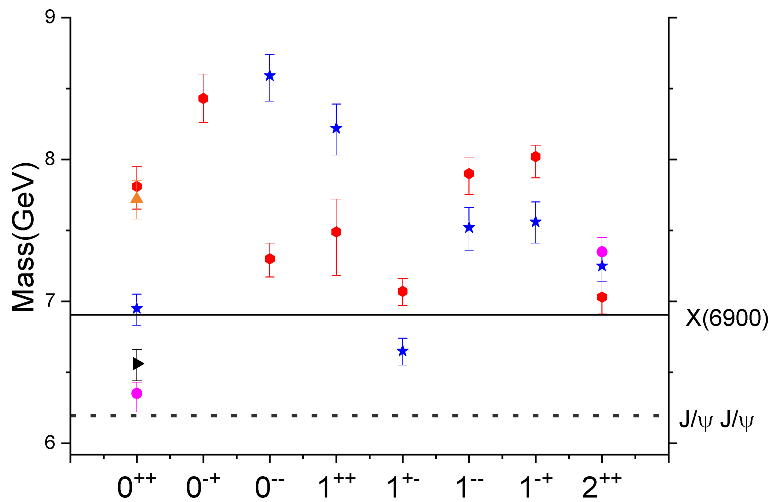

FIG. 3. The NLO mass spectra of the $\bar{c}c\bar{c}c$ system in the $\overline{\text{MS}}$ scheme. The errors of masses just come from the the parameter dependence on s_0 and M_B^2.

The most comprehensive results are listed in Tabs. IX–XVIII in Appendix B, where we include both LO and NLO, both $\overline{\text{MS}}$ scheme and on-shell scheme, and all currents of meson-meson types, diquark-antidiquark types, and also diagonalized ones. Again in these tables we set $\mu = M_B$ and thus errors of M_H are due to choices of s_0 and M_B^2. Further information of s_0 and M_B^2 dependences are shown in Figs. 5–23 in Appendix B, where only results of the more reasonable diagonalized currents are shown. In these plots, a black dot denotes to the central point (x_0, y_0), and shadows denote the Borel window determined by Eq. (49).

Let us first emphasize the importance of the NLO corrections. On one hand, NLO corrections to hadron masses are significant, which are larger than 0.5 GeV in both $\overline{\text{MS}}$ and on-shell schemes for almost all the currents involved in Tabs. IX–XVIII. On the other hand, with the NLO corrections, the quark mass scheme dependence of M_H tends to be reduced, especially for some diagonalized currents. To see this, we examine the difference of the predicted hadron masses between the two schemes,

$$\Delta M_H = M_H^{\rm OS} - M_H^{\overline{\rm MS}}\,. \tag{52}$$

From Tabs. IX–XVIII, for almost all the currents, one can find that the mass difference at LO is about $\Delta M_H^{\rm LO} \approx$ 1.2 GeV, which implies a roughly linear dependence of $\Delta M_H^{\rm LO}$ on the quark mass difference between the two scheme. One can also find that the NLO corrections to $M_H^{\overline{\rm MS}}$ are positive while those to $M_H^{\rm OS}$ are negative, therefore, the scheme dependence of M_H tends to be reduced with the NLO corrections. Taking the $J^P = 0^+$ system as an example (see Tab. IX and X), for the three diagonalized currents $J^{\rm Dia}_{S,2,3,4}$, the NLO mass difference $|\Delta M_H^{\rm NLO}| < 0.4$ GeV, which is explicitly smaller than that at LO. As for the currents $J^{\rm Dia}_{S,1}$ and $J^{\rm Dia}_{S,5}$, the NLO corrections to $M_H^{\overline{\rm MS}}$ are larger than 1 GeV, which implies that there are genuine large corrections other than the quark mass renormalizaiton effects and the perturbation convergence may be bad for these currents.

The convergence of perturbation can also be explored by the μ dependence of the NLO results. One would expect that the μ dependence of the NLO result will be significant reduced comparing with the LO one for the current for which the perturbation convergence is good, since the truncation of the perturbation series up to the NLO has weak effect on the result. On the other hand, the large μ dependence of the NLO result may imply that the perturbation convergence is bad, say, the next-to-next-to-leading-order (NNLO) corrections should be important in this case. In Tabs. IX–XVIII, we have chose $\mu = M_B$ in the $\overline{\rm MS}$ scheme. To study the μ dependence, we vary $\mu = k\ M_B$ with $k \in (0.8, 2.0)$, where the range is chosen with the requirement that the Borel platform can be achieved and the perturbative expansion is under good control. We investigate the μ dependence for the diagonalized operators with $J^{PC} = 0^{++}$, which are shown in Fig. 24–28 in Appendix B for the LO and the NLO results. From these plots, one can see that the μ dependence of the results for $J^{\rm Dia}_{S,2,3,4}$ are improved significantly after including the NLO contributions, especially for the last two operators $J^{\rm Dia}_{S,3}$ and $J^{\rm Dia}_{S,4}$, which implies that those operators have good perturbation convergence. While the NLO results of $J^{\rm Dia}_{S,1}$ and $J^{\rm Dia}_{S,5}$ are still very sensitive to the renormalization scale μ, which implies that those currents have bad perturbation convergence. Therefore, the mass difference $\Delta M_H^{\rm NLO}$ between the two schemes and the μ dependence of the NLO $M_H^{\overline{\rm MS}}$ are correlated strongly. That is, when there is a good perturbation convergence, we should expect a small $\Delta M_H^{\rm NLO}$ and weak μ-dependence at NLO.

As for the states with $J^{PC} \neq 0^{++}$, there are only three diagonalized operators that satisfy $\Delta M_H^{\rm NLO} < 0.5$ GeV. They are $J^{\rm Dia}_{P,2}$ with $J^{PC} = 0^{-+}$, $J^{\rm Dia}_{A,4}$ with $J^{PC} = 1^{+-}$ and $J^{\rm Dia}_{T,1}$ with $J^{PC} = 2^{++}$. The μ dependences of the LO and the NLO $\overline{\rm MS}$ masses for these three diagonalized operators are shown in Fig.29–31 in Appendix B. Just as one would expect, the μ dependences of the NLO results are improved significantly comparing with that of the LO one.

In cases where convergence of perturbation is bad, uncertainties from higher order corrections should be large. As higher order corrections, such as the NNLO ones for C_1, are beyond the scope of this paper, we will only choose diagonalized operators, that have good perturbation convergence, in the following analysis. For the results of the diagonalized operators $J^{\rm Dia}_{S,2,3,4}$ with $J^{PC} = 0^{++}$, $J^{\rm Dia}_{P,2}$ with $J^{PC} = 0^{-+}$, $J^{\rm Dia}_{A,4}$ with $J^{PC} = 1^{+-}$ and $J^{\rm Dia}_{T,1}$ with $J^{PC} = 2^{++}$, we also estimate the uncertainties coming from the errors of the quark masses in Eq. (47), and the uncertainties are shown in Tabs. I–VII.

Current	Order	M_H (GeV)	s_0 (GeV^2)	M_B^2 (GeV^2)	Error from s_0 and M_B^2	Error from m_Q	Error from μ
$J^{\rm Dia}_{S,2}$	LO($\overline{\rm MS}$)	$6.19^{+0.26}_{-0.23}$	51(±10%)	3.50(±10%)	$^{+0.07}_{-0.12}$	$^{+0.11}_{-0.14}$	$^{+0.22}_{-0.23}$
	NLO($\overline{\rm MS}$)	$6.95^{+0.21}_{-0.31}$	61(±10%)	5.00(±10%)	$^{+0.10}_{-0.12}$	$^{+0.15}_{-0.13}$	$^{+0.11}_{-0.26}$
	LO(OS)	$7.31^{+0.29}_{-0.24}$	64(±10%)	3.75(±10%)	$^{+0.08}_{-0.12}$	$^{+0.28}_{-0.21}$	
	NLO(OS)	$6.58^{+0.28}_{-0.29}$	48(±10%)	2.00(±10%)	$^{+0.08}_{-0.11}$	$^{+0.27}_{-0.27}$	

TABLE I. The LO and NLO results for the mass of $J^{\rm Dia}_{S,2}$ in $\overline{\rm MS}$ and On-Shell schemes. Here the errors for M_H are from s_0, M_B, the charm quark mass, and the renormalization scale μ with $\mu = kM_B$ and $k \in (0.8, 1.2)$ (the central values correspond to $\mu = M_B$).

Current	Order	M_H (GeV)	s_0 (GeV^2)	M_B^2 (GeV^2)	Error from s_0 and M_B^2	Error from m_Q	Error from μ
$J_{S,3}^{\mathrm{Dia}}$	LO($\overline{\mathrm{MS}}$)	$5.93^{+0.31}_{-0.26}$	45(±10%)	3.00(±10%)	$^{+0.07}_{-0.10}$	$^{+0.18}_{-0.09}$	$^{+0.24}_{-0.22}$
	NLO($\overline{\mathrm{MS}}$)	$6.35^{+0.20}_{-0.17}$	51(±10%)	3.50(±10%)	$^{+0.08}_{-0.13}$	$^{+0.18}_{-0.11}$	$^{+0.00}_{-0.03}$
	LO(OS)	$7.06^{+0.32}_{-0.26}$	60(±10%)	3.00(±10%)	$^{+0.07}_{-0.10}$	$^{+0.31}_{-0.24}$	
	NLO(OS)	$6.47^{+0.29}_{-0.30}$	46(±10%)	1.75(±10%)	$^{+0.08}_{-0.10}$	$^{+0.28}_{-0.28}$	

TABLE II. The LO and NLO results for the mass of $J_{S,3}^{\mathrm{Dia}}$ in $\overline{\mathrm{MS}}$ and On-Shell schemes. Here the errors for M_H are from s_0, M_B, the charm quark mass, and the renormalization scale μ with $\mu = kM_B$ and $k \in (0.8, 1.2)$ (the central values correspond to $\mu = M_B$).

Current	Order	M_H (GeV)	s_0 (GeV^2)	M_B^2 (GeV^2)	Error from s_0 and M_B^2	Error from m_Q	Error from μ
$J_{S,4}^{\mathrm{Dia}}$	LO($\overline{\mathrm{MS}}$)	$6.02^{+0.24}_{-0.28}$	49(±10%)	3.00(±10%)	$^{+0.05}_{-0.06}$	$^{+0.09}_{-0.14}$	$^{+0.22}_{-0.23}$
	NLO($\overline{\mathrm{MS}}$)	$6.56^{+0.18}_{-0.20}$	55(±10%)	4.00(±10%)	$^{+0.10}_{-0.12}$	$^{+0.15}_{-0.13}$	$^{+0.03}_{-0.10}$
	LO(OS)	$7.16^{+0.24}_{-0.30}$	66(±10%)	3.00(±10%)	$^{+0.04}_{-0.05}$	$^{+0.24}_{-0.30}$	
	NLO(OS)	$6.49^{+0.29}_{-0.30}$	46(±10%)	1.75(±10%)	$^{+0.07}_{-0.10}$	$^{+0.28}_{-0.28}$	

TABLE III. The LO and NLO results for the mass of $J_{S,4}^{\mathrm{Dia}}$ in $\overline{\mathrm{MS}}$ and On-Shell schemes. Here the errors for M_H are from s_0, M_B, the charm quark mass, and the renormalization scale μ with $\mu = kM_B$ and $k \in (0.8, 1.2)$ (the central values correspond to $\mu = M_B$).

Current	Order	M_H (GeV)	s_0 (GeV^2)	M_B^2 (GeV^2)	Error from s_0 and M_B^2	Error from m_Q	Error from μ
$J_{P,2}^{\mathrm{Dia}}$	LO($\overline{\mathrm{MS}}$)	$6.53^{+0.29}_{-0.27}$	56.(±10%)	4.25(±10%)	$^{+0.12}_{-0.14}$	$^{+0.12}_{-0.16}$	$^{+0.24}_{-0.16}$
	NLO($\overline{\mathrm{MS}}$)	$7.30^{+0.19}_{-0.20}$	68.(±10%)	6.00(±10%)	$^{+0.11}_{-0.13}$	$^{+0.14}_{-0.15}$	$^{+0.00}_{-0.03}$
	LO(OS)	$7.79^{+0.31}_{-0.27}$	74.(±10%)	4.50(±10%)	$^{+0.10}_{-0.15}$	$^{+0.29}_{-0.23}$	
	NLO(OS)	$6.89^{+0.32}_{-0.34}$	52.(±10%)	2.75(±10%)	$^{+0.14}_{-0.23}$	$^{+0.29}_{-0.25}$	

TABLE IV. The LO and NLO results for the mass of $J_{P,2}^{\mathrm{Dia}}$ in $\overline{\mathrm{MS}}$ and On-Shell schemes. Here the errors for M_H are from s_0, M_B, the charm quark mass, and the renormalization scale μ with $\mu = kM_B$ and $k \in (0.8, 1.2)$ (the central values correspond to $\mu = M_B$).

Current	Order	M_H (GeV)	s_0 (GeV^2)	M_B^2 (GeV^2)	Error from s_0 and M_B^2	Error from m_Q	Error from μ
$J_{A,4}^{\rm Dia}$	LO($\overline{\rm MS}$)	$6.04^{+0.26}_{-0.26}$	48.($\pm$10%)	3.25($\pm$10%)	$^{+0.06}_{-0.08}$	$^{+0.10}_{-0.13}$	$^{+0.23}_{-0.21}$
	NLO($\overline{\rm MS}$)	$6.65^{+0.18}_{-0.23}$	58.($\pm$10%)	4.25($\pm$10%)	$^{+0.09}_{-0.10}$	$^{+0.15}_{-0.17}$	$^{+0.01}_{-0.11}$
	LO(OS)	$7.23^{+0.24}_{-0.31}$	67.($\pm$10%)	3.25($\pm$10%)	$^{+0.04}_{-0.05}$	$^{+0.24}_{-0.31}$	
	NLO(OS)	$6.53^{+0.27}_{-0.28}$	47.($\pm$10%)	2.00($\pm$10%)	$^{+0.08}_{-0.11}$	$^{+0.26}_{-0.26}$	

TABLE V. The LO and NLO results for the mass of $J_{A,4}^{\rm Dia}$ in $\overline{\rm MS}$ and On-Shell schemes. Here the errors for M_H are from s_0, M_B, the charm quark mass, and the renormalization scale μ with $\mu = kM_B$ and $k \in (0.8, 1.2)$ (the central values correspond to $\mu = M_B$).

Current	Order	M_H (GeV)	s_0 (GeV^2)	M_B^2 (GeV^2)	Error from s_0 and M_B^2	Error from m_Q	Error from μ
$J_{T,1}^{\rm Dia}$	LO($\overline{\rm MS}$)	$6.14^{+0.25}_{-0.29}$	51($\pm$10%)	3.50($\pm$10%)	$^{+0.07}_{-0.11}$	$^{+0.07}_{-0.15}$	$^{+0.23}_{-0.22}$
	NLO($\overline{\rm MS}$)	$7.03^{+0.22}_{-0.26}$	63($\pm$10%)	5.50($\pm$10%)	$^{+0.11}_{-0.12}$	$^{+0.17}_{-0.14}$	$^{+0.08}_{-0.18}$
	LO(OS)	$7.31^{+0.25}_{-0.30}$	68($\pm$10%)	3.50($\pm$10%)	$^{+0.05}_{-0.08}$	$^{+0.24}_{-0.29}$	
	NLO(OS)	$6.56^{+0.28}_{-0.32}$	47($\pm$10%)	2.00($\pm$10%)	$^{+0.09}_{-0.15}$	$^{+0.27}_{-0.28}$	

TABLE VI. The LO and NLO results for the mass of $J_{T,1}^{\rm Dia}$ in $\overline{\rm MS}$ and On-Shell schemes. Here the errors for M_H are from s_0, M_B, the charm quark mass, and the renormalization scale μ with $\mu = kM_B$ and $k \in (0.8, 1.2)$ (the central values correspond to $\mu = M_B$).

For $J_{T,2}^{\rm Dia}$, although the $\Delta M_H^{\rm NLO} \simeq 0.7$ GeV, the μ dependence of this currents is well, as shown in Fig. [32], so we also meticulously estimate the uncertainties.

Current	Order	M_H (GeV)	s_0 (GeV^2)	M_B^2 (GeV^2)	Error from s_0 and M_B^2	Error from m_Q	Error from μ
$J_{T,2}^{\rm Dia}$	LO($\overline{\rm MS}$)	$6.15^{+0.32}_{-0.21}$	49($\pm$10%)	3.75($\pm$10%)	$^{+0.08}_{-0.10}$	$^{+0.13}_{-0.09}$	$^{+0.28}_{-0.16}$
	NLO($\overline{\rm MS}$)	$7.25^{+0.21}_{-0.35}$	67($\pm$10%)	5.75($\pm$10%)	$^{+0.10}_{-0.11}$	$^{+0.14}_{-0.17}$	$^{+0.12}_{-0.29}$
	LO(OS)	$7.32^{+0.29}_{-0.26}$	65($\pm$10%)	3.75($\pm$10%)	$^{+0.07}_{-0.13}$	$^{+0.28}_{-0.22}$	
	NLO(OS)	$6.57^{+0.30}_{-0.37}$	47($\pm$10%)	2.25($\pm$10%)	$^{+0.12}_{-0.28}$	$^{+0.27}_{-0.24}$	

TABLE VII. The LO and NLO results for the mass of $J_{T,2}^{\rm Dia}$ in $\overline{\rm MS}$ and On-Shell schemes. Here the errors for M_H are from s_0, M_B, the charm quark mass, and the renormalization scale μ with $\mu = kM_B$ and $k \in (0.8, 1.2)$ (the central values correspond to $\mu = M_B$).

Phenomenologically, it is interesting to compare our calculations with the LHCb measurements of the possible $\bar{c}c\bar{c}c$ tetraquark states in the $J/\psi J/\psi$ spectrum [5]. The most possible quantum numbers J^{PC} for the tetraquark states are 0^{++} and 2^{++}, since they can couple to $J/\psi J/\psi$ in S-wave. The predicted NLO $\overline{\rm MS}$ masses for the two operators $J_{S,3}^{\rm Dia}$ and $J_{S,4}^{\rm Dia}$ are $6.35^{+0.20}_{-0.17}$ GeV and $6.56^{+0.18}_{-0.20}$ GeV, respectively, which might account for the broad structure around $6.2 \sim 6.8$ GeV measured by the LHCb collaboration [5]. As for the narrow resonance $X(6900)$ [5], the central value of the mass is consistent with the NLO $\overline{\rm MS}$ mass for the operator $J_{S,2}^{\rm Dia}$, which gives $6.95^{+0.21}_{-0.31}$ GeV. Moreover, the predicted NLO $\overline{\text{MS}}$ mass, $7.03^{+0.22}_{-0.26}$ GeV, for the operator $J^{\text{Dia}}_{T,1}$ with $J^{PC}=2^{++}$ is also close to that of $X(6900)$, so we can not assert that the quantum number of X(6900) is 0^{++}, while 2^{++} may also be possible.

Finally, let's compare our predictions with those given in other works [23, 27, 29] within the framework of QCD sum rules. The predicted masses of the $\bar{c}c\bar{c}c$ tetraquark states are listed in table VIII. The authors of Ref. [23] adopt momentum sum rules rather than Laplace sum rules (e.g. Borel transformation) applied here. Thus, it is difficult to compare the results between theirs and ours. The Laplace sum rules were applied in Ref. [27, 29]. However, the parameters (such as the renormalization scale μ) and the scheme to determine the Borel platform in Ref. [27, 29] are different from ours. Moreover, only partial NLO contributions are considered in Ref. [27].

TABLE VIII. The mass differences of diquark-antidiquark currents obtained by different works in QCD sum rules

J^{PC}	Currents	Ours(LO)	Ours(NLO)	Ref. [23]	Ref. [27](LO)	Ref. [27](NLO)	Ref. [29]
0^{++}	$J^{\text{Di-Di}}_{\text{S},1}$	$6.07^{+0.05}_{-0.07}$	$6.60^{+0.09}_{-0.10}$	6.46 ± 0.16	6.52	6.49 ± 0.07	$6.46^{+0.13}_{-0.17}$
	$J^{\text{Di-Di}}_{\text{S},2}$	$6.19^{+0.07}_{-0.12}$	$6.90^{+0.11}_{-0.12}$	6.59 ± 0.17	6.55	6.61 ± 0.09	$6.47^{+0.12}_{-0.18}$
	$J^{\text{Di-Di}}_{\text{S},3}$	$6.96^{+0.11}_{-0.14}$	$9.25^{+0.14}_{-0.14}$	6.82 ± 0.18	7.37	7.05 ± 0.07	$6.45^{+0.14}_{-0.16}$
	$J^{\text{Di-Di}}_{\text{S},4}$	$6.17^{+0.07}_{-0.12}$	$7.36^{+0.10}_{-0.11}$	6.44 ± 0.15	6.59	6.39 ± 0.08	$6.44^{+0.15}_{-0.16}$
	$J^{\text{Di-Di}}_{\text{S},5}$	$6.07^{+0.08}_{-0.10}$	$6.69^{+0.10}_{-0.12}$	6.47 ± 0.16	-	-	-
0^{--}	$J^{\text{Di-Di}}_{\text{P},1}$	$6.55^{+0.12}_{-0.14}$	$8.43^{+0.17}_{-0.17}$	6.84 ± 0.18	-	-	-
0^{-+}	$J^{\text{Di-Di}}_{\text{P},2}$	$6.55^{+0.12}_{-0.14}$	$8.08^{+0.15}_{-0.16}$	6.40 ± 0.19	-	-	-
	$J^{\text{Di-Di}}_{\text{P},3}$	$6.54^{+0.12}_{-0.14}$	$7.51^{+0.12}_{-0.16}$	6.34 ± 0.19	-	-	-
1^{++}	$J^{\text{Di-Di}}_{\text{A},1}$	$7.00^{+0.12}_{-0.14}$	$8.84^{+0.09}_{-0.19}$	6.40 ± 0.19	-	-	-
	$J^{\text{Di-Di}}_{\text{A},2}$	$7.04^{+0.13}_{-0.15}$	$7.41^{+0.23}_{-0.30}$	6.34 ± 0.19	-	-	-
1^{+-}	$J^{\text{Di-Di}}_{\text{A},3}$	$6.95^{+0.13}_{-0.16}$	$8.81^{+0.08}_{-0.19}$	6.37 ± 0.18	-	-	-
	$J^{\text{Di-Di}}_{\text{A},4}$	$6.08^{+0.04}_{-0.10}$	$6.65^{+0.10}_{-0.13}$	6.51 ± 0.15	-	-	-
1^{--}	$J^{\text{Di-Di}}_{\text{V},1}$	$6.56^{+0.11}_{-0.13}$	$7.45^{+0.12}_{-0.14}$	6.84 ± 0.18	-	-	-
	$J^{\text{Di-Di}}_{\text{V},2}$	$6.61^{+0.12}_{-0.15}$	$7.97^{+0.10}_{-0.17}$	6.83 ± 0.18	-	-	-
1^{-+}	$J^{\text{Di-Di}}_{\text{V},3}$	$6.56^{+0.12}_{-0.15}$	$7.52^{+0.12}_{-0.14}$	6.84 ± 0.18	-	-	-
	$J^{\text{Di-Di}}_{\text{V},4}$	$6.53^{+0.11}_{-0.16}$	$8.02^{+0.08}_{-0.17}$	6.88 ± 0.18	-	-	-
2^{++}	$J^{\text{Di-Di}}_{\text{T},1}$	$6.07^{+0.08}_{-0.10}$	$6.98^{+0.09}_{-0.11}$	6.51 ± 0.15	-	-	-
	$J^{\text{Di-Di}}_{\text{T},2}$	$7.02^{+0.13}_{-0.16}$	$9.00^{+0.21}_{-0.23}$	6.37 ± 0.19	-	-	-
	$J^{\text{Di-Di}}_{\text{T},3}$	$6.15^{+0.08}_{-0.10}$	$7.25^{+0.10}_{-0.11}$	-	-	-	-

B. Numerical results and discussions for the $\bar{b}b\bar{b}b$ system

Similar to the $\bar{c}c\bar{c}c$ system, our main results for the $\bar{b}b\bar{b}b$ system are shown in Fig. 4. We set $\mu=M_B$ and choose the $\overline{\text{MS}}$ renormalization scheme, and errors of M_H include only that originated from uncertainties of s_0 and M_B^2. As references, we also plot masses of the two $\Upsilon(1S)$'s and two η_b's.

The most comprehensive results are listed in Tabs. XIX–XXVIII in Appendix C, where we include both LO and

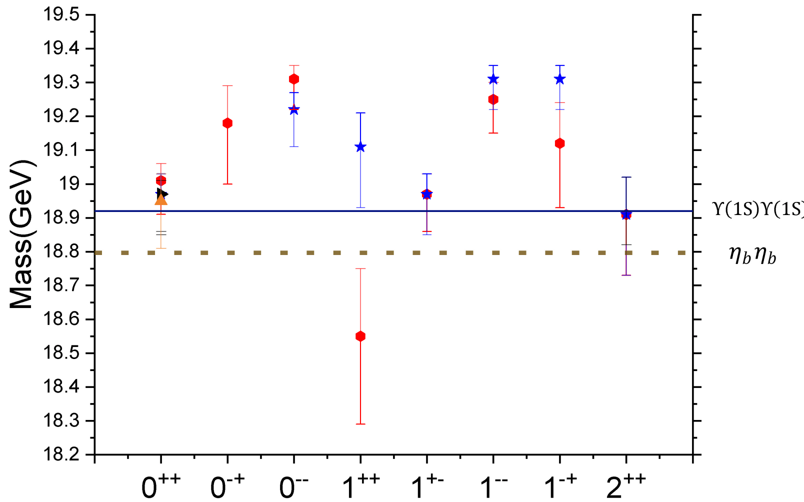

FIG. 4. The mass specturms of $\bar{b}b\bar{b}b$ system in $\overline{\text{MS}}$ scheme

NLO, both $\overline{\text{MS}}$ scheme and on-shell scheme, and all currents of meson-meson types, diquark-antidiquark types, and also diagonalized ones. Again in these tables we set $\mu = M_B$ and thus errors of M_H are due to choices of s_0 and M_B^2. Further information of s_0 and M_B^2 dependences are shown in Figs. 33–51 in Appendix C, where only results of the more reasonable diagonalized currents are shown.

From Figs. 33–51, one can see the qualities of the Borel platforms are improved evidently in most cases after considering the NLO contributions, especially for those in $\overline{\text{MS}}$ scheme. For example, in Fig. 33 (a), there is no Borel platform at LO level in $\overline{\text{MS}}$ scheme, but there is a clear and distinct platform at the NLO level. Similar phenomenon was also found in the bbb system [63]. We have checked that the $\bar{b}b$ system also has this phenomenon. This indicates that for the pure bottom system the NLO contribution is crucial to the formation of a stable Borel platform in the QCD sum rules.

Similar to the case of $\bar{c}c\bar{c}c$ system, from Tabs. XIX–XXVIII, one can see that NLO contributes non-negligible corrections, with mass corrections $|M_H^{\text{NLO}} - M_H^{\text{LO}}| \simeq$ 0.4-0.6 GeV in both $\overline{\text{MS}}$ and OS schemes. In addition, with the NLO corrections, the quark mass scheme dependence is improved significantly. The mass difference between the two schemes $|\Delta M_H| = |M_H^{\text{OS}} - M_H^{\overline{\text{MS}}}|$ is about $1.1 \sim 1.2$ GeV at LO level, while the difference is usually smaller than 0.1 GeV at NLO level except for the $J^{PC} = 1^{++}$ channel.

We choose $\mu = k\ m_B$ with $k \in (0.8, 1.2)$ to explore the renormalization scale dependence of our results, because Borel platforms can not be achieved for $k > 1.2$ even with the NLO contributions. We find that the μ dependence is improved for the NLO results comparing with the LO ones, but the μ dependences of the NLO results for the $\bar{b}b\bar{b}b$ system are more sensitive than that of the $\bar{c}c\bar{c}c$ system. Typical μ dependences at the LO and the NLO are shown in Fig. 52 and 53.

VI. SUMMARY

In this paper, we study the NLO corrections to masses of $\bar{Q}Q\bar{Q}Q$ states within QCD sum rules. As operators with the same J^{PC} can mix with each other under renormalization, we diagonalize the original operators, either in meson-meson type or diquark-antidiquark type, and use the diagonalized operators in the phenomenological study.

Numerical results show that NLO corrections are very important. On the one hand, NLO corrections to hadron masses are usually larger than 0.5 GeV in both the $\overline{\text{MS}}$ and the on-shell schemes. On the other hand, the scheme dependence tends to be reduced with the NLO corrections. More explicitly, the LO mass difference $M_H^{\text{LO-OS}} - M_H^{\text{LO-}\overline{\text{MS}}} = $ 1.1-1.3 GeV for all the operators, where the NLO corrections to $M_H^{\overline{\text{MS}}}$ are positive and those to M_H^{OS} are negtive, which results in the reduction of scheme dependence of the masses. Especially, for the $\bar{c}c\bar{c}c$ system, the NLO mass difference $M_H^{\text{NLO-OS}} - M_H^{\text{NLO-}\overline{\text{MS}}} \leq 0.5$ GeV for the operators $J_{S,2,3,4}^{\text{Dia}}$ with $J^{PC} = 0^{++}$, $J_{P,2}^{\text{Dia}}$ with $J^{PC} = 0^{-+}$, $J_{A,4}^{\text{Dia}}$ with $J^{PC} = 1^{+-}$ and $J_{T,1}^{\text{Dia}}$ with $J^{PC} = 2^{++}$, which also implies that the perturbation convergence of these operators is better than that of the others. While for the $\bar{b}b\bar{b}b$ system, the difference is usually smaller than 0.1 GeV at NLO except for the $J^{PC} = 1^{++}$ operator. We also find that NLO corrections can reduce the μ dependence.

We use currents that have good perturbative convergence in our phenomenological analysis. For the $\bar{c}c\bar{c}c$ system, we get three $J^{PC}=0^{++}$ states, with masses $6.35^{+0.20}_{-0.17}$ GeV, $6.56^{+0.18}_{-0.20}$ GeV and $6.95^{+0.21}_{-0.31}$ GeV, respectively. The first two may explain the broad structure around $6.2\sim6.8$ GeV measured by the LHCb collaboration [5], and the third one may be assigned to the observed narrow resonance $X(6900)$. For the 2^{++} states, we find one with mass $7.03^{+0.22}_{-0.26}$ GeV, which may also be a candidate to explain the $X(6900)$, and another one around 7.3 GeV, which has slightly large μ dependence.

As for the $\bar{b}b\bar{b}b$ system, we find that the NLO contribution improves the quality of the Borel platform evidently in $\overline{\rm MS}$ scheme, which is similar to the case of the bbb baryon [63]. The quark mass scheme dependence of the results are also improved significantly with the NLO contribution. However, the NLO results are still sensitive to the choice of renormalization scale μ, and we find that the Borel platforms can not be achieved for $\mu>1.2m_B$.

Finally, we would like to emphasize the importance of NLO contributions, especially in the operator mixing for multiquark systems. (i) As a key NLO contribution, the one-gluon exchange is crucial even for charmonium and bottomonium states, because it provides the color Coulomb interaction between Q and $\bar{Q}$, which is the most important short-range attractive force to form a heavy quarkonium. (ii) In the fully heavy tetraquark system discussed in this paper, if one starts from a color-singlet current-current operator, the one-gluon exchange will change it to the color-octet current-current operator, therefore leads to the operator mixing. As already shown by our result, the operator mixing induced by renormalization at NLO is inevitable and has very important consequences in the QCD sum rule calculations. (iii) In the literature some works use the color-singlet current-current local operators to describe physical hadronic molecules. However, duo to the operator mixing, the color structure of the local operators must be mixed with both color-singlet and color-octet current-current configurations. It is impossible to keep the color-singlet structure unchanged if a complete NLO QCD contribution is seriously considered. In fact, a physical molecule state means that it contains two well separated color-singlet mesons at long-distances mediated by one-meson or two-meson exchanges. And a physical molecule may not be necessarily ascribed to the color-singlet current-current local operators, which only describe the very short-distance behavior of the tetraquark and are subjected to the color configuration mixing. The description for hadronic molecules needs to understand the long-distance dynamics beyond color confinement.

ACKNOWLEDGMENTS

We thank Xiao Liu and Xin Guan for many useful and helpful discussions. We also thank Shi-Lin Zhu for helpful comments. K.T.C. thanks Cong-Feng Qiao for useful communications. The figures in this paper are drawn by using the Origin and Mathematica software. The work is supported in part by the National Natural Science Foundation of China (Grants No. 11875071, No. 11975029, No. 11745006), the National Key Research and Development Program of China under Contracts No. 2020YFA0406400, and the Deutsche Forschungsgemeinschaft (DFG, German Research Foundation) under grant 396021762 - TRR 257.

Appendix A: Operator Renormalization Matrices

1. Calculation Of Operator Renormalization Matrices

We present the calculation of operator renormalization matrices of meson-meson type operators. The operator renormalization matrices of diquark-antidiquark type operators then follows from a Fierz transformation.

A general meson-meson type operators where four quarks are different flavors, are defined as

$$\mathcal{O}_{\Gamma_1,\Gamma_2}=\left(\bar{q}_1^i\Gamma_1 q_2^j\right)\left(\bar{q}_3^k\Gamma_2 q_4^l\right)\ , \tag{A1}$$

which has two indpendent color configurations,

$$\mathcal{O}_{\Gamma_1,\Gamma_2,[1]}=\left(\bar{q}_1^i\Gamma_1 q_2^j\right)\left(\bar{q}_3^k\Gamma_2 q_4^l\right)\delta_{ij}\delta_{kl}\ , \tag{A2}$$

$$\mathcal{O}_{\Gamma_1,\Gamma_2,[2]}=\left(\bar{q}_1^i\Gamma_1 q_2^j\right)\left(\bar{q}_3^k\Gamma_2 q_4^l\right)\delta_{il}\delta_{kj}\ , \tag{A3}$$

where $\mathcal{O}_{\Gamma_1,\Gamma_2,[1]}$ is called a color-singlet operator. We can also using following relation,

$$T^a_{ij}T^a_{kl}=\frac{1}{2}\left(\delta_{il}\delta_{kj}-\frac{1}{N_c}\delta_{ij}\delta_{kl}\right)\ , \tag{A4}$$

to obtain color-octet operators,

$$\mathcal{O}_{\Gamma_1,\Gamma_2,[8]} = \left(\bar{q}_1^i \Gamma_1 T^a_{ij} q_2^j\right)\left(\bar{q}_3^k \Gamma_2 T^a_{kl} q_4^l\right) \tag{A5}$$

$$= \frac{1}{2}\left(\mathcal{O}_{\Gamma_1,\Gamma_2,[2]} - \frac{1}{N_c}\mathcal{O}_{\Gamma_1,\Gamma_2,[1]}\right) . \tag{A6}$$

For convenience, we choose $\mathcal{O}_{\Gamma_1,\Gamma_2,[1]}$ and $\mathcal{O}_{\Gamma_1,\Gamma_2,[2]}$ as bases in our calculation.

Let us first suppress the dependence of color configuration for operators. According to our operator and definition of operator renormalization matrix,

$$\mathcal{O}^B = \left(\sqrt{Z_2}\right)^4 \ \overline{\mathcal{O}}^B = Z_{\mathcal{O}}\ \mathcal{O}^R , \tag{A7}$$

where $\mathcal{O}^B = (\bar{q}_1\Gamma_1 q_2)(\bar{q}_3\Gamma_2 q_4)$ denotes the bare operator, $\overline{\mathcal{O}}^B = \left(\bar{q}_1^R\Gamma_1 q_2^R\right)\left(\bar{q}_3^R\Gamma_2 q_4^R\right)$ denotes the bare operator replaced by renormalized fields, and $\mathcal{O}^R$ denotes the renormalized operator. In our NLO calculation, we directly calculate $\overline{\mathcal{O}}^B$, and thus quark self-energy diagrams are cancelled by counter term diagrams. The remaining diagrams can be divided into three parts,

$$A = \int \frac{\mathrm{d}^D p}{(2\pi)^D}(A_1 + A_2 + A_3) , \tag{A8}$$

where A_1 denotes the contribution of gluon exchange between q_1 and q_2, A_2 denotes the contribution of gluon exchange between q_3 and q_4, and A_3 denotes others contributions e.g. contributions of gluon exchange between q_1 and q_3, q_1 and q_4 and so on. Because all infrared divergences will be cancelled, we just need to consider ultraviolet (UV) divergences therein. Therefore, the mass terms in quark propagators can be discarded. Explicitly, we have

$$A_1 = \left[ig_s\gamma_\mu \frac{i\not{p}}{p^2}\Gamma_1 \frac{i\not{p}}{p^2} ig\gamma^\mu \left(T^a\right)_{i'i}\left(T^a\right)_{jj'}\right]\left[\Gamma_2\delta_{k'k}\delta_{ll'}\right]\frac{-i}{p^2} , \tag{A9}$$

$$A_2 = \left[\Gamma_1\delta_{i'i}\delta_{jj'}\right]\left[ig\gamma_\mu \frac{i\not{p}}{p^2}\Gamma_2 \frac{i\not{p}}{p^2} ig_s\gamma^\mu \left(T^a\right)_{k'k}\left(T^a\right)_{ll'}\right]\frac{-i}{p^2} , \tag{A10}$$

$$A_3 = \left[ig_s\gamma_\mu \frac{i\not{p}}{p^2}\Gamma_1\left(T^a\right)_{i'i}\delta_{jj'} + \Gamma_1\frac{-i\not{p}}{p^2} ig_s\gamma_\mu\delta_{i'i}\left(T^a\right)_{jj'}\right]\left[ig_s\gamma^\mu\frac{-i\not{p}}{p^2}\Gamma_2\left(T^a\right)_{k'k}\delta_{ll'} + \Gamma_2\frac{i\not{p}}{p^2} ig_s\gamma^\mu\delta_{k'k}\left(T^a\right)_{ll'}\right]\frac{-i}{p^2} . \tag{A11}$$

After a simple manipulation, we get

$$A = -ig_s^2\frac{1}{D}\int\frac{\mathrm{d}^D p}{(2\pi)^D}\ \frac{1}{(p^2)^2}\ B , \tag{A12}$$

where

$$\begin{aligned} B = &\left(\gamma_\mu\gamma_\nu\Gamma_1\gamma^\nu\gamma^\mu\right)(\Gamma_2)\left(T^a\right)_{i'i}\left(T^a\right)_{jj'}\delta_{k'k}\delta_{ll'} + (\Gamma_1)\left(\gamma_\mu\gamma_v\Gamma_2\gamma^\nu\gamma^\mu\right)\delta_{i'i}\delta_{jj'}\left(T^a\right)_{k'k}\left(T^a\right)_{ll'} \\ &+ (-D)(\Gamma_1)(\Gamma_2)\left[\left(T^a\right)_{i'i}\delta_{jj'} - \delta_{i'i}\left(T^a\right)_{jj'}\right]\left[\left(T^a\right)_{k'k}\delta_{ll'} - \delta_{k'k}\left(T^a\right)_{ll'}\right] \\ &+ \frac{1}{4}\left(\{\sigma_{\mu\nu},\Gamma_1\}\right)\left(\{\sigma_{\mu\nu},\Gamma_2\}\right)\left[\left(T^a\right)_{i'i}\delta_{jj'} + \delta_{i'i}\left(T^a\right)_{jj'}\right]\left[\left(T^a\right)_{k'k}\delta_{ll'} + \delta_{k'k}\left(T^a\right)_{ll'}\right] \\ &+ \frac{1}{4}\left([\sigma_{\mu\nu},\Gamma_1]\right)\left([\sigma_{\mu\nu},\Gamma_2]\right)\left[\left(T^a\right)_{i'i}\delta_{jj'} - \delta_{i'i}\left(T^a\right)_{jj'}\right]\left[\left(T^a\right)_{k'k}\delta_{ll'} - \delta_{k'k}\left(T^a\right)_{ll'}\right] . \end{aligned} \tag{A13}$$

According to Eq. (A12), we get the UV divergences term

$$A_{UV} = -\ ig_s^2\frac{1}{4}\frac{i}{(4\pi)^2}\frac{1}{\varepsilon}B\bigg|_{D=4} = \frac{\alpha_s}{\varepsilon}\frac{B|_{D=4}}{16\pi} . \tag{A14}$$

For operators with definite color configuration $\mathcal{O}_{\Gamma_1,\Gamma_2,[c]}$, we need to multiply the corresponding color configuration ($\delta_{ij}\delta_{kl}$ or $\delta_{il}\delta_{kj}$) in Eq. (A13).

According to Eq. (A7), to use the renormalized operator we should multiply our result $M_{LO} + A_{UV} + \cdots$ by $Z_2^2 Z_{\mathcal{O}}^{-1} \approx 1 - \delta Z_{\mathcal{O}} + 2\delta Z_2$, where $M_{LO} = 1$ is the LO amplitude and $Z_2 = 1 + \delta Z_2$ and $Z_{\mathcal{O}} = 1 + \delta Z_{\mathcal{O}}$. Demanding that final results are free of UV divergences, we get

$$\delta Z_{\mathcal{O}} = A_{UV} + 2\,\delta Z_2\,, \tag{A15}$$

with

$$\delta Z_2 = -\frac{\alpha_s}{3\pi\varepsilon}\,, \tag{A16}$$

in $\overline{\text{MS}}$ scheme.

2. $J^P = 0^+$

Operator bases are defined as

$$\begin{aligned}
J^{\text{M-M}}_{S,1,[1]} &= (\bar{Q}_a\gamma^\mu Q_a)(\bar{Q}_b\gamma_\mu Q_b)\,,\\
J^{\text{M-M}}_{S,2,[1]} &= (\bar{Q}_a\gamma^\mu\gamma^5 Q_a)(\bar{Q}_b\gamma_\mu\gamma^5 Q_b)\,,\\
J^{\text{M-M}}_{S,1,[2]} &= (\bar{Q}_a\gamma^\mu Q_b)(\bar{Q}_b\gamma_\mu Q_a)\,,\\
J^{\text{M-M}}_{S,2,[2]} &= (\bar{Q}_a\gamma^\mu\gamma^5 Q_b)(\bar{Q}_b\gamma_\mu\gamma^5 Q_a)\,,\\
J^{\text{M-M}}_{S,3,[1]} &= (\bar{Q}_a Q_a)(\bar{Q}_b Q_b)\,,\\
J^{\text{M-M}}_{S,4,[1]} &= (\bar{Q}_a i\gamma^5 Q_a)(\bar{Q}_b i\gamma^5 Q_b)\,,\\
J^{\text{M-M}}_{S,5,[1]} &= (\bar{Q}_a\sigma^{\mu\nu} Q_a)(\bar{Q}_b\sigma_{\mu\nu} Q_b)\,,\\
J^{\text{M-M}}_{S,3,[2]} &= (\bar{Q}_a Q_b)(\bar{Q}_b Q_a)\,,\\
J^{\text{M-M}}_{S,4,[2]} &= (\bar{Q}_a i\gamma^5 Q_b)(\bar{Q}_b i\gamma^5 Q_a)\,,\\
J^{\text{M-M}}_{S,5,[2]} &= (\bar{Q}_a\sigma^{\mu\nu} Q_b)(\bar{Q}_b\sigma_{\mu\nu} Q_a)\,.
\end{aligned} \tag{A17}$$

The corresponding operator renormalization matrix is given by,

$$\delta Z_{O,S} = \frac{\alpha_s}{16\pi}\delta_{\overline{\text{MS}}}\begin{pmatrix}
0 & \frac{12}{N_c} & 0 & -12 & 0 & 0 & 0 & 0 & 0 & 0\\
\frac{12}{N_c} & 0 & -12 & 0 & 0 & 0 & 0 & 0 & 0 & 0\\
-6 & -6 & 6N_c & -\frac{6(N_c^2-2)}{N_c} & 0 & 0 & 0 & 0 & 0 & 0\\
-6 & -6 & -\frac{6(N_c^2-2)}{N_c} & 6N_c & 0 & 0 & 0 & 0 & 0 & 0\\
0 & 0 & 0 & 0 & \frac{12(N_c^2-1)}{N_c} & 0 & -\frac{2}{N_c} & 0 & 0 & 2\\
0 & 0 & 0 & 0 & 0 & \frac{12(N_c^2-1)}{N_c} & \frac{2}{N_c} & 0 & 0 & -2\\
0 & 0 & 0 & 0 & -\frac{48}{N_c} & \frac{48}{N_c} & -\frac{4(N_c^2-1)}{N_c} & 48 & -48 & 0\\
0 & 0 & 0 & 0 & 12 & 0 & 1 & -\frac{12}{N_c} & 0 & \frac{N_c^2-2}{N_c}\\
0 & 0 & 0 & 0 & 0 & 12 & -1 & 0 & -\frac{12}{N_c} & -\frac{N_c^2-2}{N_c}\\
0 & 0 & 0 & 0 & 24 & -24 & -12 & \frac{24(N_c^2-2)}{N_c} & -\frac{24(N_c^2-2)}{N_c} & \frac{4(2N_c^2+1)}{N_c}
\end{pmatrix}, \tag{A18}$$

where $\delta_{\overline{\text{MS}}} = \frac{1}{\epsilon} + \ln(4\pi) - \gamma_E$.

After renormalization, since there are identical particles in the operator of full heavy tetraquark system $\left(\bar{Q}\Gamma_1 Q\bar{Q}\Gamma_2 Q\right)$, 4-dimensional Fierz transformation can be used to related operators in different color configurations, which results in only 5 independent operators in $J^{PC} = 0^{++}$ channel. We can choose any 5 independent operators to perform our phenomenological study. For example, we choose $J^{\text{M-M}}_{S,i,[1]}$ in this work. According to Fierz transformation

$$J^{\text{M-M}}_{S,i,[2]} = \frac{1}{8}\begin{pmatrix} 4 & 4 & -8 & -8 & 0 \\ 4 & 4 & 8 & 8 & 0 \\ -2 & 2 & -2 & 2 & -1 \\ -2 & 2 & 2 & -2 & 1 \\ 0 & 0 & -24 & -24 & 4 \end{pmatrix} \cdot J^{\text{M-M}}_{S,i,[1]} \,, \tag{A19}$$

we can transform $J^{\text{M-M}}_{S,i,[2]}$ to $J^{\text{M-M}}_{S,i,[1]}$ to get the anomalous dimension Eq. (17),

3. $J^P = 0^-$

Operator bases for $J^P = 0^-$ are

$$\begin{aligned}
J^{\text{M-M}}_{P,1,[1]} &= (\bar{Q}_a\gamma^\mu Q_a)(\bar{Q}_b\gamma_\mu\gamma^5 Q_b)\,,\\
J^{\text{M-M}}_{P,1,[2]} &= (\bar{Q}_a\gamma^\mu Q_b)(\bar{Q}_b\gamma_\mu\gamma^5 Q_a)\,,\\
J^{\text{M-M}}_{P,2,[1]} &= (\bar{Q}_a Q_a)(\bar{Q}_b i\gamma^5 Q_b)\,,\\
J^{\text{M-M}}_{P,3,[1]} &= (\bar{Q}_a\sigma^{\mu\nu} Q_a)(\bar{Q}_b\sigma_{\mu\nu} i\gamma^5 Q_b)\,,\\
J^{\text{M-M}}_{P,2,[2]} &= (\bar{Q}_a Q_b)(\bar{Q}_b i\gamma^5 Q_a)\,,\\
J^{\text{M-M}}_{P,3,[2]} &= (\bar{Q}_a\sigma^{\mu\nu} Q_b)(\bar{Q}_b\sigma_{\mu\nu} i\gamma^5 Q_a)\,.
\end{aligned} \tag{A20}$$

The operator renormalization matrix is

$$\delta Z_{O,P} = \frac{\alpha_s}{16\pi}\delta_{\overline{\text{MS}}}\begin{pmatrix} \frac{12}{N_c} & -12 & 0 & 0 & 0 & 0 \\ -12 & \frac{12}{N_c} & 0 & 0 & 0 & 0 \\ 0 & 0 & \frac{12(N_c^2-1)}{N_c} & 0 & -\frac{2}{N_c} & 2 \\ 0 & 0 & -\frac{96}{N_c} & -\frac{4(N_c^2-24N_c-1)}{N_c} & 0 & 0 \\ 0 & 0 & 12 & \frac{4(N_c^2-4)}{N_c} & \frac{4+N_c-4N_c^2}{N_c} & \frac{N_c^2-2}{N_c} \\ 0 & 0 & 48 & \frac{48(N_c^2-2)}{N_c} & -12 & \frac{4(2N_c^2+1)}{N_c} \end{pmatrix} . \tag{A21}$$

Similay to $J^{PC} = 0^{++}$, we have the Fierz transformation

$$J^{\text{M-M}}_{P,i,[2]} = \frac{1}{8}\begin{pmatrix} 8 & 0 & 0 \\ 0 & -4 & -1 \\ 0 & -64 & 4 \end{pmatrix} \cdot J^{\text{M-M}}_{P,i,[1]}\,. \tag{A22}$$

which transforms $J^{\text{M-M}}_{P,i,[2]}$ to $J^{\text{M-M}}_{P,i,[1]}$ to get the anomalous dimension Eq. (24).

4. $J^P = 1^+$

Operator bases for $J^P = 1^+$ are

$$\begin{aligned}
J^{\text{M-M}}_{A,1,[1]} &= (\bar{Q}_a Q_a)(\bar{Q}_b\gamma^\mu\gamma^5 Q_b)\,,\\
J^{\text{M-M}}_{A,2,[1]} &= (\bar{Q}_a\sigma^{\mu\nu} i\gamma^5 Q_a)(\bar{Q}_b\gamma_\nu Q_b)\,,\\
J^{\text{M-M}}_{A,1,[2]} &= (\bar{Q}_a Q_b)(\bar{Q}_b\gamma^\mu\gamma^5 Q_a)\,,\\
J^{\text{M-M}}_{A,2,[2]} &= (\bar{Q}_a\sigma^{\mu\nu} i\gamma^5 Q_b)(\bar{Q}_b\gamma_\nu Q_a)\,,\\
J^{\text{M-M}}_{A,3,[1]} &= (\bar{Q}_a i\gamma^5 Q_a)(\bar{Q}_b\gamma^\mu Q_b)\,,\\
J^{\text{M-M}}_{A,4,[1]} &= (\bar{Q}_a\sigma^{\mu\nu} Q_a)(\bar{Q}_b\gamma_\nu\gamma^5 Q_b)\,,\\
J^{\text{M-M}}_{A,3,[2]} &= (\bar{Q}_a i\gamma^5 Q_b)(\bar{Q}_b\gamma^\mu Q_a)\,,\\
J^{\text{M-M}}_{A,4,[2]} &= (\bar{Q}_a\sigma^{\mu\nu} Q_b)(\bar{Q}_b\gamma_\nu\gamma^5 Q_a)\,.
\end{aligned} \tag{A23}$$

The operator renormalization matrix is

$$\delta Z_{O,A}=\frac{\alpha_s}{16\pi}\delta_{\overline{\rm MS}}\begin{pmatrix} \frac{6(N_c^2-1)}{N_c} & -\frac{4}{N_c} & 0 & 4 & 0 & 0 & 0 & 0\\ -\frac{12}{N_c} & -\frac{2(N_c^2-1)}{N_c} & 12 & 0 & 0 & 0 & 0 & 0\\ 6 & 2 & -\frac{6}{N_c} & \frac{2(N_c^2-2)}{N_c} & 0 & 0 & 0 & 0\\ 6 & -6 & \frac{6(N_c^2-2)}{N_c} & \frac{2(N_c^2+1)}{N_c} & 0 & 0 & 0 & 0\\ 0 & 0 & 0 & 0 & \frac{6(N_c^2-1)}{N_c} & \frac{4}{N_c} & 0 & -4\\ 0 & 0 & 0 & 0 & \frac{12}{N_c} & -\frac{2(N_c^2-1)}{N_c} & -12 & 0\\ 0 & 0 & 0 & 0 & 6 & -2 & -\frac{6}{N_c} & -\frac{2(N_c^2-2)}{N_c}\\ 0 & 0 & 0 & 0 & -6 & -6 & -\frac{6(N_c^2-2)}{N_c} & \frac{2(N_c^2+1)}{N_c} \end{pmatrix}. \tag{A24}$$

Similar to $J^{PC}=0^{++}$, the Fierz transformation

$$J^{\text{M-M}}_{A,i,[2]}=\frac{1}{2}\begin{pmatrix}-1 & -1 & 0 & 0\\ -3 & 1 & 0 & 0\\ 0 & 0 & -1 & 1\\ 0 & 0 & -3 & 1\end{pmatrix}\cdot J^{\text{M-M}}_{A,i,[1]}\,. \tag{A25}$$

transforms $J^{\text{M-M}}_{A,i,[2]}$ to $J^{\text{M-M}}_{A,i,[1]}$ and we thus get the anomalous dimension Eq. (31).

5. $J^P=1^-$

Operator bases for $J^P=1^+$ are

$$\begin{aligned} J^{\text{M-M}}_{V,1,[1]}&=(\bar{Q}_aQ_a)(\bar{Q}_b\gamma^\mu Q_b)\,,\\ J^{\text{M-M}}_{V,2,[1]}&=(\bar{Q}_a\sigma^{\mu\nu}i\gamma^5Q_a)(\bar{Q}_b\gamma_\nu\gamma^5 Q_b)\,,\\ J^{\text{M-M}}_{V,1,[2]}&=(\bar{Q}_aQ_b)(\bar{Q}_b\gamma^\mu Q_a)\,,\\ J^{\text{M-M}}_{V,2,[2]}&=(\bar{Q}_a\sigma^{\mu\nu}i\gamma^5Q_b)(\bar{Q}_b\gamma_\nu\gamma^5 Q_a)\,,\\ J^{\text{M-M}}_{V,3,[1]}&=(\bar{Q}_ai\gamma^5Q_a)(\bar{Q}_b\gamma^\mu\gamma^5 Q_b)\,,\\ J^{\text{M-M}}_{V,4,[1]}&=(\bar{Q}_a\sigma^{\mu\nu}Q_a)(\bar{Q}_b\gamma_\nu Q_b)\,,\\ J^{\text{M-M}}_{V,3,[2]}&=(\bar{Q}_ai\gamma^5Q_b)(\bar{Q}_b\gamma^\mu\gamma^5 Q_a)\,,\\ J^{\text{M-M}}_{V,4,[2]}&=(\bar{Q}_a\sigma^{\mu\nu}Q_b)(\bar{Q}_b\gamma_\nu Q_a)\,. \end{aligned} \tag{A26}$$

And the operator renormalization matrix is

$$\delta Z_{O,V}=\frac{\alpha_s}{16\pi}\delta_{\overline{\rm MS}}\begin{pmatrix} \frac{6(N_c^2-1)}{N_c} & -\frac{4}{N_c} & 0 & 4 & 0 & 0 & 0 & 0\\ -\frac{12}{N_c} & -\frac{2(N_c^2-1)}{N_c} & 12 & 0 & 0 & 0 & 0 & 0\\ 6 & 2 & -\frac{6}{N_c} & \frac{2(N_c^2-2)}{N_c} & 0 & 0 & 0 & 0\\ 6 & -6 & \frac{6(N_c^2-2)}{N_c} & \frac{2(N_c^2+1)}{N_c} & 0 & 0 & 0 & 0\\ 0 & 0 & 0 & 0 & \frac{6(N_c^2-1)}{N_c} & \frac{4}{N_c} & 0 & -4\\ 0 & 0 & 0 & 0 & \frac{12}{N_c} & -\frac{2(N_c^2-1)}{N_c} & -12 & 0\\ 0 & 0 & 0 & 0 & 6 & -2 & -\frac{6}{N_c} & -\frac{2(N_c^2-2)}{N_c}\\ 0 & 0 & 0 & 0 & -6 & -6 & -\frac{6(N_c^2-2)}{N_c} & \frac{2(N_c^2+1)}{N_c} \end{pmatrix}. \tag{A27}$$

According to Fierz transformation

$$J^{\text{M-M}}_{V,i,[2]}=\frac{1}{2}\begin{pmatrix}-1 & -1 & 0 & 0\\ -3 & 1 & 0 & 0\\ 0 & 0 & -1 & 1\\ 0 & 0 & -3 & 1\end{pmatrix}\cdot J^{\text{M-M}}_{V,i,[1]}\,, \tag{A28}$$

we can transform $J^{\text{M-M}}_{V,i,[2]}$ to $J^{\text{M-M}}_{V,i,[1]}$ to get the anomalous dimension Eq. (31).

6. $J^P = 2^+$

Operator bases for $J^P = 2^+$ are

$$\begin{aligned}
J^{\text{M-M}}_{T,1,[1]} &= (\bar{Q}_a\gamma^\mu Q_a)(\bar{Q}_b\gamma^\nu Q_b)\,, \\
J^{\text{M-M}}_{T,1,[2]} &= (\bar{Q}_a\gamma^\mu Q_b)(\bar{Q}_b\gamma^\nu Q_a)\,, \\
J^{\text{M-M}}_{T,2,[1]} &= (\bar{Q}_a\gamma^\mu\gamma^5 Q_a)(\bar{Q}_b\gamma^\nu\gamma^5 Q_b)\,, \\
J^{\text{M-M}}_{T,2,[2]} &= (\bar{Q}_a\gamma^\mu\gamma^5 Q_b)(\bar{Q}_b\gamma^\nu\gamma^5 Q_a)\,, \\
J^{\text{M-M}}_{T,3,[1]} &= (\bar{Q}_a\sigma^{\mu\alpha} Q_a)(\bar{Q}_b\sigma^{\nu\alpha} Q_b)\,, \\
J^{\text{M-M}}_{T,3,[2]} &= (\bar{Q}_a\sigma^{\mu\alpha} Q_b)(\bar{Q}_b\sigma^{\nu\alpha} Q_a)\,.
\end{aligned} \tag{A29}$$

And the operator renormalization matrix is

$$\delta Z_{O,T} = \frac{\alpha_s}{16\pi}\delta_{\overline{\text{MS}}}\begin{pmatrix} 0 & 0 & -\frac{4}{N_c} & 4 & 0 & 0 \\ 2 & -2N_c & 2 & \frac{2(N_c^2-2)}{N_c} & 0 & 0 \\ -\frac{4}{N_c} & 4 & 0 & 0 & 0 & 0 \\ 2 & \frac{2(N_c^2-2)}{N_c} & 2 & -2N_c & 0 & 0 \\ 0 & 0 & 0 & 0- & \frac{4(N_c^2-1)}{N_c} & 0 \\ 0 & 0 & 0 & 0 & -4 & \frac{4}{N_c} \end{pmatrix}. \tag{A30}$$

According to Fierz transformation

$$J^{\text{M-M}}_{T,i,[2]} = -\frac{1}{2}\begin{pmatrix} 1 & 1 & -1 \\ 1 & 1 & 1 \\ -2 & 2 & 0 \end{pmatrix} \cdot J^{\text{M-M}}_{T,i,[1]}\,, \tag{A31}$$

we can transform $J^{\text{M-M}}_{T,i,[2]}$ to $J^{\text{M-M}}_{T,i,[1]}$ to get the anomalous dimension Eq. (43).

Appendix B: Details for charm system

1. Numerical Results for $J^P = 0^+$ states

TABLE IX. The LO and NLO Results for $J^P = 0^+$ with $\bar{c}c\bar{c}c$ system in the $\overline{\text{MS}}$ scheme

Current	LO			*	NLO($\overline{\text{MS}}$)		
	M_H (GeV)	s_0 (GeV^2)	M_B^2 (GeV^2)	*	M_H (GeV)	s_0 (GeV^2)	M_B^2 (GeV^2)
$J_{S,1}^{\text{M-M}}$	$6.16^{+0.08}_{-0.10}$	49.(±10%)	3.75(±10%)	*	$7.32^{+0.09}_{-0.11}$	69.(±10%)	6.00(±10%)
$J_{S,2}^{\text{M-M}}$	$6.38^{+0.09}_{-0.15}$	53.(±10%)	3.75(±10%)	*	$8.33^{+0.13}_{-0.15}$	87.(±10%)	8.00(±10%)
$J_{S,3}^{\text{M-M}}$	$7.11^{+0.13}_{-0.15}$	65.(±10%)	5.50(±10%)	*	$7.91^{+0.16}_{-0.19}$	79.(±10%)	7.50(±10%)
$J_{S,4}^{\text{M-M}}$	$5.90^{+0.06}_{-0.08}$	45.(±10%)	3.00(±10%)	*	$6.36^{+0.06}_{-0.10}$	53.(±10%)	3.50(±10%)
$J_{S,5}^{\text{M-M}}$	$6.28^{+0.13}_{-0.17}$	51.(±10%)	4.00(±10%)	*	$7.78^{+0.13}_{-0.13}$	77.(±10%)	6.75(±10%)
$J_{S,1}^{\text{Di-Di}}$	$6.07^{+0.05}_{-0.07}$	49.(±10%)	3.25(±10%)	*	$6.60^{+0.09}_{-0.10}$	57.(±10%)	4.00(±10%)
$J_{S,2}^{\text{Di-Di}}$	$6.19^{+0.07}_{-0.12}$	51.(±10%)	3.25(±10%)	*	$6.90^{+0.11}_{-0.12}$	61.(±10%)	4.75(±10%)
$J_{S,3}^{\text{Di-Di}}$	$6.96^{+0.11}_{-0.14}$	63.(±10%)	4.75(±10%)	*	$9.25^{+0.14}_{-0.14}$	105.(±10%)	10.00(±10%)
$J_{S,4}^{\text{Di-Di}}$	$6.17^{+0.07}_{-0.12}$	51.(±10%)	3.50(±10%)	*	$7.36^{+0.10}_{-0.11}$	69.(±10%)	6.25(±10%)
$J_{S,5}^{\text{Di-Di}}$	$6.07^{+0.08}_{-0.10}$	47.(±10%)	3.50(±10%)	*	$6.69^{+0.10}_{-0.12}$	57.(±10%)	4.25(±10%)
$J_{S,1}^{\text{Dia}}$	$6.18^{+0.08}_{-0.10}$	49.(±10%)	3.75(±10%)	*	$7.81^{+0.14}_{-0.16}$	77.(±10%)	7.25(±10%)
$J_{S,2}^{\text{Dia}}$	$6.19^{+0.07}_{-0.12}$	51.(±10%)	3.50(±10%)	*	$6.95^{+0.10}_{-0.12}$	61.(±10%)	5.00(±10%)
$J_{S,3}^{\text{Dia}}$	$5.93^{+0.07}_{-0.10}$	45.(±10%)	3.00(±10%)	*	$6.35^{+0.08}_{-0.13}$	51.(±10%)	3.50(±10%)
$J_{S,4}^{\text{Dia}}$	$6.02^{+0.05}_{-0.06}$	49.(±10%)	3.00(±10%)	*	$6.56^{+0.10}_{-0.12}$	55.(±10%)	4.00(±10%)
$J_{S,5}^{\text{Dia}}$	$6.33^{+0.12}_{-0.14}$	53.(±10%)	4.00(±10%)	*	$7.72^{+0.13}_{-0.14}$	75.(±10%)	6.50(±10%)

TABLE X. The LO and NLO Results for $J^P = 0^+$ with $\bar{c}c\bar{c}c$ system in the On-Shell scheme

Current	LO			*	NLO(OS)		
	M_H (GeV)	s_0 (GeV^2)	M_B^2 (GeV^2)	*	M_H (GeV)	s_0 (GeV^2)	M_B^2 (GeV^2)
$J_{S,1}^{\text{M-M}}$	$7.35^{+0.07}_{-0.10}$	66.(±10%)	3.75(±10%)	*	$6.60^{+0.09}_{-0.12}$	48.(±10%)	2.25(±10%)
$J_{S,2}^{\text{M-M}}$	$7.44^{+0.12}_{-0.15}$	66.(±10%)	4.00(±10%)	*	$6.60^{+0.10}_{-0.15}$	48.(±10%)	2.25(±10%)
$J_{S,3}^{\text{M-M}}$	$8.43^{+0.14}_{-0.18}$	86.(±10%)	6.00(±10%)	*	$7.40^{+0.15}_{-0.21}$	62.(±10%)	3.75(±10%)
$J_{S,4}^{\text{M-M}}$	$7.05^{+0.06}_{-0.09}$	60.(±10%)	3.00(±10%)	*	$6.44^{+0.08}_{-0.09}$	44.(±10%)	1.75(±10%)
$J_{S,5}^{\text{M-M}}$	$7.45^{+0.10}_{-0.11}$	68.(±10%)	4.00(±10%)	*	$6.62^{+0.09}_{-0.13}$	48.(±10%)	2.25(±10%)
$J_{S,1}^{\text{Di-Di}}$	$7.23^{+0.04}_{-0.07}$	66.(±10%)	3.25(±10%)	*	$6.54^{+0.06}_{-0.08}$	48.(±10%)	1.75(±10%)
$J_{S,2}^{\text{Di-Di}}$	$7.27^{+0.08}_{-0.11}$	64.(±10%)	3.50(±10%)	*	$6.52^{+0.10}_{-0.14}$	46.(±10%)	2.00(±10%)
$J_{S,3}^{\text{Di-Di}}$	$8.17^{+0.15}_{-0.19}$	80.(±10%)	5.25(±10%)	*	$7.19^{+0.16}_{-0.26}$	58.(±10%)	3.25(±10%)
$J_{S,4}^{\text{Di-Di}}$	$7.31^{+0.08}_{-0.11}$	64.(±10%)	3.75(±10%)	*	$6.59^{+0.09}_{-0.12}$	48.(±10%)	2.25(±10%)
$J_{S,5}^{\text{Di-Di}}$	$7.22^{+0.08}_{-0.12}$	62.(±10%)	3.50(±10%)	*	$6.51^{+0.09}_{-0.13}$	46.(±10%)	2.00(±10%)
$J_{S,1}^{\text{Dia}}$	$7.36^{+0.07}_{-0.10}$	66.(±10%)	3.75(±10%)	*	$6.60^{+0.09}_{-0.12}$	48.(±10%)	2.25(±10%)
$J_{S,2}^{\text{Dia}}$	$7.31^{+0.08}_{-0.12}$	64.(±10%)	3.75(±10%)	*	$6.58^{+0.08}_{-0.11}$	48.(±10%)	2.00(±10%)
$J_{S,3}^{\text{Dia}}$	$7.06^{+0.07}_{-0.10}$	60.(±10%)	3.00(±10%)	*	$6.47^{+0.08}_{-0.10}$	46.(±10%)	1.75(±10%)
$J_{S,4}^{\text{Dia}}$	$7.16^{+0.04}_{-0.05}$	66.(±10%)	3.00(±10%)	*	$6.49^{+0.07}_{-0.10}$	46.(±10%)	1.75(±10%)
$J_{S,5}^{\text{Dia}}$	$7.44^{+0.12}_{-0.14}$	66.(±10%)	4.25(±10%)	*	$6.62^{+0.09}_{-0.13}$	48.(±10%)	2.25(±10%)

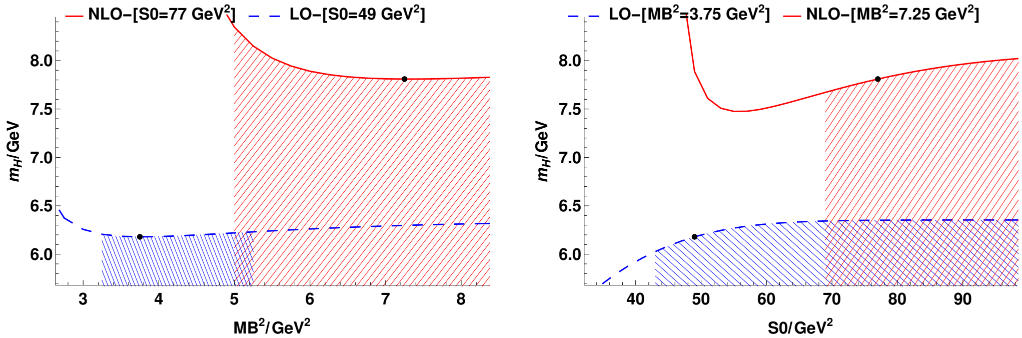

(a)$\overline{\mathrm{MS}}$

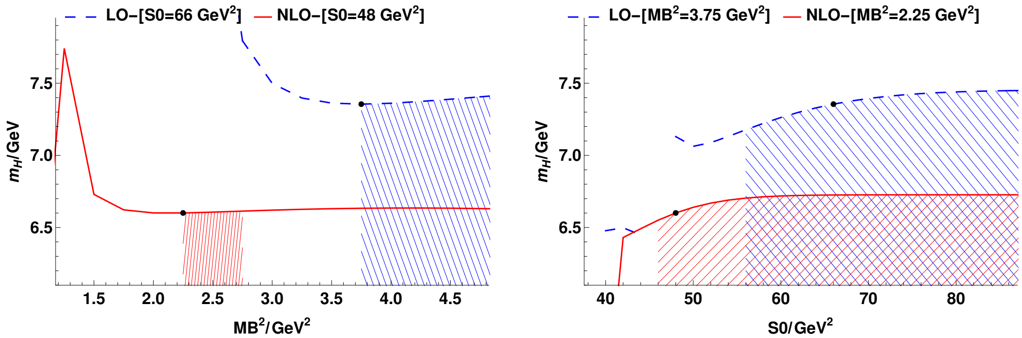

(b)OS

FIG. 5. The Borel platform curves for $J_{S,1}^{\mathrm{Dia}}$ in the $\overline{\mathrm{MS}}$ and On-Shell schemes

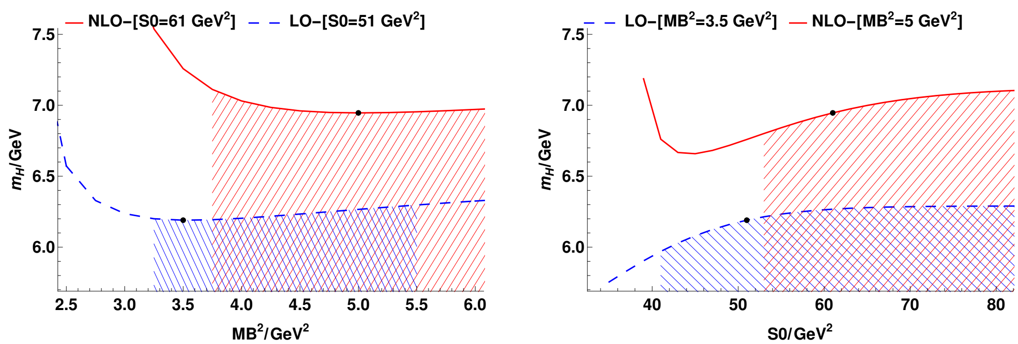

(a)$\overline{\mathrm{MS}}$

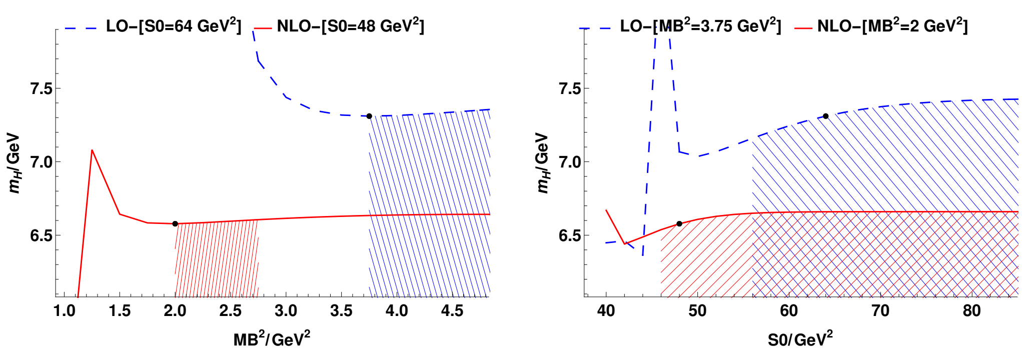

(b)OS

FIG. 6. The Borel platform curves for $J_{S,2}^{\mathrm{Dia}}$ in the $\overline{\mathrm{MS}}$ and On-Shell schemes

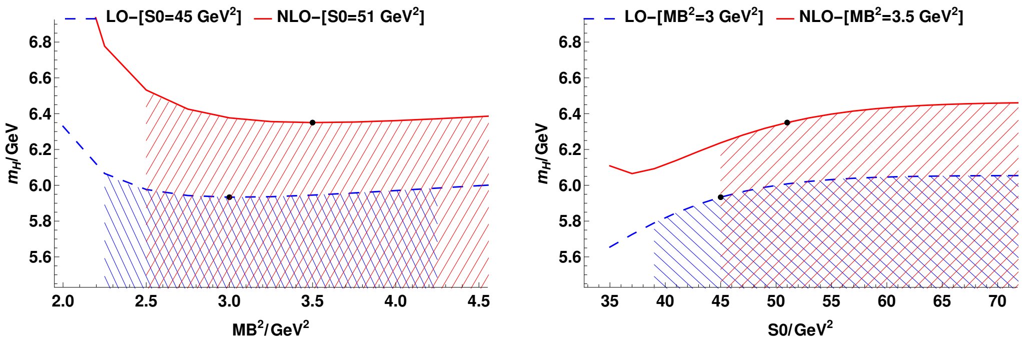

(a)$\overline{\text{MS}}$

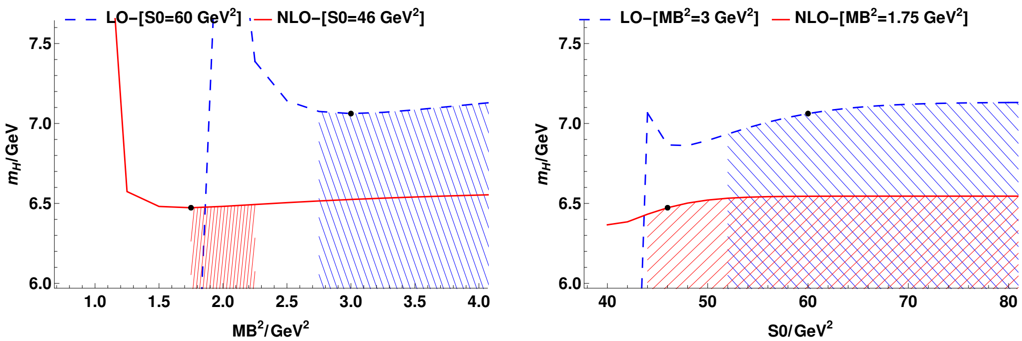

(b)OS

FIG. 7. The Borel platform curves for $J_{S,3}^{\text{Dia}}$ in the $\overline{\text{MS}}$ and On-Shell schemes

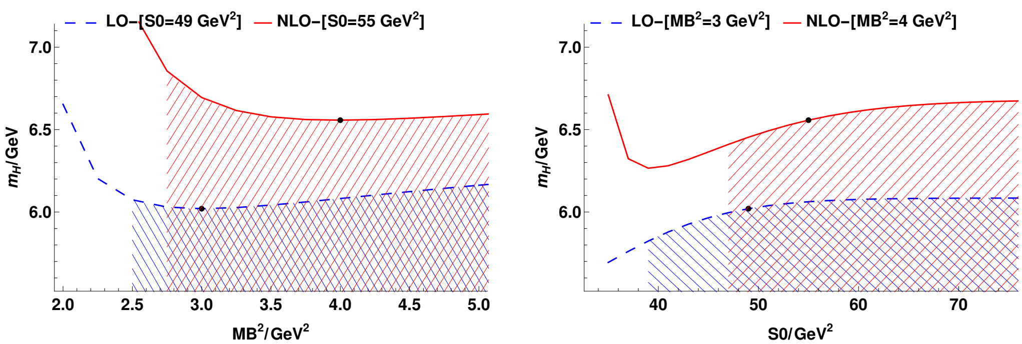

(a)$\overline{\text{MS}}$

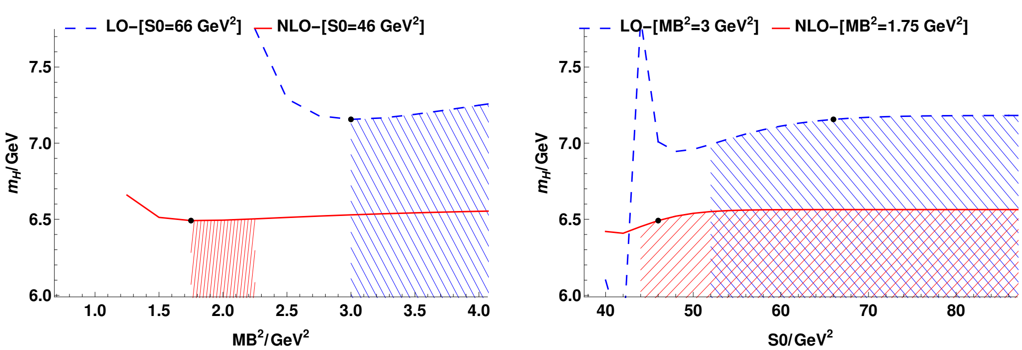

(b)OS

FIG. 8. The Borel platform curves for $J_{S,4}^{\text{Dia}}$ in the $\overline{\text{MS}}$ and On-Shell schemes

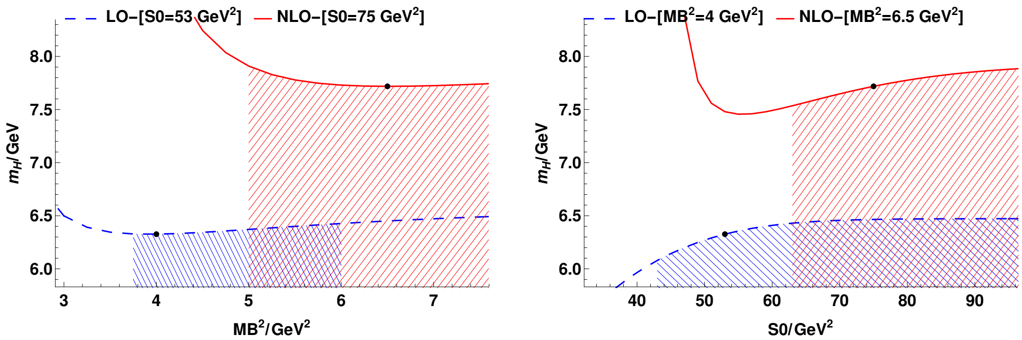

(a)$\overline{\text{MS}}$

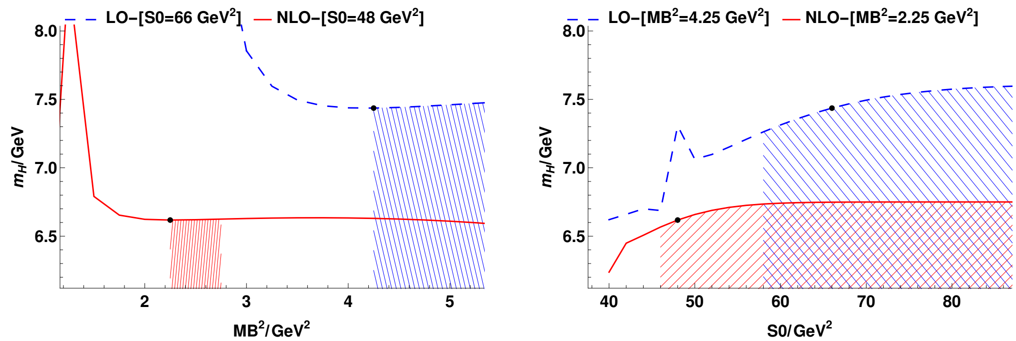

(b)OS

FIG. 9. The Borel platform curves for $J_{S,5}^{\text{Dia}}$ in the $\overline{\text{MS}}$ and On-Shell schemes

2. Numerical Results for $J^P = 0^-$ states

TABLE XI. The LO and NLO Results for $J^P = 0^-$ with $\bar{c}c\bar{c}c$ system in the $\overline{\text{MS}}$ scheme

Current	LO			*	NLO($\overline{\text{MS}}$)		
	M_H (GeV)	s_0 (GeV^2)	M_B^2 (GeV^2)	*	M_H (GeV)	s_0 (GeV^2)	M_B^2 (GeV^2)
$J_{P,1}^{\text{M-M}}$	$6.55^{+0.12}_{-0.14}$	56.(±10%)	4.25(±10%)	*	$8.43^{+0.17}_{-0.17}$	88.(±10%)	9.50(±10%)
$J_{P,2}^{\text{M-M}}$	$6.53^{+0.12}_{-0.14}$	56.(±10%)	4.25(±10%)	*	$7.30^{+0.11}_{-0.13}$	68.(±10%)	6.00(±10%)
$J_{P,3}^{\text{M-M}}$	$6.56^{+0.12}_{-0.15}$	56.(±10%)	4.25(±10%)	*	$8.53^{+0.15}_{-0.19}$	90.(±10%)	9.00(±10%)
$J_{P,1}^{\text{Di-Di}}$	$6.55^{+0.12}_{-0.14}$	56.(±10%)	4.25(±10%)	*	$8.43^{+0.17}_{-0.17}$	88.(±10%)	9.50(±10%)
$J_{P,2}^{\text{Di-Di}}$	$6.55^{+0.12}_{-0.14}$	56.(±10%)	4.25(±10%)	*	$8.08^{+0.15}_{-0.16}$	82.(±10%)	8.00(±10%)
$J_{P,3}^{\text{Di-Di}}$	$6.54^{+0.12}_{-0.14}$	56.(±10%)	4.25(±10%)	*	$7.51^{+0.12}_{-0.16}$	72.(±10%)	6.25(±10%)
$J_{P,1}^{\text{Dia}}$	$6.55^{+0.12}_{-0.14}$	56.(±10%)	4.25(±10%)	*	$8.43^{+0.17}_{-0.17}$	88.(±10%)	9.50(±10%)
$J_{P,2}^{\text{Dia}}$	$6.53^{+0.12}_{-0.14}$	56.(±10%)	4.25(±10%)	*	$7.30^{+0.11}_{-0.13}$	68.(±10%)	6.00(±10%)
$J_{P,3}^{\text{Dia}}$	$6.56^{+0.12}_{-0.15}$	56.(±10%)	4.25(±10%)	*	$8.59^{+0.15}_{-0.18}$	92.(±10%)	9.00(±10%)

TABLE XII. The LO and NLO Results for $J^P=0^-$ with $\bar{c}c\bar{c}c$ system in the On-Shell scheme

Current	LO			*	NLO(OS)		
	M_H (GeV)	s_0 (GeV^2)	M_B^2 (GeV^2)	*	M_H (GeV)	s_0 (GeV^2)	M_B^2 (GeV^2)
$J_{P,1}^{\text{M-M}}$	$7.74^{+0.14}_{-0.18}$	72.(±10%)	4.50(±10%)	*	$6.87^{+0.15}_{-0.27}$	52.(±10%)	2.75(±10%)
$J_{P,2}^{\text{M-M}}$	$7.79^{+0.10}_{-0.15}$	74.(±10%)	4.50(±10%)	*	$6.89^{+0.14}_{-0.23}$	52.(±10%)	2.75(±10%)
$J_{P,3}^{\text{M-M}}$	$7.70^{+0.12}_{-0.21}$	70.(±10%)	4.50(±10%)	*	$6.84^{+0.13}_{-0.23}$	52.(±10%)	2.50(±10%)
$J_{P,1}^{\text{Di-Di}}$	$7.74^{+0.14}_{-0.18}$	72.(±10%)	4.50(±10%)	*	$6.87^{+0.15}_{-0.27}$	52.(±10%)	2.75(±10%)
$J_{P,2}^{\text{Di-Di}}$	$7.74^{+0.14}_{-0.18}$	72.(±10%)	4.50(±10%)	*	$6.86^{+0.15}_{-0.26}$	52.(±10%)	2.75(±10%)
$J_{P,3}^{\text{Di-Di}}$	$7.75^{+0.13}_{-0.18}$	72.(±10%)	4.50(±10%)	*	$6.87^{+0.14}_{-0.25}$	52.(±10%)	2.75(±10%)
$J_{P,1}^{\text{Dia}}$	$7.74^{+0.14}_{-0.18}$	72.(±10%)	4.50(±10%)	*	$6.87^{+0.15}_{-0.27}$	52.(±10%)	2.75(±10%)
$J_{P,2}^{\text{Dia}}$	$7.79^{+0.10}_{-0.15}$	74.(±10%)	4.50(±10%)	*	$6.89^{+0.14}_{-0.23}$	52.(±10%)	2.75(±10%)
$J_{P,3}^{\text{Dia}}$	$7.70^{+0.12}_{-0.21}$	70.(±10%)	4.50(±10%)	*	$6.84^{+0.13}_{-0.23}$	52.(±10%)	2.50(±10%)

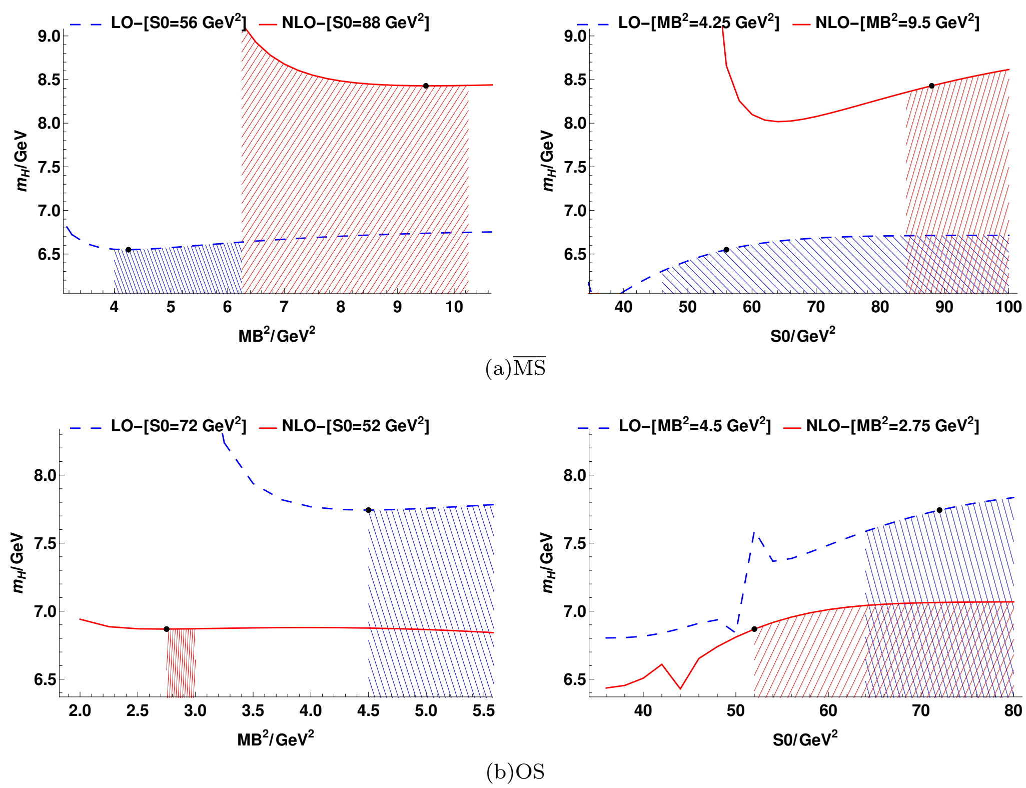

FIG. 10. The Borel platform curves for $J_{P,1}^{\text{Dia}}$ in the $\overline{\text{MS}}$ and On-Shell schemes

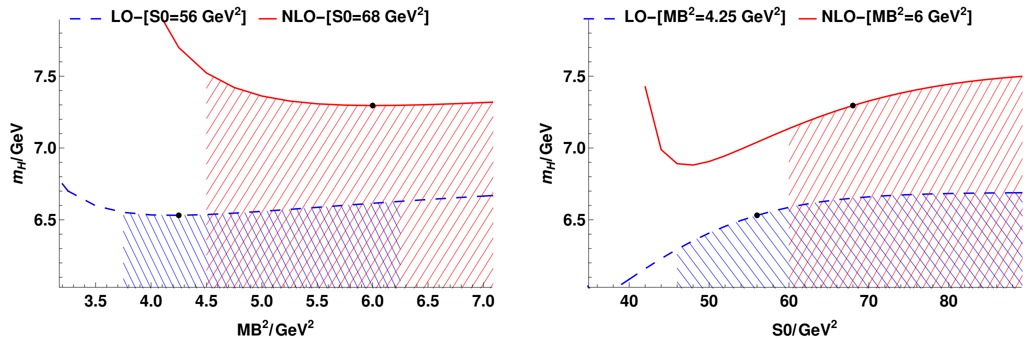

(a)$\overline{\text{MS}}$

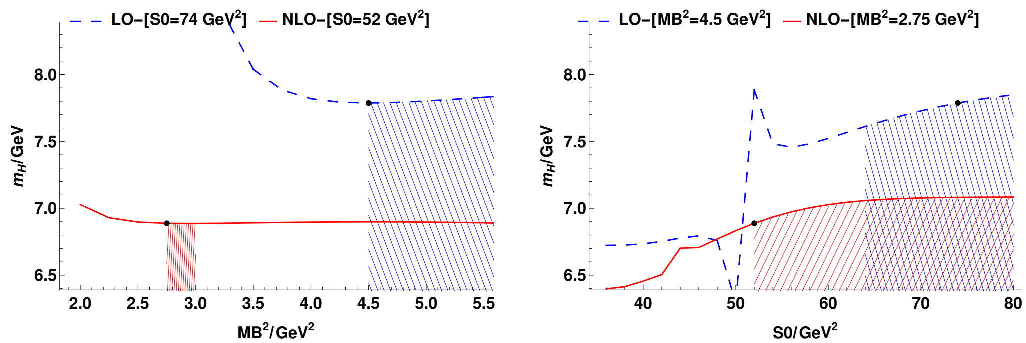

(b)OS

FIG. 11. The Borel platform curves for $J^{\text{Dia}}_{P,2}$ in the $\overline{\text{MS}}$ and On-Shell schemes

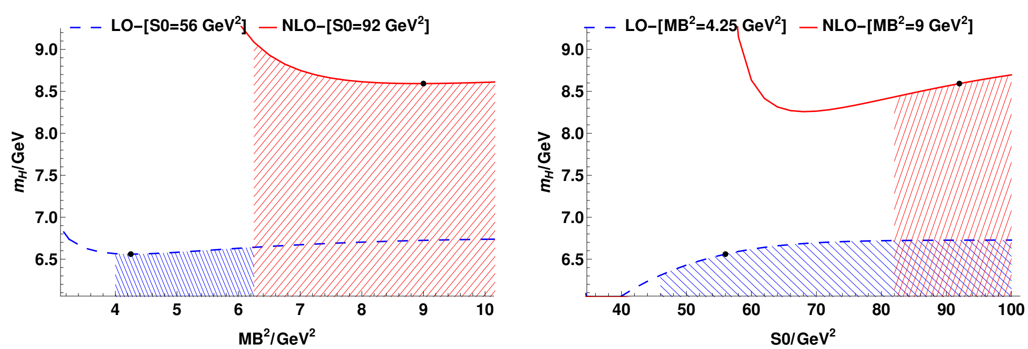

(a)$\overline{\text{MS}}$

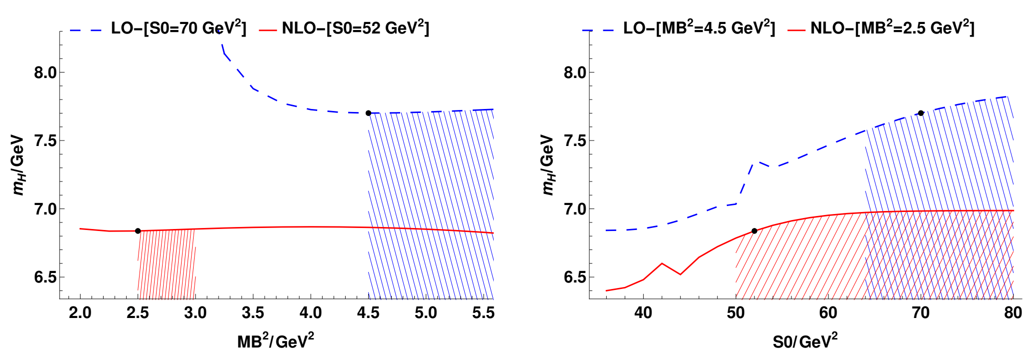

(b)OS

FIG. 12. The Borel platform curves for $J^{\text{Dia}}_{P,3}$ in the $\overline{\text{MS}}$ and On-Shell schemes

3. Numerical Results for $J^P = 1^+$ states

TABLE XIII. The LO and NLO Results for $J^P = 1^+$ with $\bar{c}c\bar{c}c$ system in the $\overline{\text{MS}}$ scheme

Current	LO			*	NLO($\overline{\text{MS}}$)		
	M_H (GeV)	s_0 (GeV^2)	M_B^2 (GeV^2)	*	M_H (GeV)	s_0 (GeV^2)	M_B^2 (GeV^2)
$J_{A,1}^{\text{M-M}}$	$7.07^{+0.14}_{-0.16}$	64.(±10%)	5.50(±10%)	*	$8.32^{+0.18}_{-0.20}$	86.(±10%)	9.00(±10%)
$J_{A,2}^{\text{M-M}}$	$6.93^{+0.12}_{-0.15}$	62.(±10%)	4.75(±10%)	*	$7.59^{+0.10}_{-0.06}$	62.(±10%)	5.50(±10%)
$J_{A,3}^{\text{M-M}}$	$6.04^{+0.06}_{-0.08}$	48.(±10%)	3.25(±10%)	*	$6.65^{+0.09}_{-0.10}$	58.(±10%)	4.25(±10%)
$J_{A,4}^{\text{M-M}}$	$6.38^{+0.08}_{-0.13}$	54.(±10%)	3.75(±10%)	*	$7.73^{+0.10}_{-0.12}$	76.(±10%)	6.00(±10%)
$J_{A,1}^{\text{Di-Di}}$	$7.00^{+0.12}_{-0.14}$	64.(±10%)	5.00(±10%)	*	$8.84^{+0.09}_{-0.19}$	96.(±10%)	10.00(±10%)
$J_{A,2}^{\text{Di-Di}}$	$7.04^{+0.13}_{-0.15}$	64.(±10%)	5.25(±10%)	*	$7.41^{+0.23}_{-0.30}$	70.(±10%)	7.75(±10%)
$J_{A,3}^{\text{Di-Di}}$	$6.95^{+0.13}_{-0.16}$	62.(±10%)	5.00(±10%)	*	$8.81^{+0.08}_{-0.19}$	96.(±10%)	10.00(±10%)
$J_{A,4}^{\text{Di-Di}}$	$6.08^{+0.04}_{-0.10}$	50.(±10%)	3.25(±10%)	*	$6.65^{+0.10}_{-0.13}$	56.(±10%)	4.50(±10%)
$J_{A,1}^{\text{Dia}}$	$6.92^{+0.12}_{-0.15}$	62.(±10%)	4.75(±10%)	*	$7.49^{+0.23}_{-0.31}$	70.(±10%)	7.50(±10%)
$J_{A,2}^{\text{Dia}}$	$7.08^{+0.13}_{-0.16}$	64.(±10%)	5.50(±10%)	*	$8.22^{+0.17}_{-0.19}$	84.(±10%)	8.50(±10%)
$J_{A,3}^{\text{Dia}}$	$6.21^{+0.07}_{-0.11}$	52.(±10%)	3.50(±10%)	*	$7.07^{+0.09}_{-0.10}$	64.(±10%)	5.00(±10%)
$J_{A,4}^{\text{Dia}}$	$6.04^{+0.06}_{-0.08}$	48.(±10%)	3.25(±10%)	*	$6.65^{+0.09}_{-0.10}$	58.(±10%)	4.25(±10%)

TABLE XIV. The LO and NLO Results for $J^P = 1^+$ with $\bar{c}c\bar{c}c$ system in the On-Shell scheme

Current	LO			*	NLO(OS)		
	M_H (GeV)	s_0 (GeV^2)	M_B^2 (GeV^2)	*	M_H (GeV)	s_0 (GeV^2)	M_B^2 (GeV^2)
$J_{A,1}^{\text{M-M}}$	$8.38^{+0.08}_{-0.18}$	85.(±10%)	5.75(±10%)	*	$7.35^{+0.14}_{-0.21}$	61.(±10%)	3.50(±10%)
$J_{A,2}^{\text{M-M}}$	$8.10^{+0.17}_{-0.23}$	77.(±10%)	5.25(±10%)	*	$6.74^{+0.21}_{-0.56}$	51.(±10%)	2.75(±10%)
$J_{A,3}^{\text{M-M}}$	$7.22^{+0.04}_{-0.05}$	67.(±10%)	3.25(±10%)	*	$6.53^{+0.08}_{-0.11}$	47.(±10%)	2.00(±10%)
$J_{A,4}^{\text{M-M}}$	$7.46^{+0.11}_{-0.13}$	67.(±10%)	4.00(±10%)	*	$6.58^{+0.11}_{-0.17}$	47.(±10%)	2.25(±10%)
$J_{A,1}^{\text{Di-Di}}$	$8.18^{+0.17}_{-0.22}$	79.(±10%)	5.50(±10%)	*	$7.23^{+0.14}_{-0.23}$	59.(±10%)	3.25(±10%)
$J_{A,2}^{\text{Di-Di}}$	$8.27^{+0.16}_{-0.21}$	81.(±10%)	5.75(±10%)	*	$6.63^{+0.16}_{-0.28}$	49.(±10%)	2.50(±10%)
$J_{A,3}^{\text{Di-Di}}$	$8.21^{+0.14}_{-0.18}$	81.(±10%)	5.25(±10%)	*	$7.23^{+0.15}_{-0.23}$	59.(±10%)	3.25(±10%)
$J_{A,4}^{\text{Di-Di}}$	$7.22^{+0.07}_{-0.10}$	63.(±10%)	3.50(±10%)	*	$6.54^{+0.08}_{-0.11}$	47.(±10%)	2.00(±10%)
$J_{A,1}^{\text{Dia}}$	$8.09^{+0.17}_{-0.23}$	77.(±10%)	5.25(±10%)	*	$6.62^{+0.16}_{-0.24}$	49.(±10%)	2.50(±10%)
$J_{A,2}^{\text{Dia}}$	$8.39^{+0.08}_{-0.18}$	85.(±10%)	5.75(±10%)	*	$7.25^{+0.16}_{-0.27}$	59.(±10%)	3.50(±10%)
$J_{A,3}^{\text{Dia}}$	$7.33^{+0.08}_{-0.11}$	65.(±10%)	3.75(±10%)	*	$6.56^{+0.08}_{-0.12}$	47.(±10%)	2.00(±10%)
$J_{A,4}^{\text{Dia}}$	$7.23^{+0.04}_{-0.05}$	67.(±10%)	3.25(±10%)	*	$6.53^{+0.08}_{-0.11}$	47.(±10%)	2.00(±10%)

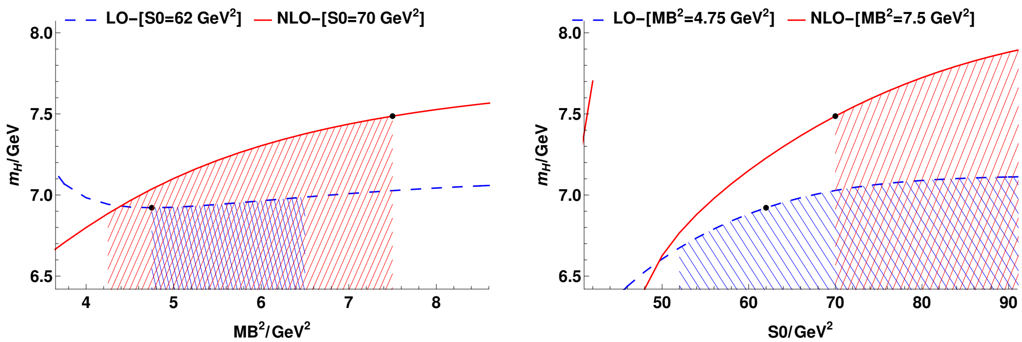

(a)$\overline{\text{MS}}$

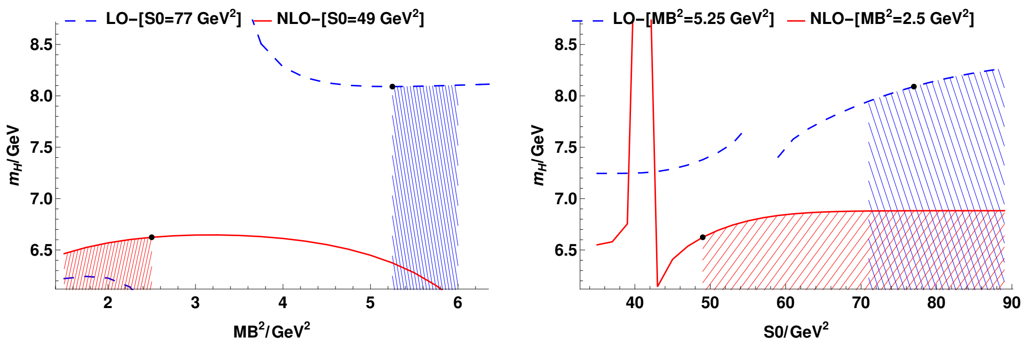

(b)OS

FIG. 13. The Borel platform curves for $J_{A,1}^{\text{Dia}}$ in the $\overline{\text{MS}}$ and On-Shell schemes

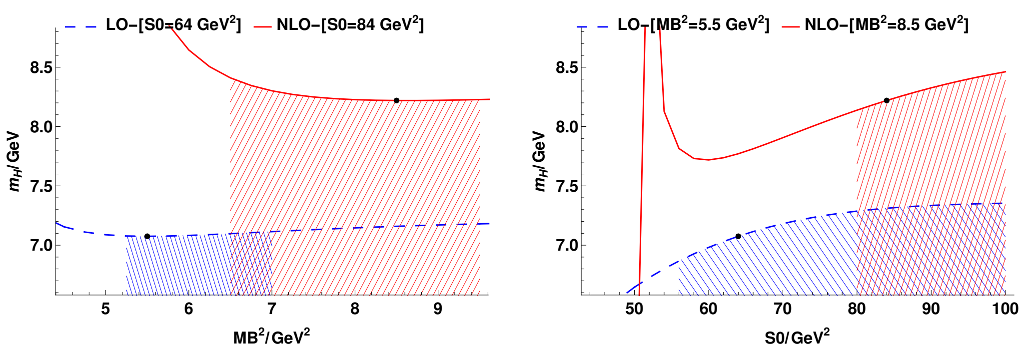

(a)$\overline{\text{MS}}$

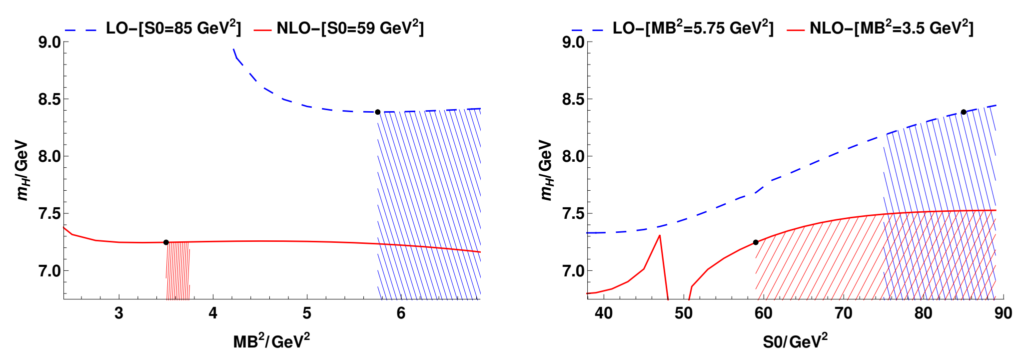

(b)OS

FIG. 14. The Borel platform curves for $J_{A,2}^{\text{Dia}}$ in the $\overline{\text{MS}}$ and On-Shell schemes

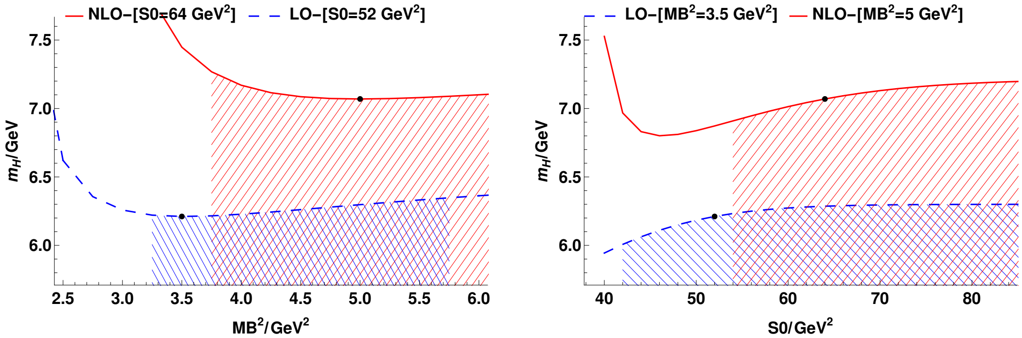

(a)$\overline{\text{MS}}$

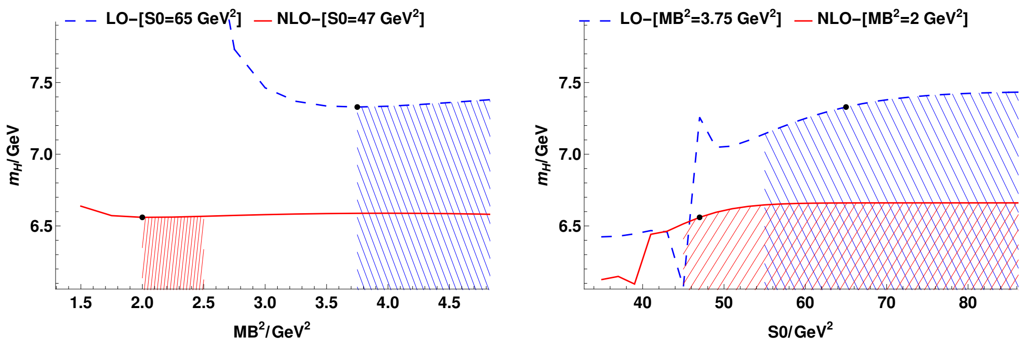

(b)OS

FIG. 15. The Borel platform curves for $J_{A,3}^{\text{Dia}}$ in the $\overline{\text{MS}}$ and On-Shell schemes

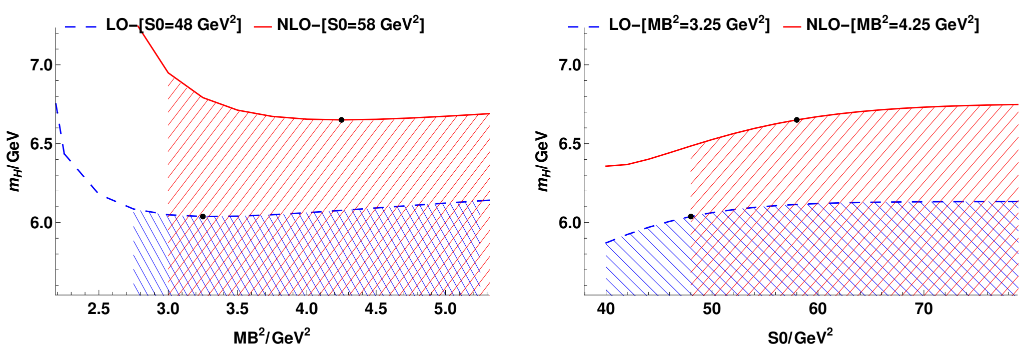

(a)$\overline{\text{MS}}$

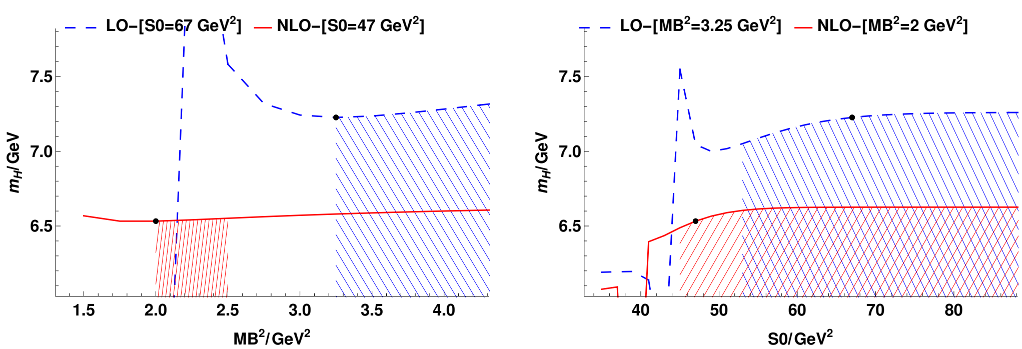

(b)OS

FIG. 16. The Borel platform curves for $J_{A,4}^{\text{Dia}}$ in the $\overline{\text{MS}}$ and On-Shell schemes

4. Numerical Results for $J^P = 1^-$ states

TABLE XV. The LO and NLO Results for $J^P = 1^-$ with $\bar{c}c\bar{c}c$ system in the $\overline{\text{MS}}$ scheme

Current	LO			*	NLO($\overline{\text{MS}}$)		
	M_H (GeV)	s_0 (GeV^2)	M_B^2 (GeV^2)	*	M_H (GeV)	s_0 (GeV^2)	M_B^2 (GeV^2)
$J_{V,1}^{\text{M-M}}$	$6.61^{+0.12}_{-0.14}$	57.(±10%)	4.50(±10%)	*	$7.55^{+0.14}_{-0.15}$	73.(±10%)	6.75(±10%)
$J_{V,2}^{\text{M-M}}$	$6.55^{+0.11}_{-0.17}$	55.(±10%)	4.50(±10%)	*	$7.98^{+0.10}_{-0.16}$	80.(±10%)	7.75(±10%)
$J_{V,3}^{\text{M-M}}$	$6.59^{+0.11}_{-0.14}$	57.(±10%)	4.25(±10%)	*	$7.57^{+0.13}_{-0.15}$	73.(±10%)	6.50(±10%)
$J_{V,4}^{\text{M-M}}$	$6.53^{+0.11}_{-0.14}$	56.(±10%)	4.00(±10%)	*	$8.09^{+0.06}_{-0.16}$	82.(±10%)	7.75(±10%)
$J_{V,1}^{\text{Di-Di}}$	$6.56^{+0.11}_{-0.13}$	57.(±10%)	4.25(±10%)	*	$7.45^{+0.12}_{-0.14}$	71.(±10%)	6.25(±10%)
$J_{V,2}^{\text{Di-Di}}$	$6.61^{+0.12}_{-0.15}$	57.(±10%)	4.50(±10%)	*	$7.97^{+0.10}_{-0.17}$	80.(±10%)	8.00(±10%)
$J_{V,3}^{\text{Di-Di}}$	$6.56^{+0.12}_{-0.15}$	56.(±10%)	4.25(±10%)	*	$7.52^{+0.12}_{-0.14}$	72.(±10%)	6.25(±10%)
$J_{V,4}^{\text{Di-Di}}$	$6.53^{+0.11}_{-0.16}$	55.(±10%)	4.25(±10%)	*	$8.02^{+0.08}_{-0.17}$	81.(±10%)	7.75(±10%)
$J_{V,1}^{\text{Dia}}$	$6.57^{+0.11}_{-0.13}$	57.(±10%)	4.25(±10%)	*	$7.90^{+0.11}_{-0.15}$	79.(±10%)	7.25(±10%)
$J_{V,2}^{\text{Dia}}$	$6.60^{+0.12}_{-0.14}$	57.(±10%)	4.50(±10%)	*	$7.52^{+0.14}_{-0.16}$	72.(±10%)	6.75(±10%)
$J_{V,3}^{\text{Dia}}$	$6.53^{+0.11}_{-0.13}$	56.(±10%)	4.00(±10%)	*	$8.02^{+0.08}_{-0.15}$	81.(±10%)	7.25(±10%)
$J_{V,4}^{\text{Dia}}$	$6.59^{+0.11}_{-0.14}$	57.(±10%)	4.25(±10%)	*	$7.56^{+0.14}_{-0.15}$	73.(±10%)	6.50(±10%)

TABLE XVI. The LO and NLO Results for $J^P = 1^-$ with $\bar{c}c\bar{c}c$ system in the On-Shell scheme

Current	LO			*	NLO(OS)		
	M_H (GeV)	s_0 (GeV^2)	M_B^2 (GeV^2)	*	M_H (GeV)	s_0 (GeV^2)	M_B^2 (GeV^2)
$J_{V,1}^{\text{M-M}}$	$7.87^{+0.12}_{-0.15}$	76.(±10%)	4.75(±10%)	*	$6.96^{+0.12}_{-0.17}$	54.(±10%)	3.00(±10%)
$J_{V,2}^{\text{M-M}}$	$7.78^{+0.13}_{-0.17}$	72.(±10%)	4.75(±10%)	*	$6.88^{+0.12}_{-0.20}$	52.(±10%)	2.75(±10%)
$J_{V,3}^{\text{M-M}}$	$7.86^{+0.11}_{-0.13}$	77.(±10%)	4.50(±10%)	*	$6.95^{+0.11}_{-0.15}$	54.(±10%)	2.75(±10%)
$J_{V,4}^{\text{M-M}}$	$7.69^{+0.12}_{-0.15}$	71.(±10%)	4.25(±10%)	*	$6.80^{+0.12}_{-0.20}$	51.(±10%)	2.50(±10%)
$J_{V,1}^{\text{Di-Di}}$	$7.79^{+0.11}_{-0.13}$	74.(±10%)	4.50(±10%)	*	$6.87^{+0.13}_{-0.19}$	52.(±10%)	2.75(±10%)
$J_{V,2}^{\text{Di-Di}}$	$7.85^{+0.11}_{-0.16}$	75.(±10%)	4.75(±10%)	*	$6.96^{+0.12}_{-0.18}$	54.(±10%)	3.00(±10%)
$J_{V,3}^{\text{Di-Di}}$	$7.78^{+0.12}_{-0.15}$	73.(±10%)	4.50(±10%)	*	$6.87^{+0.13}_{-0.20}$	52.(±10%)	2.75(±10%)
$J_{V,4}^{\text{Di-Di}}$	$7.70^{+0.14}_{-0.18}$	70.(±10%)	4.50(±10%)	*	$6.86^{+0.11}_{-0.17}$	52.(±10%)	2.50(±10%)
$J_{V,1}^{\text{Dia}}$	$7.78^{+0.11}_{-0.13}$	74.(±10%)	4.50(±10%)	*	$6.87^{+0.13}_{-0.20}$	52.(±10%)	2.75(±10%)
$J_{V,2}^{\text{Dia}}$	$7.85^{+0.11}_{-0.16}$	75.(±10%)	4.75(±10%)	*	$6.98^{+0.10}_{-0.17}$	55.(±10%)	2.75(±10%)
$J_{V,3}^{\text{Dia}}$	$7.68^{+0.12}_{-0.15}$	71.(±10%)	4.25(±10%)	*	$6.80^{+0.13}_{-0.20}$	51.(±10%)	2.50(±10%)
$J_{V,4}^{\text{Dia}}$	$7.86^{+0.11}_{-0.13}$	77.(±10%)	4.50(±10%)	*	$6.95^{+0.11}_{-0.15}$	54.(±10%)	2.75(±10%)

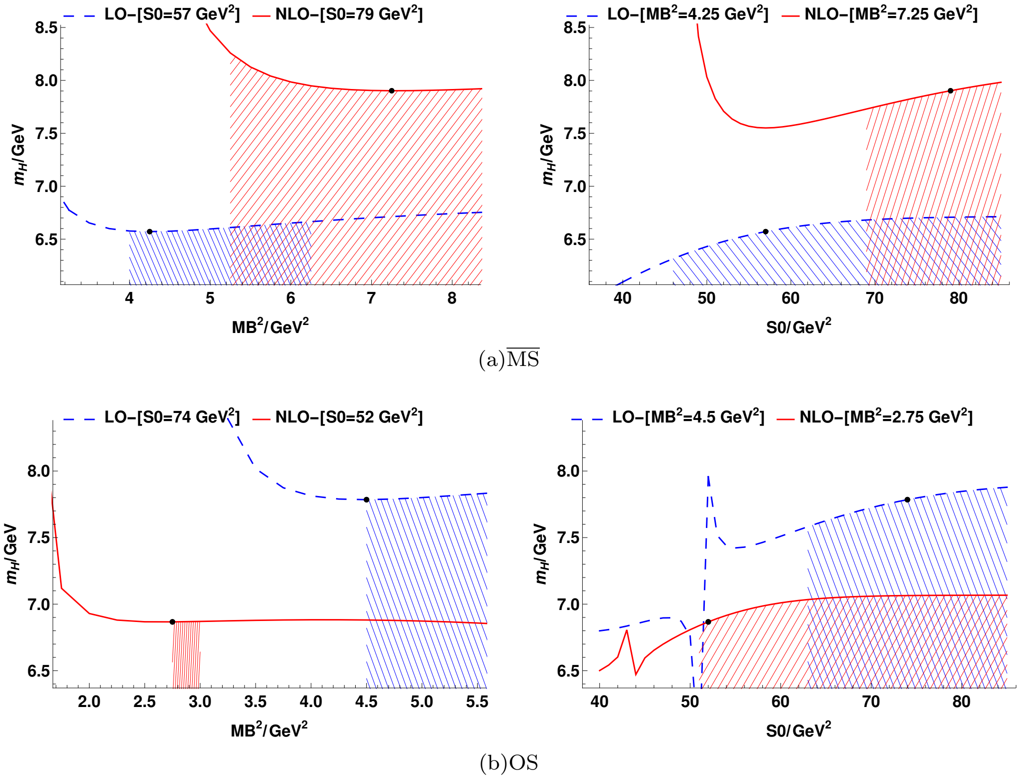

FIG. 17. The Borel platform curves for $J_{V,1}^{\text{Dia}}$ in the $\overline{\text{MS}}$ and On-Shell schemes

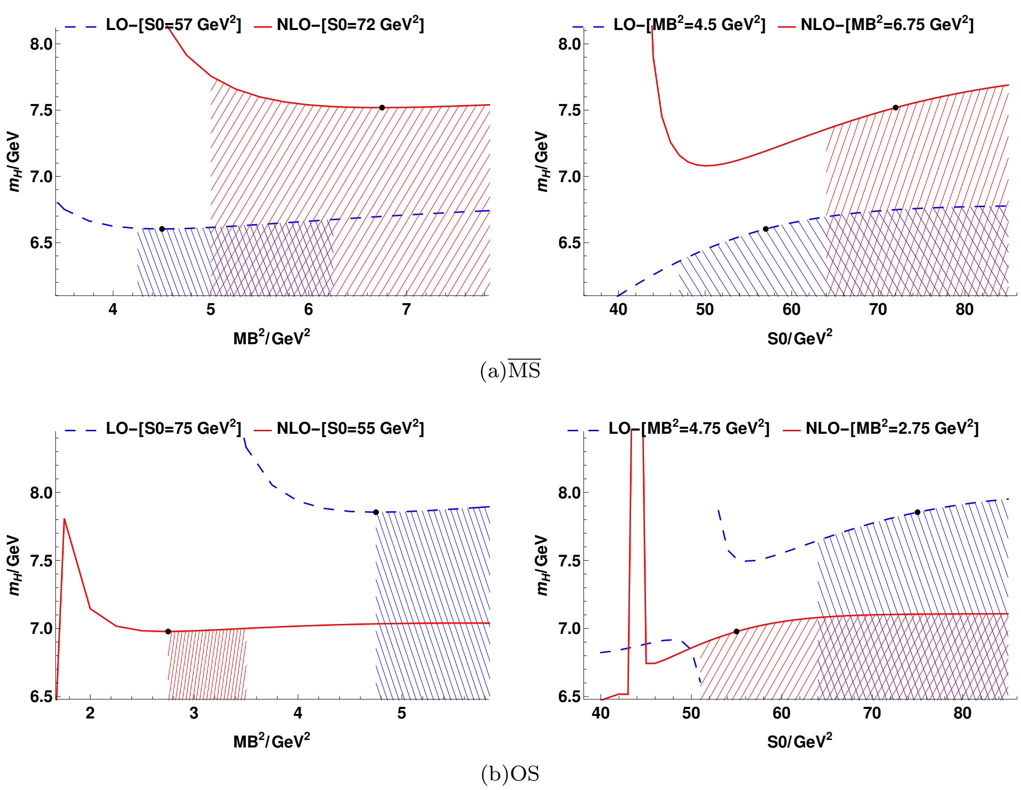

FIG. 18. The Borel platform curves for $J_{V,2}^{\text{Dia}}$ in the $\overline{\text{MS}}$ and On-Shell schemes

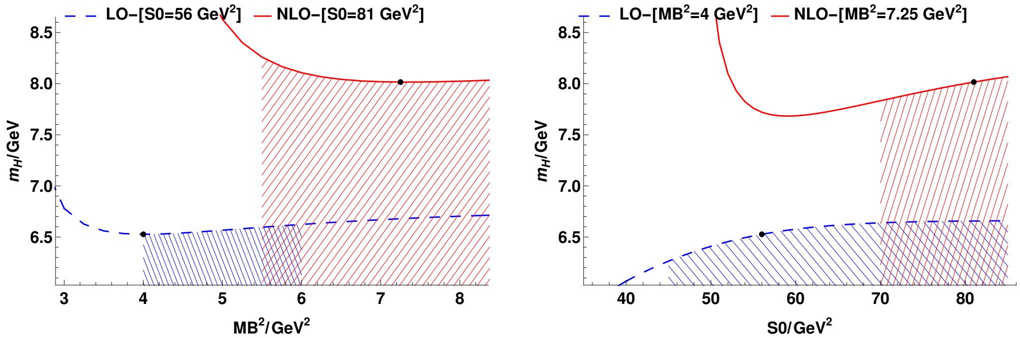

(a)$\overline{\text{MS}}$

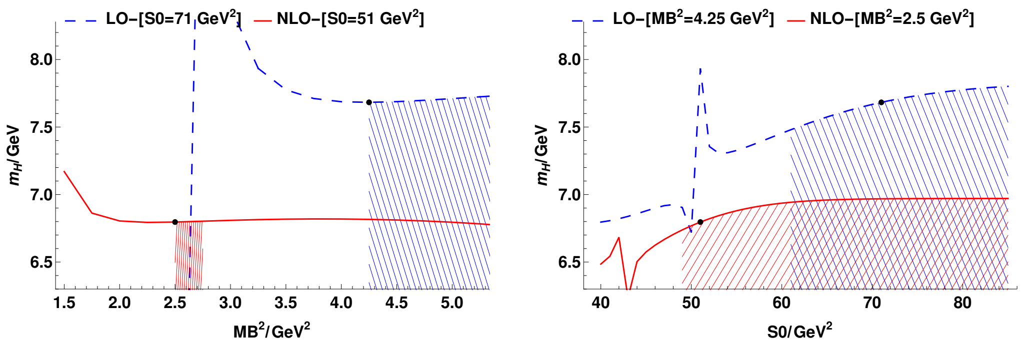

(b)OS

FIG. 19. The Borel platform curves for $J_{V,3}^{\text{Dia}}$ in the $\overline{\text{MS}}$ and On-Shell schemes

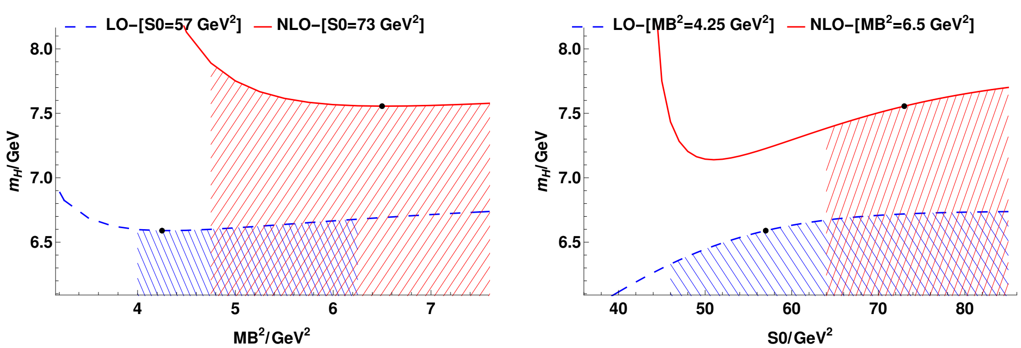

(a)$\overline{\text{MS}}$

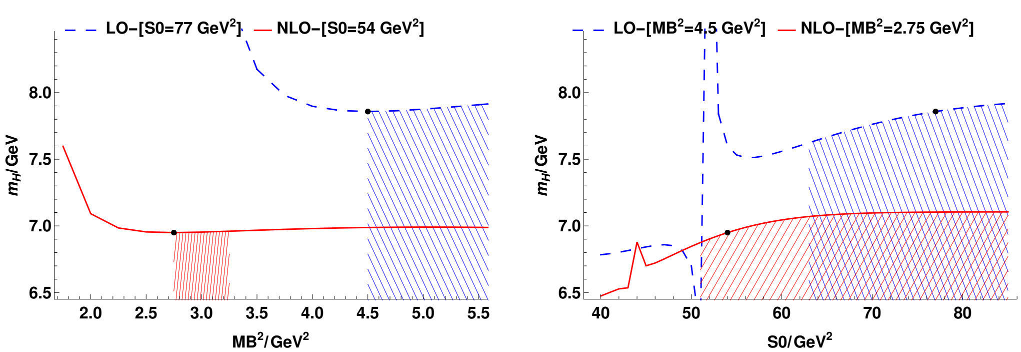

(b)OS

FIG. 20. The Borel platform curves for $J_{V,4}^{\text{Dia}}$ in the $\overline{\text{MS}}$ and On-Shell schemes

5. Numerical Results for $J^P = 2^+$ states

TABLE XVII. The LO and NLO Results for $J^P = 2^+$ with $\bar{c}c\bar{c}c$ system in the $\overline{\text{MS}}$ scheme

Current	LO			*	NLO($\overline{\text{MS}}$)		
	M_H (GeV)	s_0 (GeV^2)	M_B^2 (GeV^2)	*	M_H (GeV)	s_0 (GeV^2)	M_B^2 (GeV^2)
$J_{T,1}^{\text{M-M}}$	$6.11^{+0.06}_{-0.08}$	49.($\pm$10%)	3.50($\pm$10%)	*	$7.03^{+0.10}_{-0.12}$	63.($\pm$10%)	5.50($\pm$10%)
$J_{T,2}^{\text{M-M}}$	$7.10^{+0.13}_{-0.15}$	65.($\pm$10%)	5.50($\pm$10%)	*	$8.89^{+0.21}_{-0.24}$	97.($\pm$10%)	11.00($\pm$10%)
$J_{T,3}^{\text{M-M}}$	$6.23^{+0.10}_{-0.14}$	51.($\pm$10%)	3.75($\pm$10%)	*	$7.35^{+0.10}_{-0.10}$	69.($\pm$10%)	5.75($\pm$10%)
$J_{T,1}^{\text{Di-Di}}$	$6.07^{+0.08}_{-0.10}$	47.($\pm$10%)	3.75($\pm$10%)	*	$6.98^{+0.09}_{-0.11}$	63.($\pm$10%)	5.25($\pm$10%)
$J_{T,2}^{\text{Di-Di}}$	$7.02^{+0.13}_{-0.16}$	63.($\pm$10%)	5.25($\pm$10%)	*	$9.00^{+0.21}_{-0.23}$	99.($\pm$10%)	11.25($\pm$10%)
$J_{T,3}^{\text{Di-Di}}$	$6.15^{+0.08}_{-0.10}$	49.($\pm$10%)	3.75($\pm$10%)	*	$7.25^{+0.10}_{-0.11}$	67.($\pm$10%)	5.75($\pm$10%)
$J_{T,1}^{\text{Dia}}$	$6.14^{+0.07}_{-0.11}$	51.($\pm$10%)	3.50($\pm$10%)	*	$7.03^{+0.11}_{-0.12}$	63.($\pm$10%)	5.50($\pm$10%)
$J_{T,2}^{\text{Dia}}$	$6.15^{+0.08}_{-0.10}$	49.($\pm$10%)	3.75($\pm$10%)	*	$7.25^{+0.10}_{-0.11}$	67.($\pm$10%)	5.75($\pm$10%)
$J_{T,3}^{\text{Dia}}$	$6.23^{+0.10}_{-0.14}$	51.($\pm$10%)	3.75($\pm$10%)	*	$7.35^{+0.10}_{-0.10}$	69.($\pm$10%)	5.75($\pm$10%)

TABLE XVIII. The LO and NLO Results for $J^P = 2^+$ with $\bar{c}c\bar{c}c$ system in the On-Shell scheme

Current	LO			*	NLO(OS)		
	M_H (GeV)	s_0 (GeV^2)	M_B^2 (GeV^2)	*	M_H (GeV)	s_0 (GeV^2)	M_B^2 (GeV^2)
$J_{T,1}^{\text{M-M}}$	$7.31^{+0.05}_{-0.08}$	68.($\pm$10%)	3.50($\pm$10%)	*	$6.56^{+0.09}_{-0.14}$	47.($\pm$10%)	2.00($\pm$10%)
$J_{T,2}^{\text{M-M}}$	$8.38^{+0.14}_{-0.20}$	85.($\pm$10%)	5.75($\pm$10%)	*	$7.37^{+0.16}_{-0.25}$	61.($\pm$10%)	3.75($\pm$10%)
$J_{T,3}^{\text{M-M}}$	$7.39^{+0.08}_{-0.11}$	68.($\pm$10%)	3.75($\pm$10%)	*	$6.57^{+0.12}_{-0.19}$	47.($\pm$10%)	2.25($\pm$10%)
$J_{T,1}^{\text{Di-Di}}$	$7.32^{+0.04}_{-0.07}$	69.($\pm$10%)	3.50($\pm$10%)	*	$6.56^{+0.09}_{-0.14}$	47.($\pm$10%)	2.00($\pm$10%)
$J_{T,2}^{\text{Di-Di}}$	$8.27^{+0.16}_{-0.22}$	81.($\pm$10%)	5.75($\pm$10%)	*	$7.30^{+0.15}_{-0.24}$	60.($\pm$10%)	3.50($\pm$10%)
$J_{T,3}^{\text{Di-Di}}$	$7.32^{+0.07}_{-0.13}$	65.($\pm$10%)	3.75($\pm$10%)	*	$6.57^{+0.12}_{-0.18}$	47.($\pm$10%)	2.25($\pm$10%)
$J_{T,1}^{\text{Dia}}$	$7.31^{+0.05}_{-0.08}$	68.($\pm$10%)	3.50($\pm$10%)	*	$6.56^{+0.09}_{-0.15}$	47.($\pm$10%)	2.00($\pm$10%)
$J_{T,2}^{\text{Dia}}$	$7.32^{+0.07}_{-0.13}$	65.($\pm$10%)	3.75($\pm$10%)	*	$6.57^{+0.12}_{-0.18}$	47.($\pm$10%)	2.25($\pm$10%)
$J_{T,3}^{\text{Dia}}$	$7.39^{+0.08}_{-0.11}$	68.($\pm$10%)	3.75($\pm$10%)	*	$6.57^{+0.12}_{-0.19}$	47.($\pm$10%)	2.25($\pm$10%)

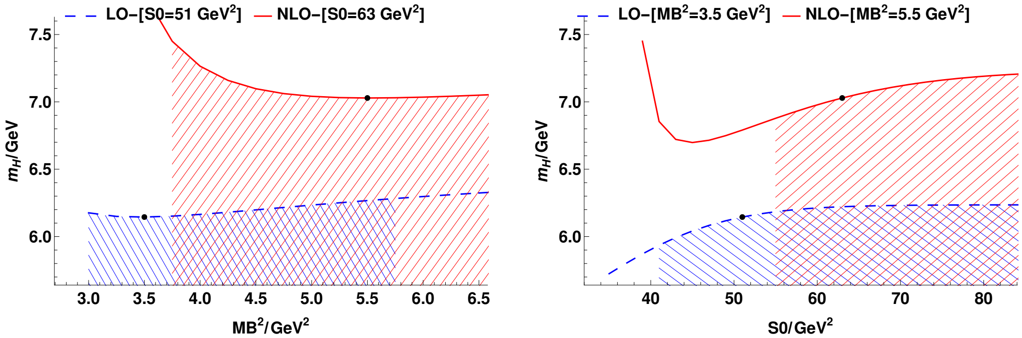

(a)$\overline{\mathrm{MS}}$

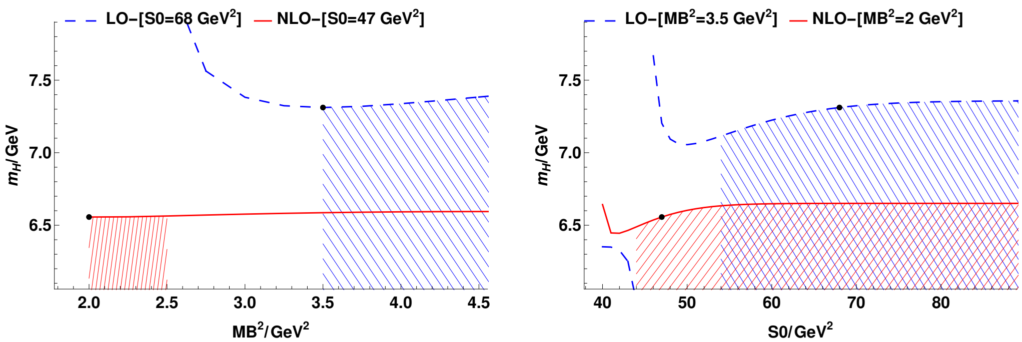

(b)OS

FIG. 21. The Borel platform curves for $J_{T,1}^{\mathrm{Dia}}$ in the $\overline{\mathrm{MS}}$ and On-Shell schemes

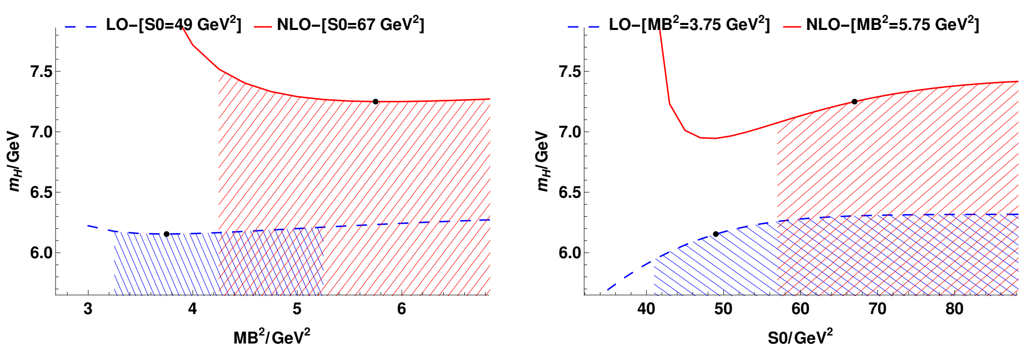

(a)$\overline{\mathrm{MS}}$

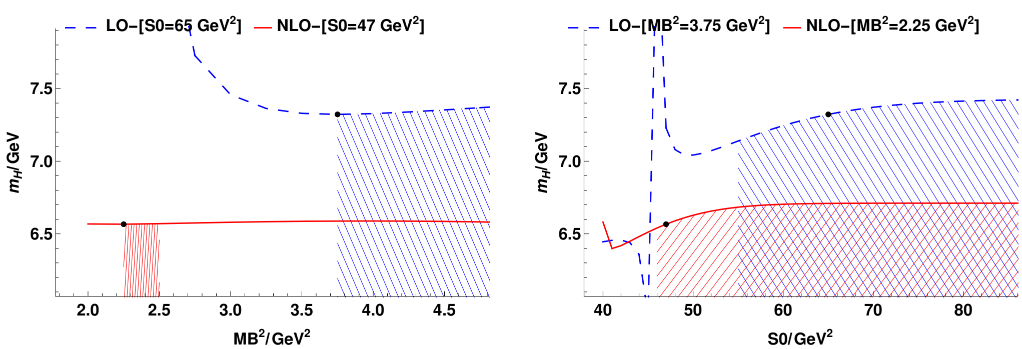

(b)OS

FIG. 22. The Borel platform curves for $J_{T,2}^{\mathrm{Dia}}$ in the $\overline{\mathrm{MS}}$ and On-Shell schemes

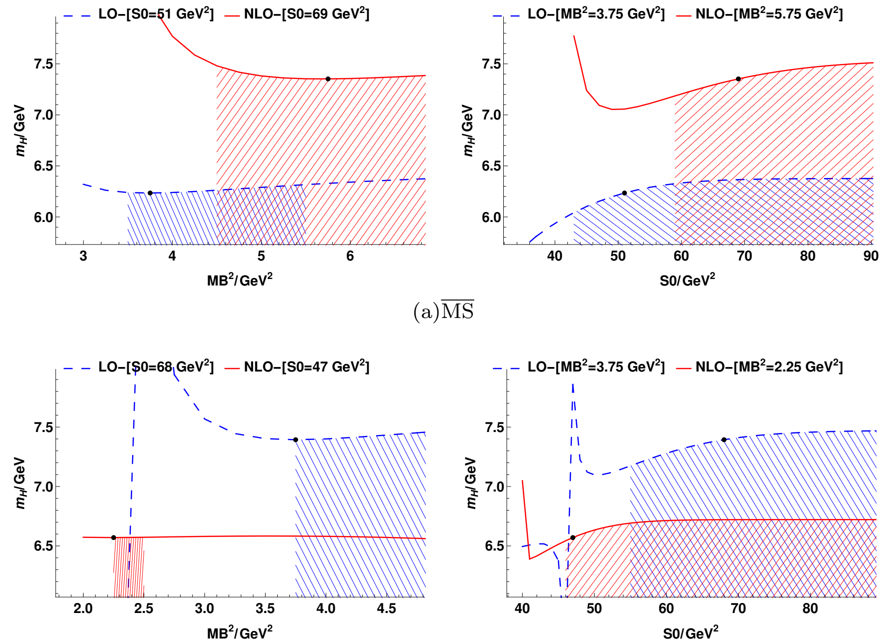

(a)$\overline{\text{MS}}$

(b)OS

FIG. 23. The Borel platform curves for $J_{T,3}^{\text{Dia}}$ in the $\overline{\text{MS}}$ and On-Shell schemes

6. Renormalization scale dependence

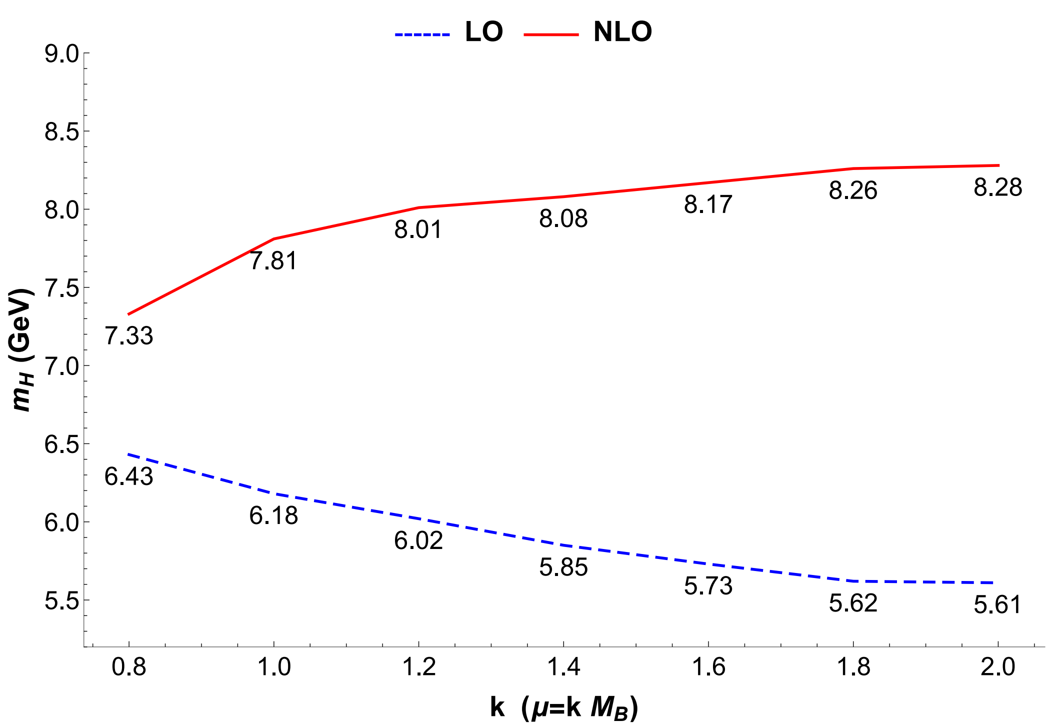

FIG. 24. The renormalization scale μ dependence of the LO and NLO results of $J_{S,1}^{\text{Dia}}$ in $\overline{\text{MS}}$ scheme

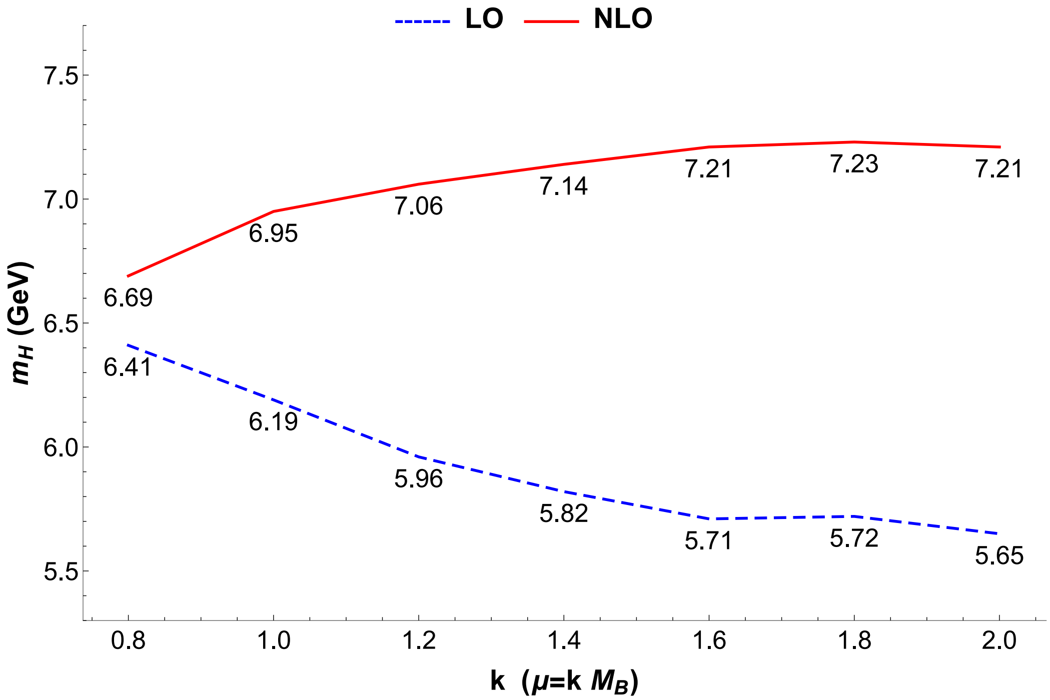

FIG. 25. The renormalization scale μ dependence of the LO and NLO results of $J_{S,2}^{\mathrm{Dia}}$ in $\overline{\mathrm{MS}}$ scheme

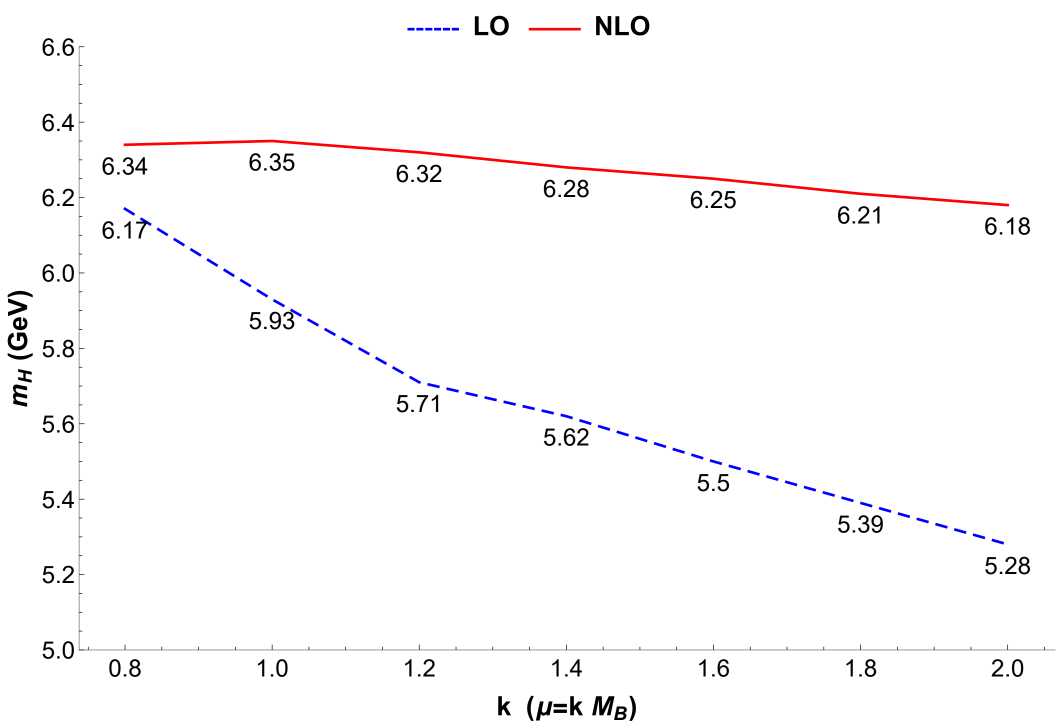

FIG. 26. The renormalization scale μ dependence of the LO and NLO results of $J_{S,3}^{\mathrm{Dia}}$ in $\overline{\mathrm{MS}}$ scheme

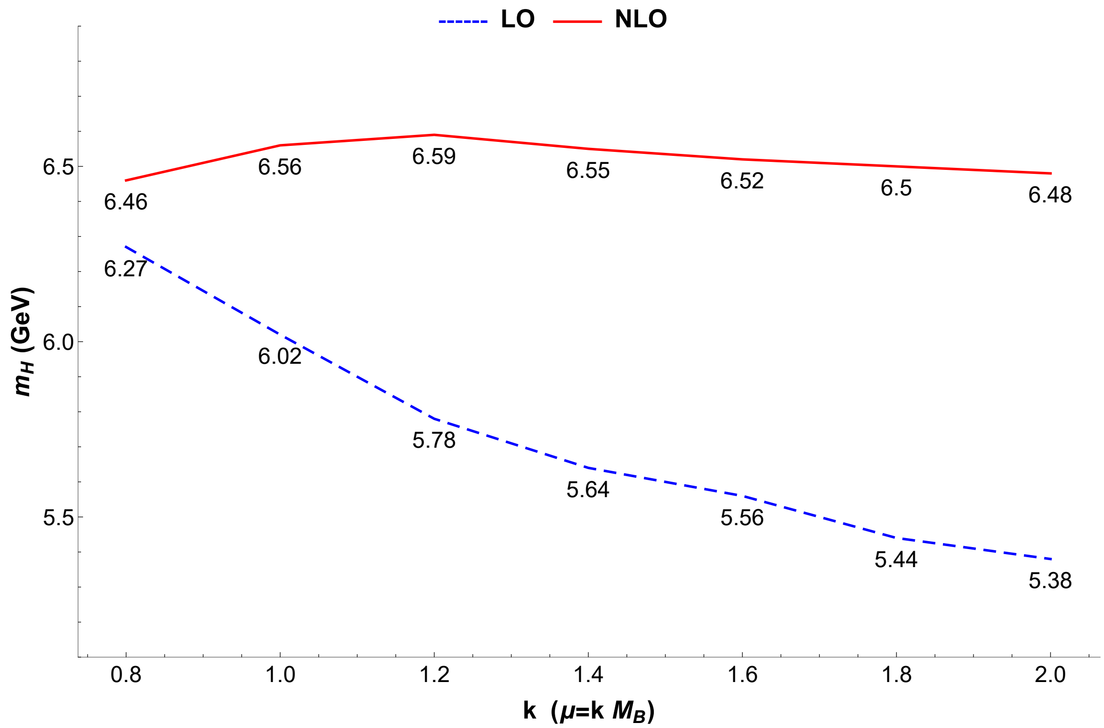

FIG. 27. The renormalization scale μ dependence of the LO and NLO results of $J_{S,4}^{\mathrm{Dia}}$ in $\overline{\mathrm{MS}}$ scheme

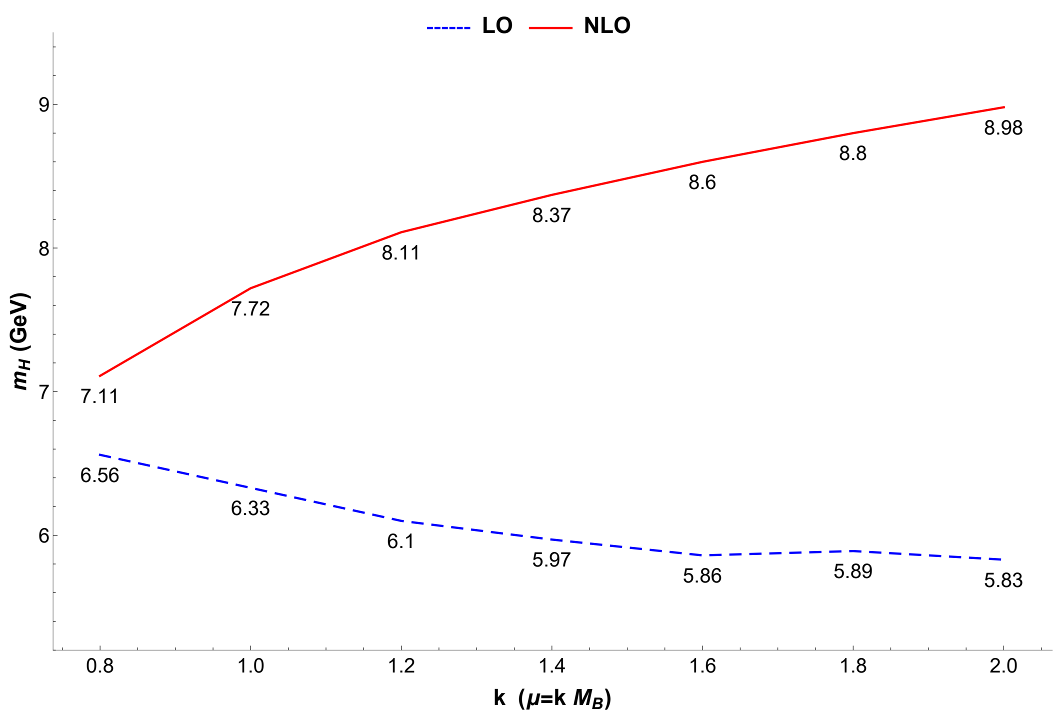

FIG. 28. The renormalization scale μ dependence of the LO and NLO results of $J_{S,5}^{\mathrm{Dia}}$ in $\overline{\mathrm{MS}}$ scheme

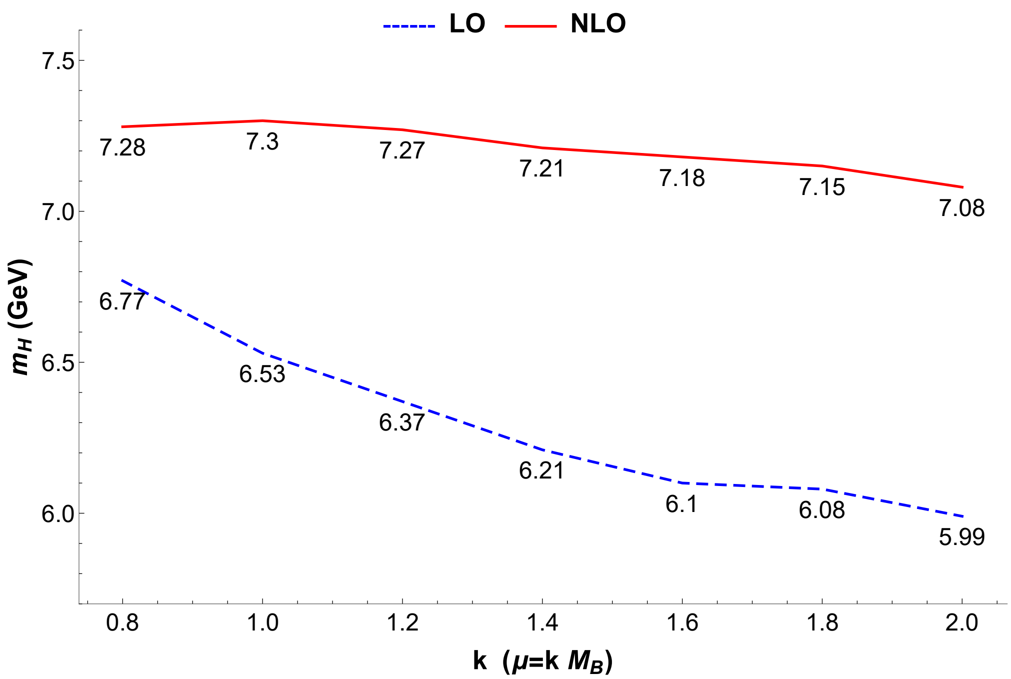

FIG. 29. The renormalization scale μ dependence of the LO and NLO results of $J^{\rm Dia}_{P,2}$ in $\overline{\rm MS}$ scheme

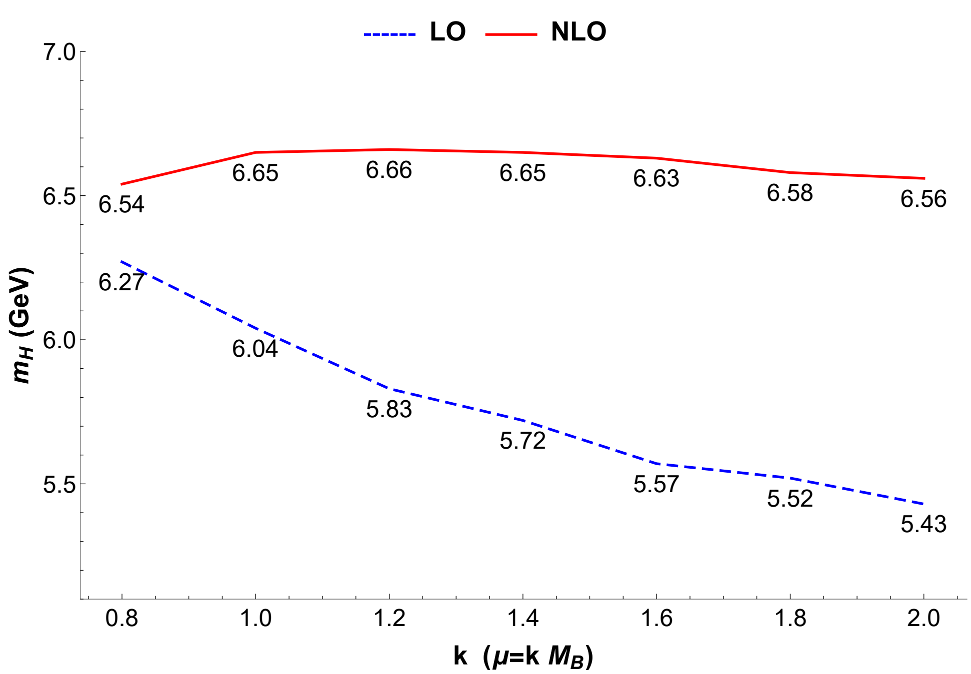

FIG. 30. The renormalization scale μ dependence of the LO and NLO results of $J^{\rm Dia}_{A,4}$ in $\overline{\rm MS}$ scheme

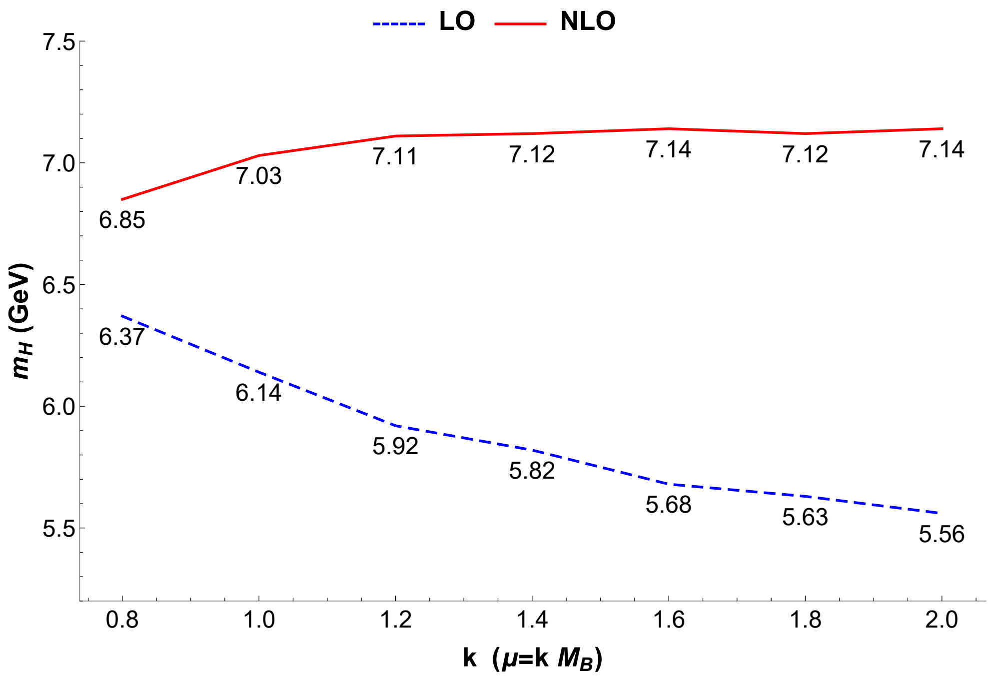

FIG. 31. The renormalization scale μ dependence of the LO and NLO results of $J_{T,1}^{\mathrm{Dia}}$ in $\overline{\mathrm{MS}}$ scheme

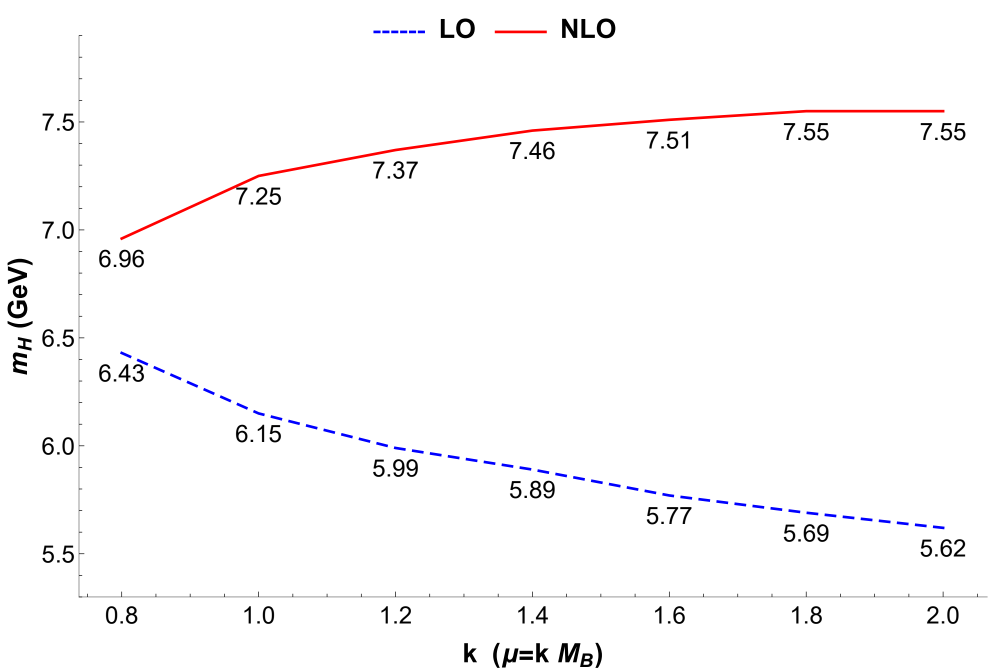

FIG. 32. The renormalization scale μ dependence of the LO and NLO results of $J_{T,2}^{\mathrm{Dia}}$ in $\overline{\mathrm{MS}}$ scheme

Appendix C: Details for bottom system

1. Numerical Results with $J^P = 0^+$

TABLE XIX. The LO and NLO Results for $J^P = 0^+$ with $\bar{b}b\bar{b}b$ system in the $\overline{\mathrm{MS}}$ scheme. (Δ denotes this result is got in Borel condition ($\leq 40\%$))

Current	LO			*	NLO($\overline{\mathrm{MS}}$)		
	M_H (GeV)	S_0 (GeV^2)	M_B^2 (GeV^2)	*	M_H (GeV)	S_0 (GeV^2)	M_B^2 (GeV^2)
$J_{S,1}^{\text{M-M}}$	$18.51^{+0.17}_{-0.26}$	380.(±5%)	19.00(±5%)	*	$19.00^{+0.05}_{-0.10}$	400.(±5%)	9.00(±5%)
$J_{S,2}^{\text{M-M}}$	$18.55^{+0.19}_{-0.26}$	382.(±5%)	18.00(±5%)	*	$18.92^{+0.10}_{-0.17}$	384.(±5%)	9.50(±5%)
$J_{S,3}^{\text{M-M}}$	$19.21^{+0.20}_{-0.26}$	408.(±5%)	18.00(±5%)	*	$(\Delta)19.66^{+0.05}_{-0.10}$	420.(±5%)	7.00(±5%)
$J_{S,4}^{\text{M-M}}$	$18.50^{+0.17}_{-0.26}$	380.(±5%)	19.00(±5%)	*	$18.97^{+0.05}_{-0.11}$	398.(±5%)	9.50(±5%)
$J_{S,5}^{\text{M-M}}$	$18.51^{+0.17}_{-0.26}$	380.(±5%)	19.00(±5%)	*	$18.93^{+0.09}_{-0.16}$	386.(±5%)	9.50(±5%)
$J_{S,1}^{\text{Di-Di}}$	$18.50^{+0.17}_{-0.26}$	380.(±5%)	19.00(±5%)	*	$18.97^{+0.05}_{-0.11}$	398.(±5%)	9.50(±5%)
$J_{S,2}^{\text{Di-Di}}$	$18.52^{+0.17}_{-0.26}$	380.(±5%)	18.00(±5%)	*	$18.95^{+0.08}_{-0.14}$	390.(±5%)	9.50(±5%)
$J_{S,3}^{\text{Di-Di}}$	$19.17^{+0.20}_{-0.26}$	406.(±5%)	17.50(±5%)	*	$19.42^{+0.10}_{-0.17}$	404.(±5%)	8.00(±5%)
$J_{S,4}^{\text{Di-Di}}$	$18.50^{+0.17}_{-0.26}$	380.(±5%)	19.00(±5%)	*	$19.00^{+0.05}_{-0.10}$	400.(±5%)	9.00(±5%)
$J_{S,5}^{\text{Di-Di}}$	$18.51^{+0.17}_{-0.26}$	380.(±5%)	19.00(±5%)	*	$18.97^{+0.05}_{-0.11}$	398.(±5%)	9.50(±5%)
$J_{S,1}^{\text{Dia}}$	$18.51^{+0.17}_{-0.26}$	380.(±5%)	19.00(±5%)	*	$19.01^{+0.05}_{-0.10}$	400.(±5%)	9.00(±5%)
$J_{S,2}^{\text{Dia}}$	$18.51^{+0.17}_{-0.26}$	380.(±5%)	19.00(±5%)	*	$18.97^{+0.06}_{-0.11}$	398.(±5%)	9.50(±5%)
$J_{S,3}^{\text{Dia}}$	$18.50^{+0.18}_{-0.26}$	380.(±5%)	19.00(±5%)	*	$18.96^{+0.05}_{-0.11}$	398.(±5%)	9.50(±5%)
$J_{S,4}^{\text{Dia}}$	$18.50^{+0.17}_{-0.26}$	380.(±5%)	19.00(±5%)	*	$18.97^{+0.06}_{-0.11}$	398.(±5%)	9.50(±5%)
$J_{S,5}^{\text{Dia}}$	$18.51^{+0.17}_{-0.26}$	380.(±5%)	19.00(±5%)	*	$18.95^{+0.08}_{-0.14}$	390.(±5%)	9.50(±5%)

TABLE XX. The LO and NLO Results for $J^P = 0^+$ with $\bar{b}b\bar{b}b$ system in the On-Shell scheme

Current	LO			*	NLO(OS)		
	M_H (GeV)	S_0 (GeV^2)	M_B^2 (GeV^2)	*	M_H (GeV)	S_0 (GeV^2)	M_B^2 (GeV^2)
$J_{S,1}^{\text{M-M}}$	$19.68^{+0.04}_{-0.10}$	$420.(\pm5\%)$	$7.50(\pm5\%)$	*	$18.98^{+0.07}_{-0.28}$	$366.(\pm5\%)$	$3.50(\pm5\%)$
$J_{S,2}^{\text{M-M}}$	$19.68^{+0.04}_{-0.10}$	$420.(\pm5\%)$	$7.50(\pm5\%)$	*	$18.98^{+0.07}_{-0.28}$	$366.(\pm5\%)$	$3.50(\pm5\%)$
$J_{S,3}^{\text{M-M}}$	$20.51^{+0.05}_{-0.18}$	$452.(\pm5\%)$	$11.00(\pm5\%)$	*	$19.51^{+0.72}_{-1.55}$	$392.(\pm5\%)$	$6.00(\pm5\%)$
$J_{S,4}^{\text{M-M}}$	$19.64^{+0.02}_{-0.06}$	$426.(\pm5\%)$	$7.00(\pm5\%)$	*	$18.98^{+0.07}_{-0.35}$	$366.(\pm5\%)$	$3.50(\pm5\%)$
$J_{S,5}^{\text{M-M}}$	$19.71^{+0.03}_{-0.08}$	$426.(\pm5\%)$	$7.50(\pm5\%)$	*	$18.98^{+0.07}_{-0.27}$	$366.(\pm5\%)$	$3.50(\pm5\%)$
$J_{S,1}^{\text{Di-Di}}$	$19.64^{+0.06}_{-0.12}$	$412.(\pm5\%)$	$7.50(\pm5\%)$	*	$18.98^{+0.07}_{-0.31}$	$366.(\pm5\%)$	$3.50(\pm5\%)$
$J_{S,2}^{\text{Di-Di}}$	$19.64^{+0.06}_{-0.12}$	$412.(\pm5\%)$	$7.50(\pm5\%)$	*	$18.98^{+0.07}_{-0.30}$	$366.(\pm5\%)$	$3.50(\pm5\%)$
$J_{S,3}^{\text{Di-Di}}$	$20.25^{+0.12}_{-0.20}$	$436.(\pm5\%)$	$9.50(\pm5\%)$	*	$19.31^{+0.10}_{-1.33}$	$382.(\pm5\%)$	$4.50(\pm5\%)$
$J_{S,4}^{\text{Di-Di}}$	$19.68^{+0.04}_{-0.10}$	$420.(\pm5\%)$	$7.50(\pm5\%)$	*	$18.98^{+0.07}_{-0.28}$	$366.(\pm5\%)$	$3.50(\pm5\%)$
$J_{S,5}^{\text{Di-Di}}$	$19.65^{+0.05}_{-0.11}$	$414.(\pm5\%)$	$7.50(\pm5\%)$	*	$18.98^{+0.07}_{-0.31}$	$366.(\pm5\%)$	$3.50(\pm5\%)$
$J_{S,1}^{\text{Dia}}$	$19.68^{+0.04}_{-0.10}$	$420.(\pm5\%)$	$7.50(\pm5\%)$	*	$18.98^{+0.07}_{-0.28}$	$366.(\pm5\%)$	$3.50(\pm5\%)$
$J_{S,2}^{\text{Dia}}$	$19.67^{+0.04}_{-0.10}$	$418.(\pm5\%)$	$7.50(\pm5\%)$	*	$18.98^{+0.07}_{-0.28}$	$366.(\pm5\%)$	$3.50(\pm5\%)$
$J_{S,3}^{\text{Dia}}$	$19.64^{+0.02}_{-0.06}$	$426.(\pm5\%)$	$7.00(\pm5\%)$	*	$18.98^{+0.07}_{-0.36}$	$366.(\pm5\%)$	$3.50(\pm5\%)$
$J_{S,4}^{\text{Dia}}$	$19.61^{+0.07}_{-0.14}$	$408.(\pm5\%)$	$7.50(\pm5\%)$	*	$18.98^{+0.07}_{-0.33}$	$366.(\pm5\%)$	$3.50(\pm5\%)$
$J_{S,5}^{\text{Dia}}$	$19.66^{+0.08}_{-0.15}$	$410.(\pm5\%)$	$8.00(\pm5\%)$	*	$18.98^{+0.07}_{-0.26}$	$366.(\pm5\%)$	$3.50(\pm5\%)$

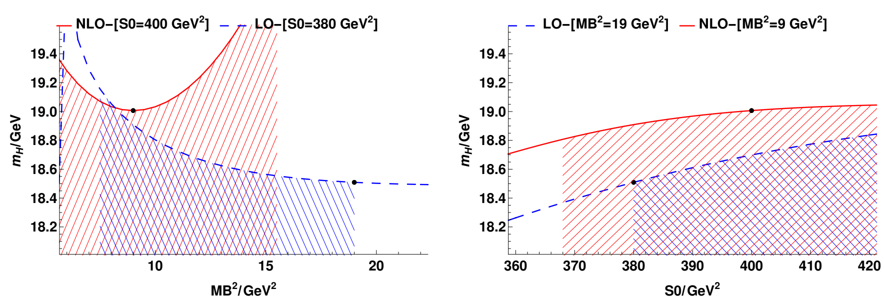

(a)$\overline{\text{MS}}$

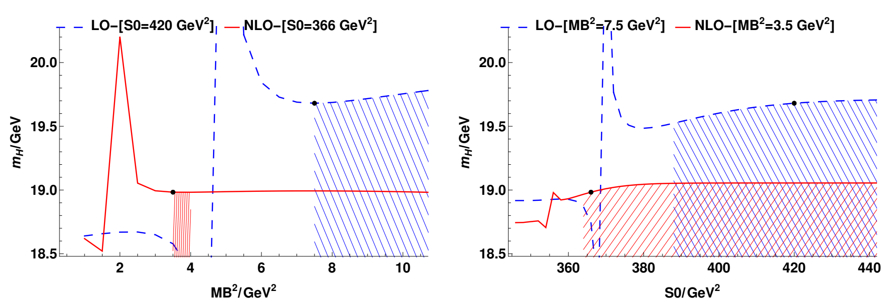

(b)OS

FIG. 33. The Borel platform curves for $J_{S,1}^{\text{Dia}}$ with $\bar{b}b\bar{b}b$ system in the $\overline{\text{MS}}$ and On-Shell schemes

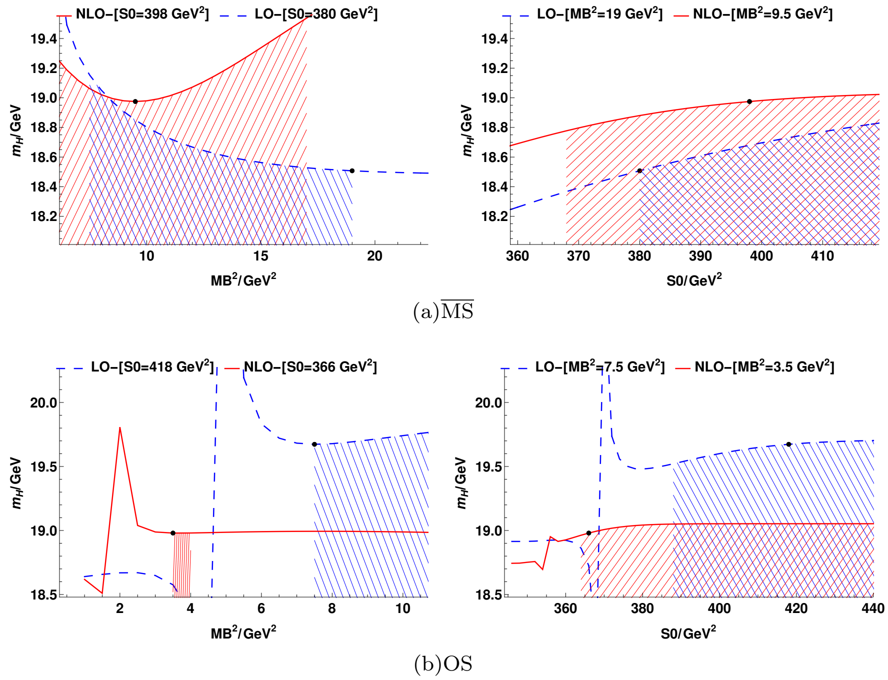

FIG. 34. The Borel platform curves for $J_{S,2}^{\rm Dia}$ with $\bar{b}b\bar{b}b$ system in the $\overline{\rm MS}$ and On-Shell schemes

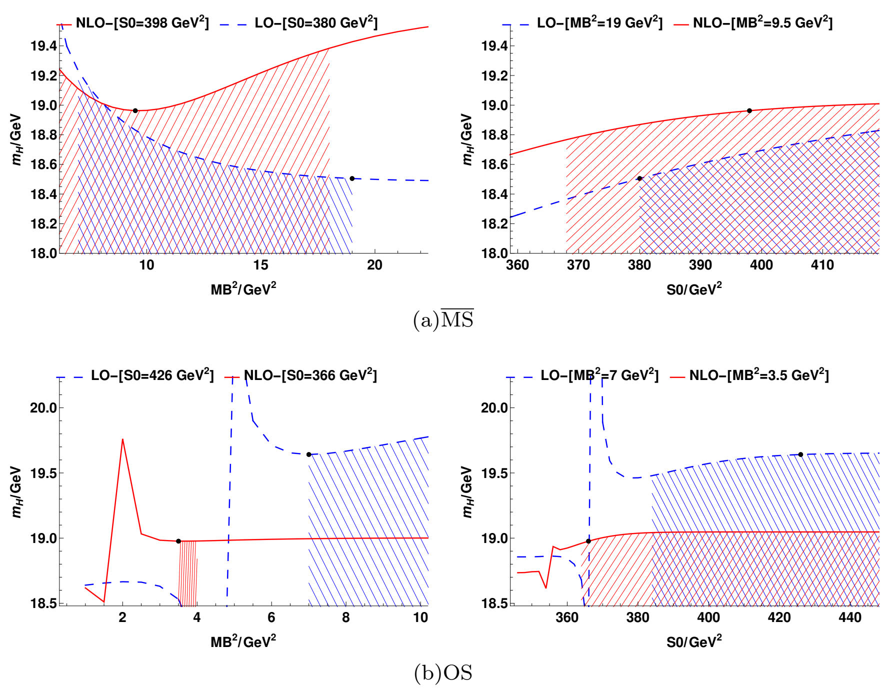

FIG. 35. The Borel platform curves for $J_{S,3}^{\rm Dia}$ with $\bar{b}b\bar{b}b$ system in the $\overline{\rm MS}$ and On-Shell schemes

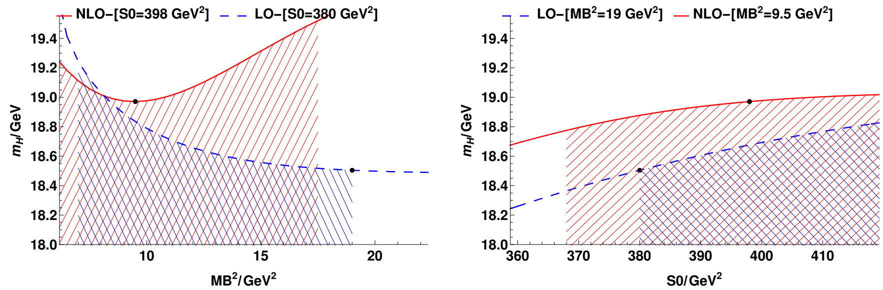

(a)$\overline{\mathrm{MS}}$

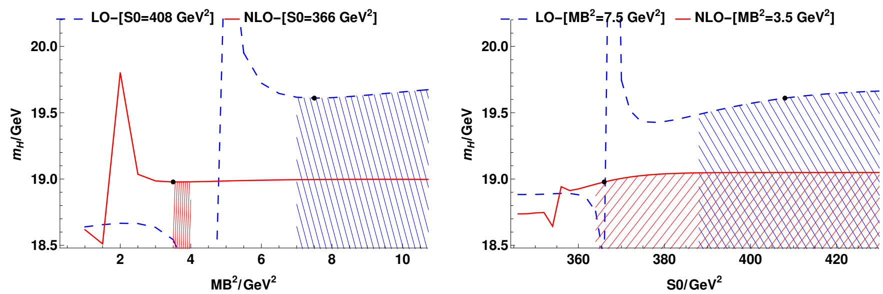

(b)OS

FIG. 36. The Borel platform curves for $J_{S,4}^{\mathrm{Dia}}$ with $\bar{b}b\bar{b}b$ system in the $\overline{\mathrm{MS}}$ and On-Shell schemes

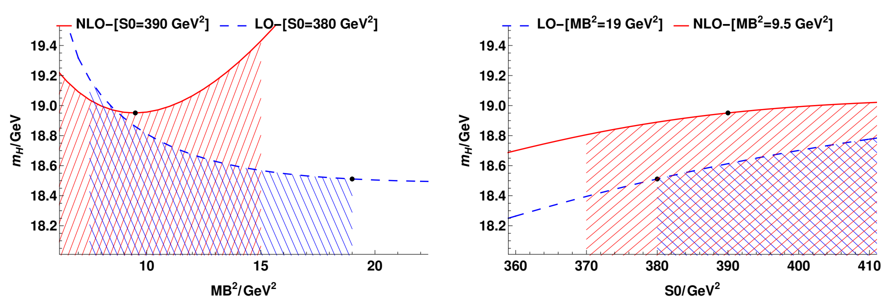

(a)$\overline{\mathrm{MS}}$

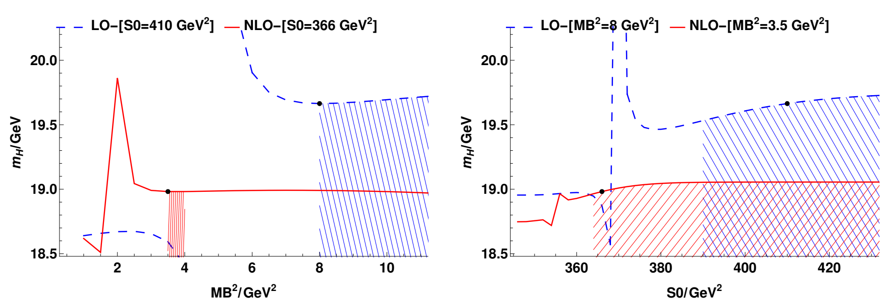

(b)OS

FIG. 37. The Borel platform curves for $J_{S,5}^{\mathrm{Dia}}$ with $\bar{b}b\bar{b}b$ system in the $\overline{\mathrm{MS}}$ and On-Shell schemes

2. Numerical Results with $J^P = 0^-$

TABLE XXI. The LO and NLO Results for $J^P = 0^-$ with $\bar{b}b\bar{b}b$ system in the $\overline{\text{MS}}$ scheme

Current	LO			*	NLO($\overline{\text{MS}}$)		
	M_H (GeV)	S_0 (GeV^2)	M_B^2 (GeV^2)	*	M_H (GeV)	S_0 (GeV^2)	M_B^2 (GeV^2)
$J_{P,1}^{\text{M-M}}$	$18.85^{+0.19}_{-0.26}$	394.(±5%)	18.00(±5%)	*	$19.18^{+0.11}_{-0.18}$	392.(±5%)	8.50(±5%)
$J_{P,2}^{\text{M-M}}$	$18.86^{+0.19}_{-0.26}$	394.(±5%)	18.00(±5%)	*	$19.31^{+0.04}_{-0.09}$	412.(±5%)	8.00(±5%)
$J_{P,3}^{\text{M-M}}$	$18.85^{+0.19}_{-0.26}$	394.(±5%)	18.00(±5%)	*	$19.23^{+0.05}_{-0.11}$	408.(±5%)	8.50(±5%)
$J_{P,1}^{\text{Di-Di}}$	$18.85^{+0.19}_{-0.24}$	394.(±5%)	18.00(±5%)	*	$19.18^{+0.11}_{-0.18}$	392.(±5%)	8.50(±5%)
$J_{P,2}^{\text{Di-Di}}$	$18.85^{+0.19}_{-0.24}$	394.(±5%)	18.00(±5%)	*	$19.24^{+0.06}_{-0.12}$	406.(±5%)	8.50(±5%)
$J_{P,3}^{\text{Di-Di}}$	$18.86^{+0.19}_{-0.24}$	394.(±5%)	18.00(±5%)	*	$19.23^{+0.08}_{-0.14}$	400.(±5%)	8.50(±5%)
$J_{P,1}^{\text{Dia}}$	$18.85^{+0.19}_{-0.26}$	394.(±5%)	18.00(±5%)	*	$19.18^{+0.11}_{-0.18}$	392.(±5%)	8.50(±5%)
$J_{P,2}^{\text{Dia}}$	$18.86^{+0.19}_{-0.26}$	394.(±5%)	18.00(±5%)	*	$19.31^{+0.04}_{-0.09}$	412.(±5%)	8.00(±5%)
$J_{P,3}^{\text{Dia}}$	$18.85^{+0.19}_{-0.26}$	394.(±5%)	18.00(±5%)	*	$19.22^{+0.05}_{-0.11}$	408.(±5%)	8.50(±5%)

TABLE XXII. The LO and NLO Results for $J^P = 0^-$ with $\bar{b}b\bar{b}b$ system in the On-Shell scheme

Current	LO			*	NLO(OS)		
	M_H (GeV)	S_0 (GeV^2)	M_B^2 (GeV^2)	*	M_H (GeV)	S_0 (GeV^2)	M_B^2 (GeV^2)
$J_{P,1}^{\text{M-M}}$	$19.97^{+0.08}_{-0.15}$	428.(±5%)	8.50(±5%)	*	$19.14^{+0.08}_{-0.55}$	374.(±5%)	4.00(±5%)
$J_{P,2}^{\text{M-M}}$	$20.08^{+0.06}_{-0.12}$	438.(±5%)	9.00(±5%)	*	$19.24^{+0.07}_{-1.29}$	380.(±5%)	4.50(±5%)
$J_{P,3}^{\text{M-M}}$	$19.89^{+0.10}_{-0.18}$	418.(±5%)	8.50(±5%)	*	$19.12^{+0.08}_{-0.21}$	374.(±5%)	4.00(±5%)
$J_{P,1}^{\text{Di-Di}}$	$19.97^{+0.08}_{-0.15}$	428.(±5%)	8.50(±5%)	*	$19.14^{+0.08}_{-0.55}$	374.(±5%)	4.00(±5%)
$J_{P,2}^{\text{Di-Di}}$	$19.97^{+0.08}_{-0.15}$	428.(±5%)	8.50(±5%)	*	$19.14^{+0.08}_{-0.93}$	374.(±5%)	4.00(±5%)
$J_{P,3}^{\text{Di-Di}}$	$20.01^{+0.09}_{-0.17}$	428.(±5%)	9.00(±5%)	*	$19.18^{+0.09}_{-0.21}$	376.(±5%)	4.50(±5%)
$J_{P,1}^{\text{Dia}}$	$19.97^{+0.08}_{-0.15}$	428.(±5%)	8.50(±5%)	*	$19.14^{+0.08}_{-0.55}$	374.(±5%)	4.00(±5%)
$J_{P,2}^{\text{Dia}}$	$20.09^{+0.06}_{-0.12}$	438.(±5%)	9.00(±5%)	*	$19.24^{+0.07}_{-1.24}$	380.(±5%)	4.50(±5%)
$J_{P,3}^{\text{Dia}}$	$19.92^{+0.07}_{-0.14}$	426.(±5%)	8.00(±5%)	*	$19.12^{+0.08}_{-0.22}$	374.(±5%)	4.00(±5%)

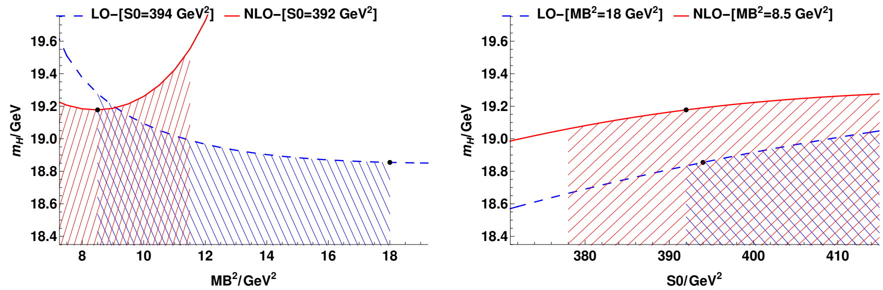

(a)$\overline{\mathrm{MS}}$

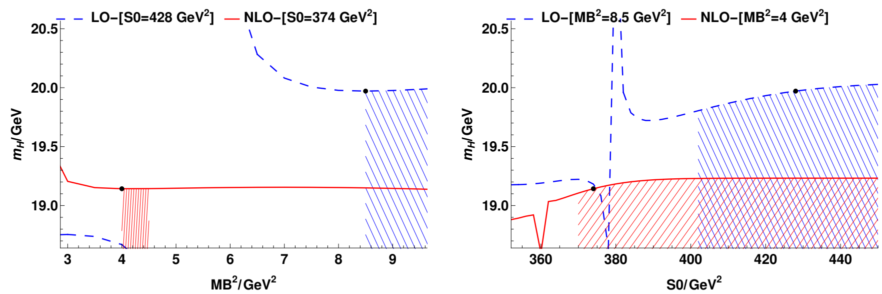

(b)OS

FIG. 38. The Borel platform curves for $J_{P,1}^{\mathrm{Dia}}$ with $\bar{b}b\bar{b}b$ system in the $\overline{\mathrm{MS}}$ and On-Shell schemes

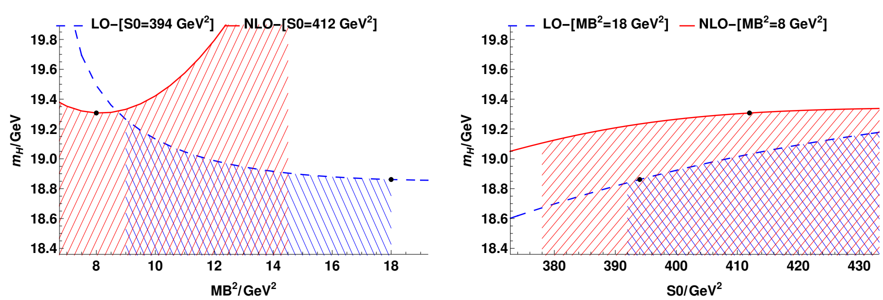

(a)$\overline{\mathrm{MS}}$

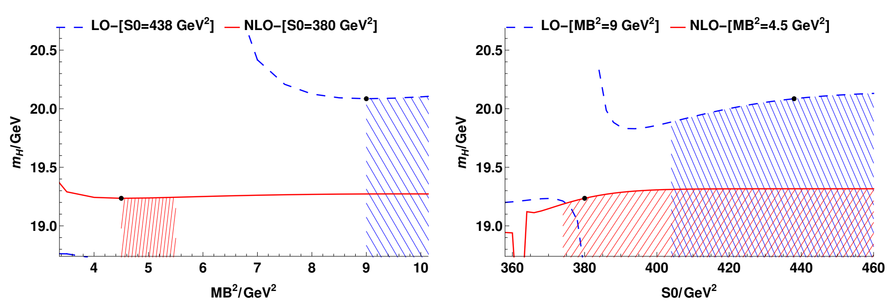

(b)OS

FIG. 39. The Borel platform curves for $J_{P,2}^{\mathrm{Dia}}$ with $\bar{b}b\bar{b}b$ system in the $\overline{\mathrm{MS}}$ and On-Shell schemes

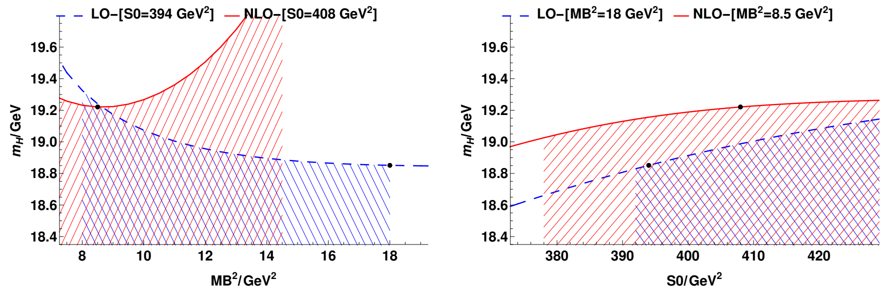

(a)$\overline{\rm MS}$

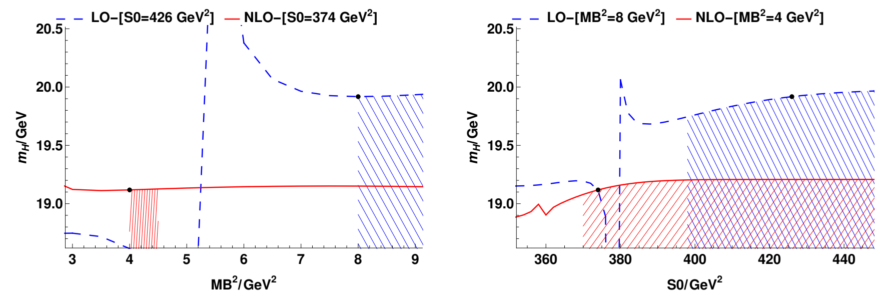

(b)OS

FIG. 40. The Borel platform curves for $J^{\rm Dia}_{P,3}$ with $\bar{b}b\bar{b}b$ system in the $\overline{\rm MS}$ and On-Shell schemes

3. Numerical Results with $J^P = 1^+$

TABLE XXIII. The LO and NLO Results for $J^P = 1^+$ with $\bar{b}b\bar{b}b$ system in the $\overline{\rm MS}$ scheme

Current	LO			*	NLO($\overline{\rm MS}$)		
	M_H (GeV)	S_0 (GeV^2)	M_B^2 (GeV^2)	*	M_H (GeV)	S_0 (GeV^2)	M_B^2 (GeV^2)
$J^{\rm M\text{-}M}_{A,1}$	$19.21^{+0.20}_{-0.26}$	408.(±5%)	18.00(±5%)	*	$19.53^{+0.11}_{-0.17}$	402.(±5%)	7.50(±5%)
$J^{\rm M\text{-}M}_{A,2}$	$19.17^{+0.20}_{-0.26}$	406.(±5%)	17.50(±5%)	*	$18.60^{+0.19}_{-0.26}$	384.(±5%)	16.50(±5%)
$J^{\rm M\text{-}M}_{A,3}$	$18.50^{+0.17}_{-0.26}$	380.(±5%)	19.00(±5%)	*	$18.97^{+0.06}_{-0.12}$	396.(±5%)	9.50(±5%)
$J^{\rm M\text{-}M}_{A,4}$	$18.55^{+0.18}_{-0.25}$	382.(±5%)	18.00(±5%)	*	$18.97^{+0.06}_{-0.11}$	398.(±5%)	9.50(±5%)
$J^{\rm Di\text{-}Di}_{A,1}$	$19.17^{+0.20}_{-0.26}$	406.(±5%)	17.50(±5%)	*	$19.40^{+0.12}_{-0.20}$	398.(±5%)	8.00(±5%)
$J^{\rm Di\text{-}Di}_{A,2}$	$19.20^{+0.20}_{-0.26}$	408.(±5%)	18.00(±5%)	*	$18.55^{+0.19}_{-0.26}$	382.(±5%)	17.00(±5%)
$J^{\rm Di\text{-}Di}_{A,3}$	$19.17^{+0.20}_{-0.26}$	406.(±5%)	17.50(±5%)	*	$19.40^{+0.12}_{-0.20}$	398.(±5%)	8.00(±5%)
$J^{\rm Di\text{-}Di}_{A,4}$	$18.50^{+0.17}_{-0.25}$	380.(±5%)	19.00(±5%)	*	$18.97^{+0.06}_{-0.11}$	398.(±5%)	9.50(±5%)
$J^{\rm Dia}_{A,1}$	$19.17^{+0.20}_{-0.26}$	406.(±5%)	17.00(±5%)	*	$18.55^{+0.20}_{-0.26}$	382.(±5%)	17.50(±5%)
$J^{\rm Dia}_{A,2}$	$19.21^{+0.20}_{-0.26}$	408.(±5%)	18.00(±5%)	*	$19.11^{+0.10}_{-0.18}$	404.(±5%)	10.00(±5%)
$J^{\rm Dia}_{A,3}$	$18.51^{+0.17}_{-0.26}$	380.(±5%)	19.00(±5%)	*	$18.97^{+0.06}_{-0.11}$	398.(±5%)	9.50(±5%)
$J^{\rm Dia}_{A,4}$	$18.50^{+0.17}_{-0.26}$	380.(±5%)	19.00(±5%)	*	$18.97^{+0.06}_{-0.12}$	396.(±5%)	9.50(±5%)

TABLE XXIV. The LO and NLO Results for $J^P = 1^+$ with $\bar{b}b\bar{b}b$ system in the On-Shell scheme

Current	LO			*	NLO(OS)		
	M_H (GeV)	S_0 (GeV^2)	M_B^2 (GeV^2)	*	M_H (GeV)	S_0 (GeV^2)	M_B^2 (GeV^2)
$J_{A,1}^{\text{M-M}}$	$20.46^{+0.11}_{-0.18}$	450.(±5%)	10.50(±5%)	*	$19.47^{+0.32}_{-0.82}$	390.(±5%)	5.50(±5%)
$J_{A,2}^{\text{M-M}}$	$20.21^{+0.14}_{-0.22}$	432.(±5%)	9.50(±5%)	*	$18.97^{+0.12}_{-1.47}$	368.(±5%)	4.00(±5%)
$J_{A,3}^{\text{M-M}}$	$19.64^{+0.06}_{-0.12}$	412.(±5%)	7.50(±5%)	*	$18.98^{+0.07}_{-0.31}$	366.(±5%)	3.50(±5%)
$J_{A,4}^{\text{M-M}}$	$19.70^{+0.04}_{-0.09}$	424.(±5%)	7.50(±5%)	*	$18.98^{+0.07}_{-0.27}$	366.(±5%)	3.50(±5%)
$J_{A,1}^{\text{Di-Di}}$	$20.28^{+0.14}_{-0.22}$	436.(±5%)	10.00(±5%)	*	$19.36^{+0.11}_{-0.47}$	386.(±5%)	5.00(±5%)
$J_{A,2}^{\text{Di-Di}}$	$20.40^{+0.10}_{-0.17}$	448.(±5%)	10.00(±5%)	*	$19.20^{+0.18}_{-0.32}$	382.(±5%)	6.50(±5%)
$J_{A,3}^{\text{Di-Di}}$	$20.32^{+0.09}_{-0.17}$	444.(±5%)	9.50(±5%)	*	$19.36^{+0.11}_{-0.46}$	386.(±5%)	5.00(±5%)
$J_{A,4}^{\text{Di-Di}}$	$19.65^{+0.05}_{-0.11}$	414.(±5%)	7.50(±5%)	*	$18.98^{+0.07}_{-0.30}$	366.(±5%)	3.50(±5%)
$J_{A,1}^{\text{Dia}}$	$20.18^{+0.14}_{-0.23}$	430.(±5%)	9.50(±5%)	*	$19.20^{+0.18}_{-0.31}$	382.(±5%)	6.50(±5%)
$J_{A,2}^{\text{Dia}}$	$20.47^{+0.10}_{-0.17}$	452.(±5%)	10.50(±5%)	*	$19.02^{+2.93}_{-0.42}$	370.(±5%)	4.00(±5%)
$J_{A,3}^{\text{Dia}}$	$19.68^{+0.04}_{-0.10}$	420.(±5%)	7.50(±5%)	*	$18.98^{+0.07}_{-0.29}$	366.(±5%)	3.50(±5%)
$J_{A,4}^{\text{Dia}}$	$19.64^{+0.05}_{-0.11}$	414.(±5%)	7.50(±5%)	*	$18.98^{+0.07}_{-0.31}$	366.(±5%)	3.50(±5%)

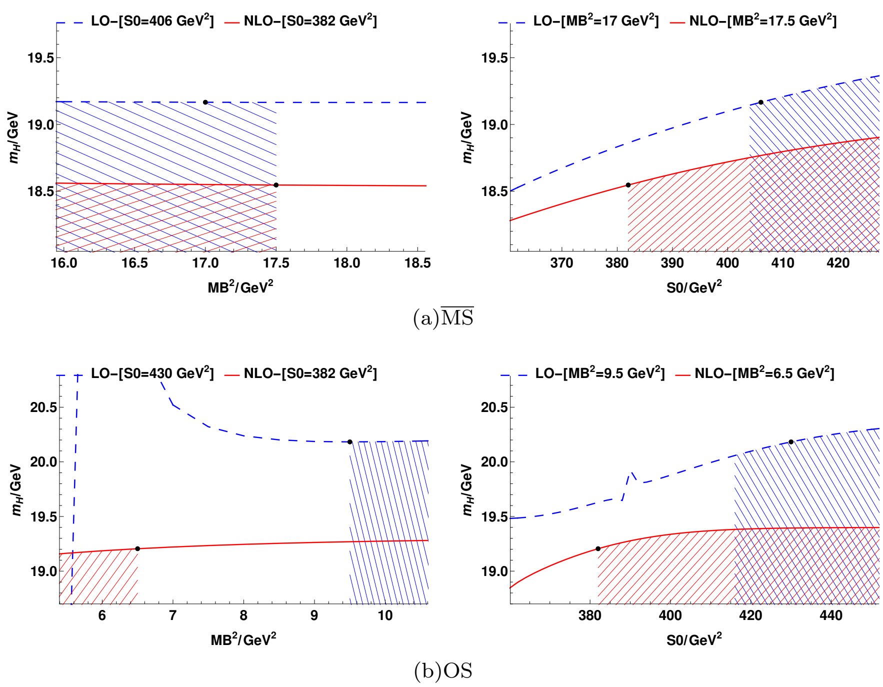

FIG. 41. The Borel platform curves for $J_{A,1}^{\text{Dia}}$ with $\bar{b}b\bar{b}b$ system in the $\overline{\text{MS}}$ and On-Shell schemes

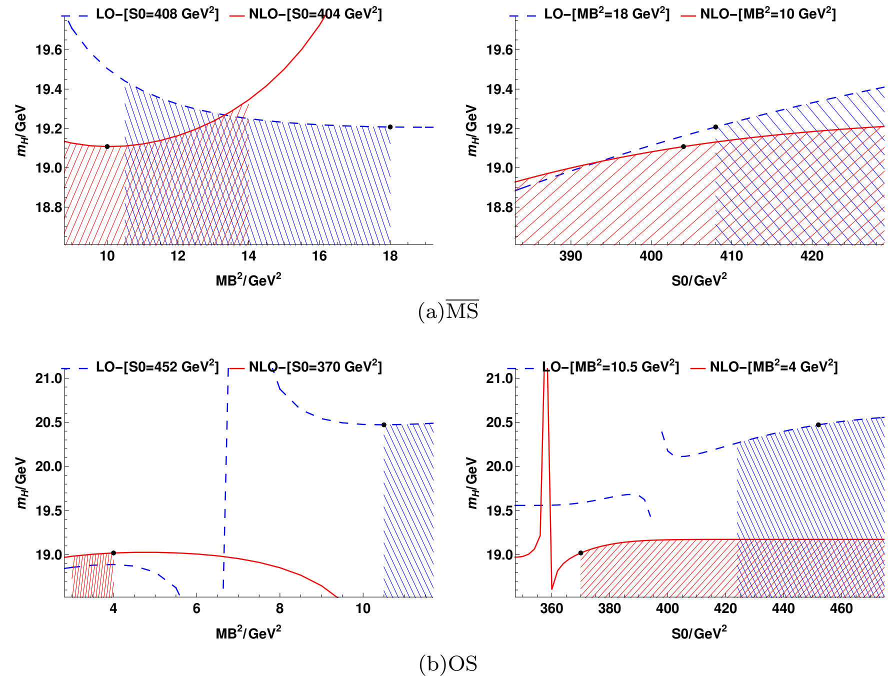

FIG. 42. The Borel platform curves for $J_{A,2}^{\mathrm{Dia}}$ with $\bar{b}b\bar{b}b$ system in the $\overline{\mathrm{MS}}$ and On-Shell schemes

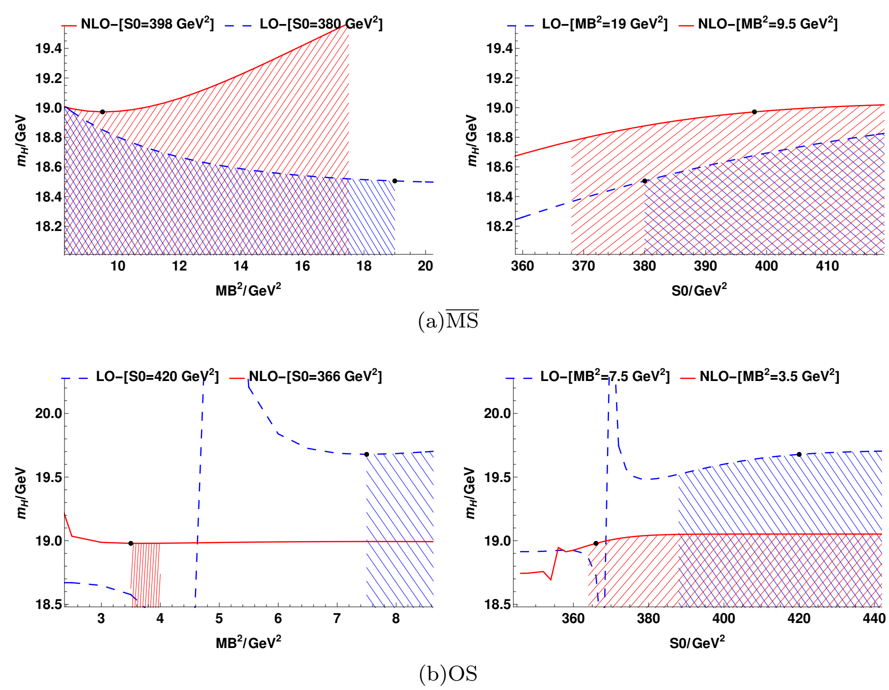

FIG. 43. The Borel platform curves for $J_{A,3}^{\mathrm{Dia}}$ with $\bar{b}b\bar{b}b$ system in the $\overline{\mathrm{MS}}$ and On-Shell schemes

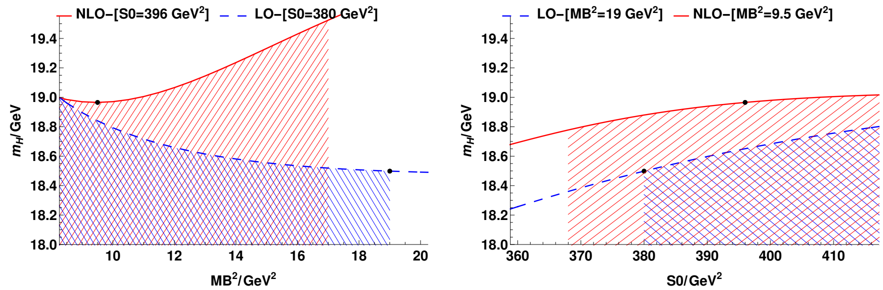

(a)$\overline{\mathrm{MS}}$

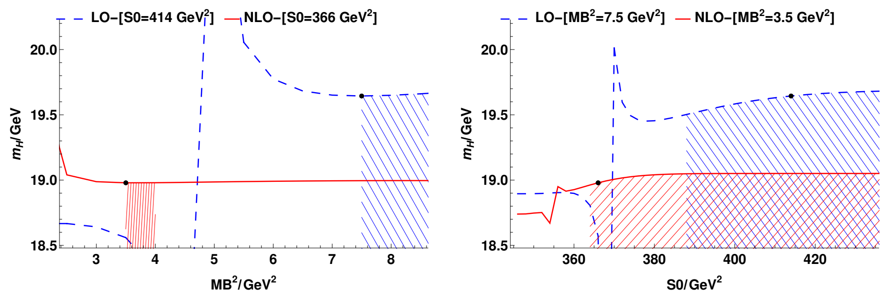

(b)OS

FIG. 44. The Borel platform curves for $J^{\mathrm{Dia}}_{A,4}$ with $\bar{b}b\bar{b}b$ system in the $\overline{\mathrm{MS}}$ and On-Shell schemes

4. Numerical Results with $J^P = 1^-$

TABLE XXV. The LO and NLO Results for $J^P = 1^-$ with $\bar{b}b\bar{b}b$ system in the $\overline{\mathrm{MS}}$ scheme

Current	LO			*	NLO($\overline{\mathrm{MS}}$)		
	M_H (GeV)	S_0 (GeV^2)	M_B^2 (GeV^2)	*	M_H (GeV)	S_0 (GeV^2)	M_B^2 (GeV^2)
$J^{\text{M-M}}_{V,1}$	$18.86^{+0.19}_{-0.25}$	394.(±5%)	18.50(±5%)	*	$19.31^{+0.04}_{-0.09}$	412.(±5%)	8.00(±5%)
$J^{\text{M-M}}_{V,2}$	$18.85^{+0.19}_{-0.26}$	394.(±5%)	18.00(±5%)	*	$19.23^{+0.07}_{-0.13}$	402.(±5%)	8.50(±5%)
$J^{\text{M-M}}_{V,3}$	$18.87^{+0.19}_{-0.26}$	394.(±5%)	18.00(±5%)	*	$19.31^{+0.04}_{-0.09}$	412.(±5%)	8.00(±5%)
$J^{\text{M-M}}_{V,4}$	$18.85^{+0.20}_{-0.26}$	394.(±5%)	18.00(±5%)	*	$19.22^{+0.05}_{-0.11}$	408.(±5%)	8.50(±5%)
$J^{\text{Di-Di}}_{V,1}$	$18.85^{+0.19}_{-0.25}$	394.(±5%)	18.00(±5%)	*	$19.26^{+0.05}_{-0.11}$	408.(±5%)	8.50(±5%)
$J^{\text{Di-Di}}_{V,2}$	$18.86^{+0.19}_{-0.26}$	394.(±5%)	18.00(±5%)	*	$19.18^{+0.13}_{-0.20}$	388.(±5%)	8.50(±5%)
$J^{\text{Di-Di}}_{V,3}$	$18.86^{+0.19}_{-0.26}$	394.(±5%)	18.00(±5%)	*	$19.25^{+0.07}_{-0.13}$	404.(±5%)	8.50(±5%)
$J^{\text{Di-Di}}_{V,4}$	$18.86^{+0.19}_{-0.26}$	394.(±5%)	18.00(±5%)	*	$19.23^{+0.07}_{-0.13}$	402.(±5%)	8.50(±5%)
$J^{\text{Dia}}_{V,1}$	$18.85^{+0.19}_{-0.25}$	394.(±5%)	18.00(±5%)	*	$19.25^{+0.05}_{-0.10}$	410.(±5%)	8.50(±5%)
$J^{\text{Dia}}_{V,2}$	$18.86^{+0.19}_{-0.25}$	394.(±5%)	18.50(±5%)	*	$19.31^{+0.04}_{-0.09}$	412.(±5%)	8.00(±5%)
$J^{\text{Dia}}_{V,3}$	$18.85^{+0.20}_{-0.26}$	394.(±5%)	18.00(±5%)	*	$19.12^{+0.12}_{-0.19}$	390.(±5%)	9.00(±5%)
$J^{\text{Dia}}_{V,4}$	$18.87^{+0.19}_{-0.26}$	394.(±5%)	18.00(±5%)	*	$19.31^{+0.04}_{-0.09}$	412.(±5%)	8.00(±5%)

TABLE XXVI. The LO and NLO Results for $J^P = 1^-$ with $\bar{b}b\bar{b}b$ system in the On-Shell scheme

Current	LO			*	NLO(OS)		
	M_H (GeV)	S_0 (GeV^2)	M_B^2 (GeV^2)	*	M_H (GeV)	S_0 (GeV^2)	M_B^2 (GeV^2)
$J_{V,1}^{\text{M-M}}$	$20.06^{+0.10}_{-0.17}$	430.(±5%)	9.50(±5%)	*	$19.24^{+0.07}_{-0.77}$	380.(±5%)	4.50(±5%)
$J_{V,2}^{\text{M-M}}$	$19.99^{+0.10}_{-0.18}$	426.(±5%)	9.00(±5%)	*	$19.17^{+0.09}_{-0.20}$	376.(±5%)	4.50(±5%)
$J_{V,3}^{\text{M-M}}$	$20.10^{+0.06}_{-0.12}$	440.(±5%)	9.00(±5%)	*	$19.24^{+0.07}_{-1.03}$	380.(±5%)	4.50(±5%)
$J_{V,4}^{\text{M-M}}$	$19.92^{+0.07}_{-0.14}$	426.(±5%)	8.00(±5%)	*	$19.12^{+0.08}_{-0.20}$	374.(±5%)	4.00(±5%)
$J_{V,1}^{\text{Di-Di}}$	$20.00^{+0.10}_{-0.17}$	426.(±5%)	9.00(±5%)	*	$19.18^{+0.09}_{-0.21}$	376.(±5%)	4.50(±5%)
$J_{V,2}^{\text{Di-Di}}$	$20.06^{+0.07}_{-0.14}$	434.(±5%)	9.00(±5%)	*	$19.19^{+0.09}_{-0.23}$	376.(±5%)	4.50(±5%)
$J_{V,3}^{\text{Di-Di}}$	$20.01^{+0.09}_{-0.17}$	428.(±5%)	9.00(±5%)	*	$19.18^{+0.10}_{-0.21}$	376.(±5%)	4.50(±5%)
$J_{V,4}^{\text{Di-Di}}$	$19.96^{+0.08}_{-0.16}$	426.(±5%)	8.50(±5%)	*	$19.14^{+0.08}_{-0.92}$	374.(±5%)	4.00(±5%)
$J_{V,1}^{\text{Dia}}$	$20.00^{+0.06}_{-0.13}$	432.(±5%)	8.50(±5%)	*	$19.15^{+0.08}_{-0.44}$	374.(±5%)	4.00(±5%)
$J_{V,2}^{\text{Dia}}$	$20.05^{+0.10}_{-0.18}$	428.(±5%)	9.50(±5%)	*	$19.23^{+0.07}_{-1.02}$	380.(±5%)	4.50(±5%)
$J_{V,3}^{\text{Dia}}$	$19.90^{+0.07}_{-0.15}$	424.(±5%)	8.00(±5%)	*	$19.12^{+0.08}_{-0.21}$	374.(±5%)	4.00(±5%)
$J_{V,4}^{\text{Dia}}$	$20.10^{+0.06}_{-0.12}$	440.(±5%)	9.00(±5%)	*	$19.24^{+0.07}_{-1.03}$	380.(±5%)	4.50(±5%)

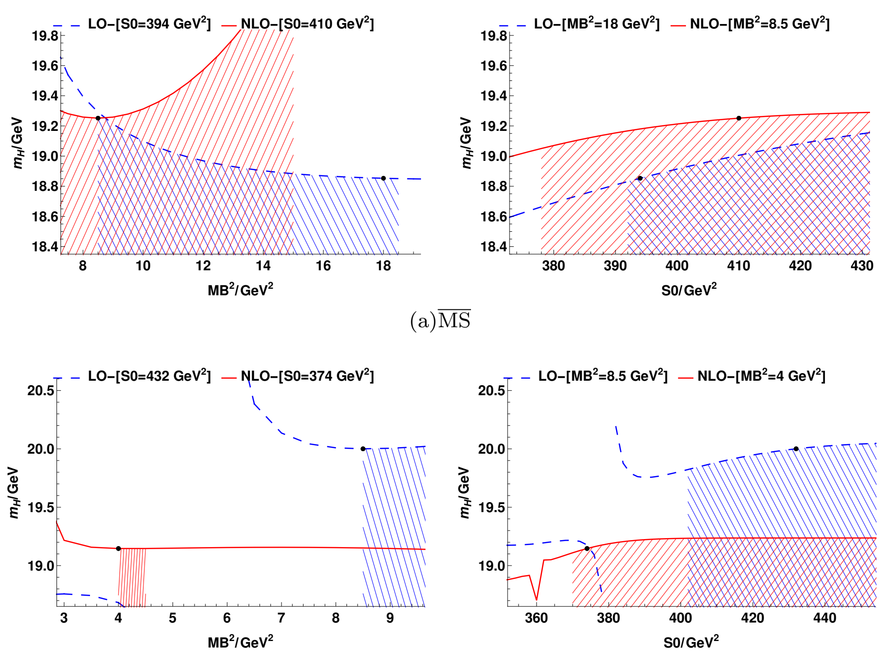

(a)$\overline{\text{MS}}$

(b)OS

FIG. 45. The Borel platform curves for $J_{V,1}^{\text{Dia}}$ with $\bar{b}b\bar{b}b$ system in the $\overline{\text{MS}}$ and On-Shell schemes

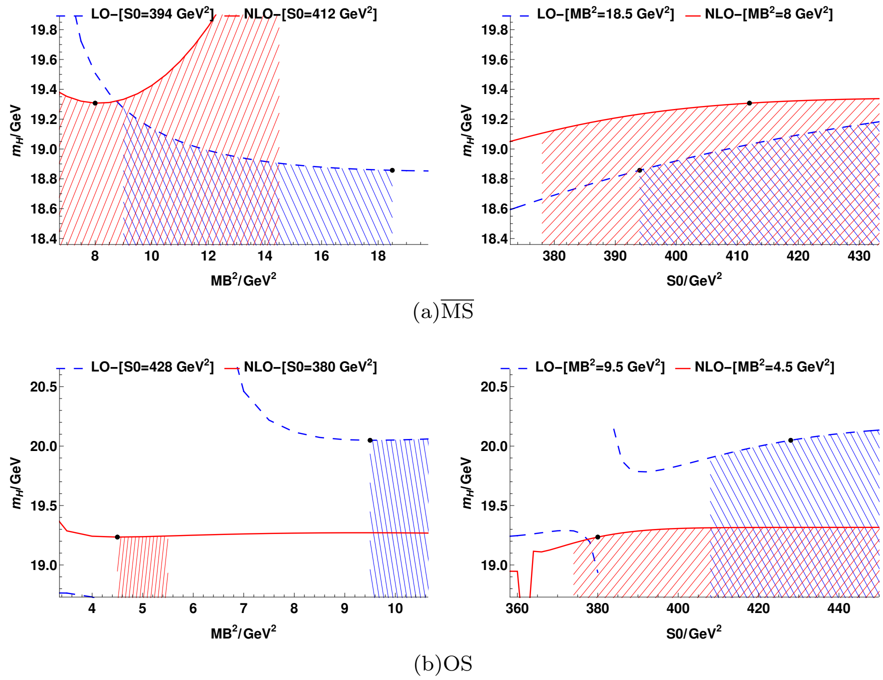

FIG. 46. The Borel platform curves for $J_{V,2}^{\text{Dia}}$ with $\bar{b}b\bar{b}b$ system in the $\overline{\text{MS}}$ and On-Shell schemes

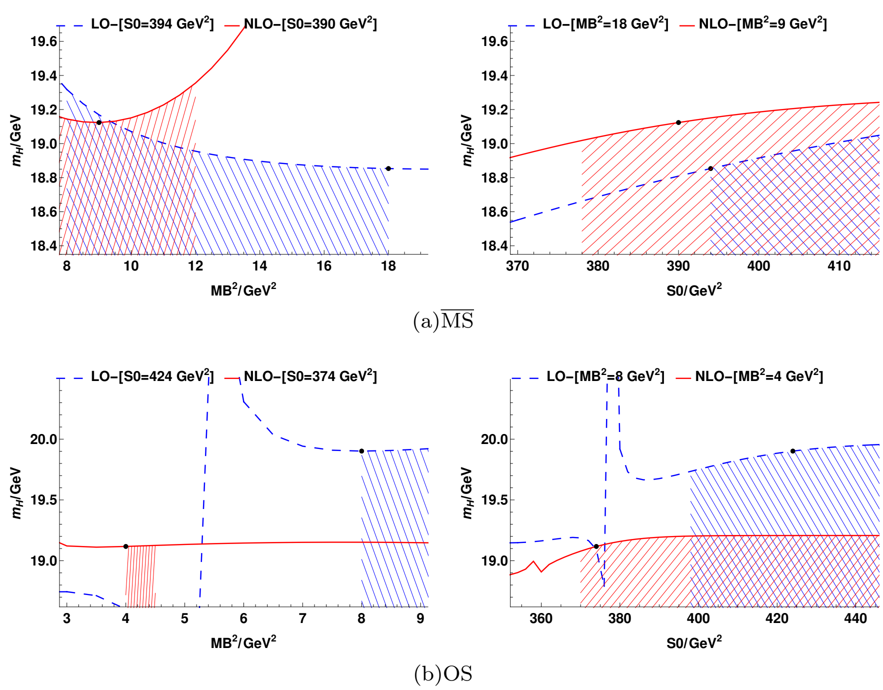

FIG. 47. The Borel platform curves for $J_{V,3}^{\text{Dia}}$ with $\bar{b}b\bar{b}b$ system in the $\overline{\text{MS}}$ and On-Shell schemes

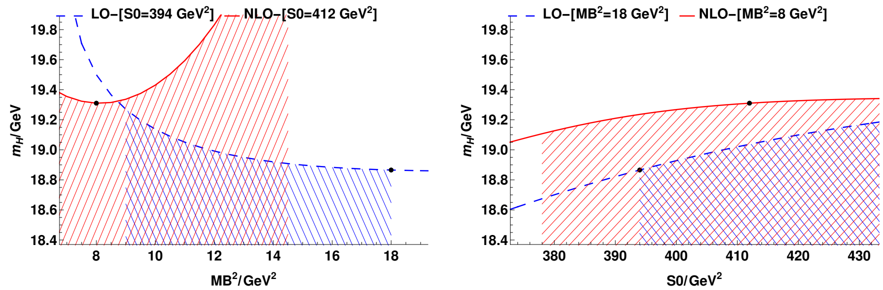

(a)$\overline{\mathrm{MS}}$

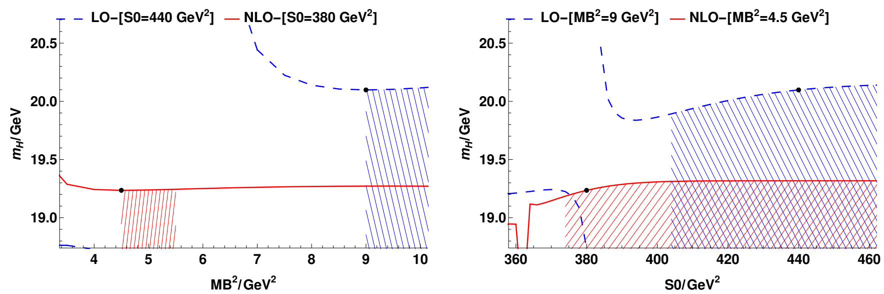

(b)OS

FIG. 48. The Borel platform curves for $J_{V,4}^{\mathrm{Dia}}$ with $\bar{b}b\bar{b}b$ system in the $\overline{\mathrm{MS}}$ and On-Shell schemes

5. Numerical Results with $J^P = 2^+$

TABLE XXVII. The LO and NLO Results for $J^P = 2^+$ with $\bar{b}b\bar{b}b$ system in the $\overline{\mathrm{MS}}$ scheme

Current	LO			*	NLO($\overline{\mathrm{MS}}$)		
	M_H (GeV)	S_0 (GeV^2)	M_B^2 (GeV^2)	*	M_H (GeV)	S_0 (GeV^2)	M_B^2 (GeV^2)
$J_{T,1}^{\mathrm{M\text{-}M}}$	$18.50^{+0.17}_{-0.25}$	380.(±5%)	19.00(±5%)	*	$18.89^{+0.11}_{-0.18}$	380.(±5%)	9.50(±5%)
$J_{T,2}^{\mathrm{M\text{-}M}}$	$19.21^{+0.20}_{-0.26}$	408.(±5%)	18.00(±5%)	*	$19.62^{+0.04}_{-0.08}$	424.(±5%)	7.00(±5%)
$J_{T,3}^{\mathrm{M\text{-}M}}$	$18.50^{+0.17}_{-0.26}$	380.(±5%)	19.00(±5%)	*	$18.95^{+0.07}_{-0.13}$	392.(±5%)	9.50(±5%)
$J_{T,1}^{\mathrm{Di\text{-}Di}}$	$18.50^{+0.17}_{-0.25}$	380.(±5%)	19.00(±5%)	*	$18.93^{+0.09}_{-0.16}$	386.(±5%)	9.50(±5%)
$J_{T,2}^{\mathrm{Di\text{-}Di}}$	$19.20^{+0.21}_{-0.26}$	408.(±5%)	18.00(±5%)	*	$19.55^{+0.04}_{-0.10}$	422.(±5%)	7.50(±5%)
$J_{T,3}^{\mathrm{Di\text{-}Di}}$	$18.50^{+0.17}_{-0.26}$	380.(±5%)	19.00(±5%)	*	$18.91^{+0.11}_{-0.18}$	382.(±5%)	9.50(±5%)
$J_{T,1}^{\mathrm{Dia}}$	$18.50^{+0.17}_{-0.26}$	380.(±5%)	19.00(±5%)	*	$18.91^{+0.11}_{-0.18}$	382.(±5%)	9.50(±5%)
$J_{T,2}^{\mathrm{Dia}}$	$18.50^{+0.17}_{-0.26}$	380.(±5%)	19.00(±5%)	*	$18.91^{+0.11}_{-0.18}$	382.(±5%)	9.50(±5%)
$J_{T,3}^{\mathrm{Dia}}$	$18.50^{+0.17}_{-0.26}$	380.(±5%)	19.00(±5%)	*	$18.95^{+0.07}_{-0.13}$	392.(±5%)	9.50(±5%)

TABLE XXVIII. The LO and NLO Results for $J^P = 2^+$ with $\bar{b}b\bar{b}b$ system in the On-Shell scheme

Current	LO			*	NLO(OS)		
	M_H (GeV)	S_0 (GeV^2)	M_B^2 (GeV^2)	*	M_H (GeV)	S_0 (GeV^2)	M_B^2 (GeV^2)
$J_{T,1}^{\text{M-M}}$	$19.67^{+0.04}_{-0.09}$	418.($\pm$5%)	7.50($\pm$5%)	*	$18.98^{+0.07}_{-0.29}$	366.($\pm$5%)	3.50($\pm$5%)
$J_{T,2}^{\text{M-M}}$	$20.44^{+0.11}_{-0.18}$	448.($\pm$5%)	10.50($\pm$5%)	*	$19.44^{+0.54}_{-1.79}$	388.($\pm$5%)	5.50($\pm$5%)
$J_{T,3}^{\text{M-M}}$	$19.68^{+0.04}_{-0.10}$	420.($\pm$5%)	7.50($\pm$5%)	*	$18.98^{+0.07}_{-0.28}$	366.($\pm$5%)	3.50($\pm$5%)
$J_{T,1}^{\text{Di-Di}}$	$19.67^{+0.04}_{-0.10}$	418.($\pm$5%)	7.50($\pm$5%)	*	$18.98^{+0.07}_{-0.29}$	366.($\pm$5%)	3.50($\pm$5%)
$J_{T,2}^{\text{Di-Di}}$	$20.38^{+0.11}_{-0.18}$	446.($\pm$5%)	10.00($\pm$5%)	*	$19.39^{+0.23}_{-1.89}$	386.($\pm$5%)	5.00($\pm$5%)
$J_{T,3}^{\text{Di-Di}}$	$19.68^{+0.04}_{-0.10}$	420.($\pm$5%)	7.50($\pm$5%)	*	$18.98^{+0.07}_{-0.28}$	366.($\pm$5%)	3.50($\pm$5%)
$J_{T,1}^{\text{Dia}}$	$19.67^{+0.04}_{-0.09}$	418.($\pm$5%)	7.50($\pm$5%)	*	$18.98^{+0.07}_{-0.29}$	366.($\pm$5%)	3.50($\pm$5%)
$J_{T,2}^{\text{Dia}}$	$19.68^{+0.04}_{-0.10}$	420.($\pm$5%)	7.50($\pm$5%)	*	$18.98^{+0.07}_{-0.28}$	366.($\pm$5%)	3.50($\pm$5%)
$J_{T,3}^{\text{Dia}}$	$19.68^{+0.04}_{-0.10}$	420.($\pm$5%)	7.50($\pm$5%)	*	$18.98^{+0.07}_{-0.28}$	366.($\pm$5%)	3.50($\pm$5%)

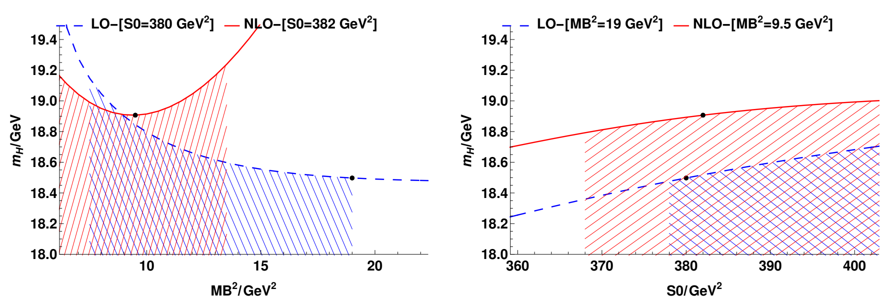

(a)$\overline{\text{MS}}$

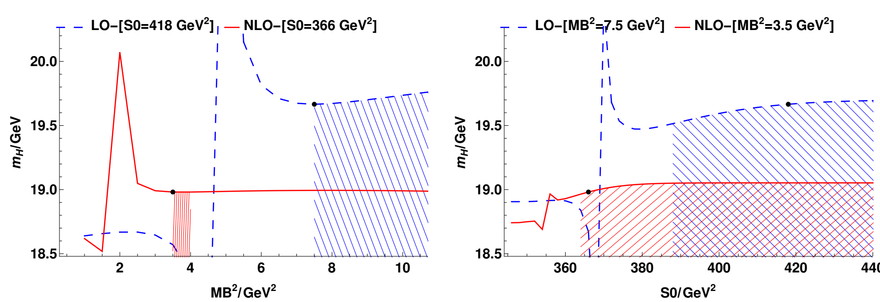

(b)OS

FIG. 49. The Borel platform curves for $J_{T,1}^{\text{Dia}}$ with $\bar{b}b\bar{b}b$ system in the $\overline{\text{MS}}$ and On-Shell schemes

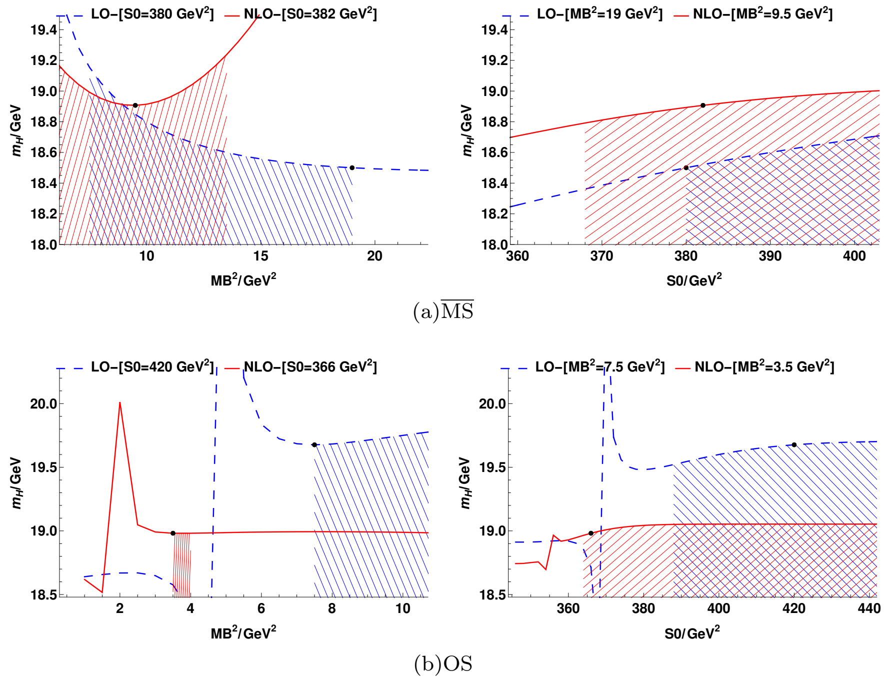

FIG. 50. The Borel platform curves for $J_{T,2}^{\rm Dia}$ with $\bar{b}b\bar{b}b$ system in the $\overline{\rm MS}$ and On-Shell schemes

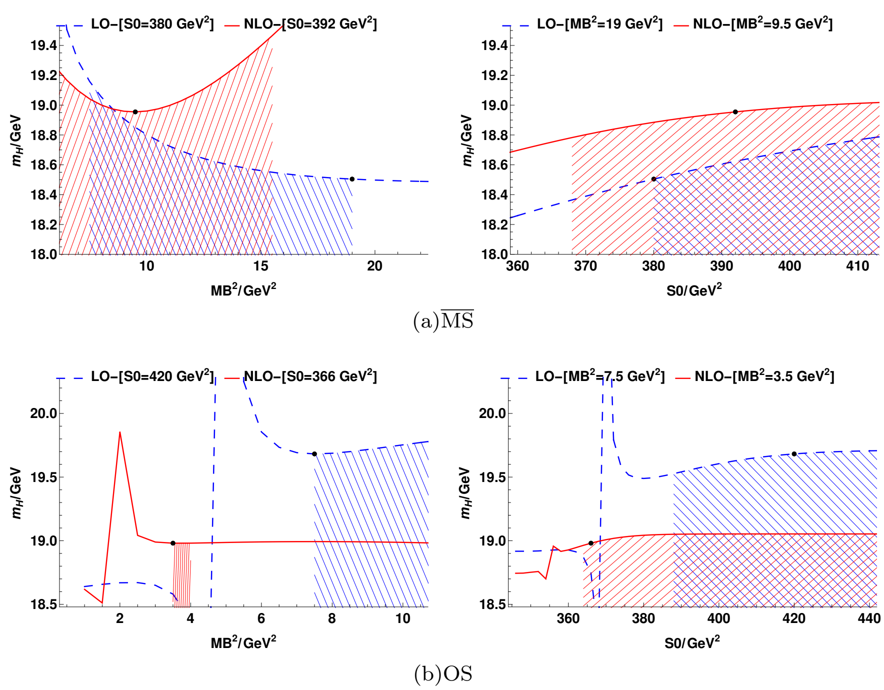

FIG. 51. The Borel platform curves for $J_{T,3}^{\rm Dia}$ with $\bar{b}b\bar{b}b$ system in the $\overline{\rm MS}$ and On-Shell schemes

6. Renormalization scale dependence

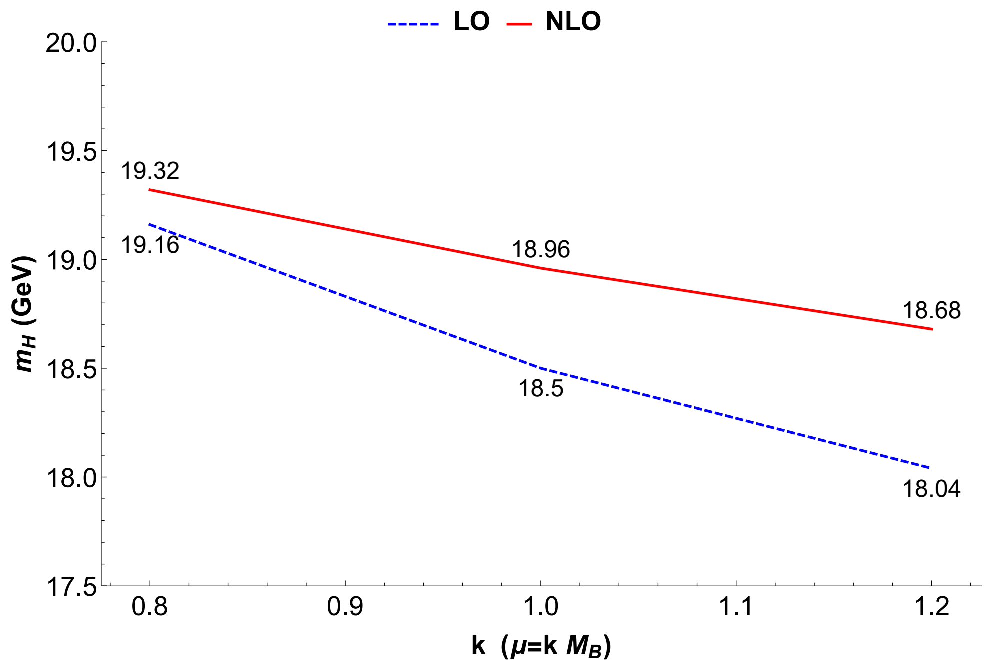

FIG. 52. The renormalization scale μ dependence of the LO and NLO results of $J_{S,3}^{\rm Dia}$ in $\overline{\rm MS}$ scheme

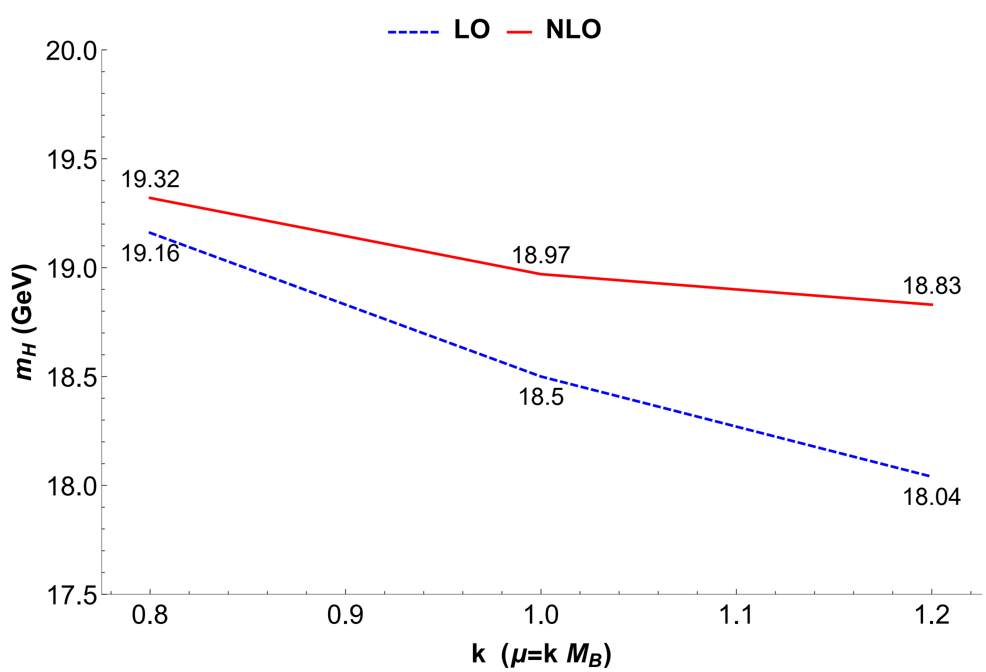

FIG. 53. The renormalization scale μ dependence of the LO and NLO results of $J_{S,4}^{\rm Dia}$ in $\overline{\rm MS}$ scheme

[1] **Particle Data Group** , M. Tanabashi *et al.*, *Review of Particle Physics*, *Phys. Rev. D* **98** (2018) 030001 [InSPIRE].
[2] H.-X. Chen, W. Chen, X. Liu, and S.-L. Zhu, *The hidden-charm pentaquark and tetraquark states*, *Phys. Rept.* **639** (2016) 1–121 [arXiv:1601.02092] [InSPIRE].
[3] Y.-R. Liu, H.-X. Chen, W. Chen, X. Liu, and S.-L. Zhu, *Pentaquark and Tetraquark states*, *Prog. Part. Nucl. Phys.* **107** (2019) 237–320 [arXiv:1903.11976] [InSPIRE].
[4] N. Brambilla, S. Eidelman, C. Hanhart, A. Nefediev, C.-P. Shen, C. E. Thomas, A. Vairo, and C.-Z. Yuan, *The XYZ states: experimental and theoretical status and perspectives*, *Phys. Rept.* **873** (2020) 1–154 [arXiv:1907.07583] [InSPIRE].
[5] **LHCb** , R. Aaij *et al.*, *Observation of structure in the J/ψ -pair mass spectrum*, *Sci. Bull.* **65** (2020) 1983–1993 [arXiv:2006.16957] [InSPIRE].
[6] Y. Iwasaki, *A Possible Model for New Resonances-Exotics and Hidden Charm*, *Prog. Theor. Phys.* **54** (1975) 492 [InSPIRE].
[7] K.-T. Chao, *The (cc) - ($\bar{c}\bar{c}$) (Diquark - Anti-Diquark) States in e^+e^- Annihilation*, *Z. Phys. C* **7** (1981) 317 [InSPIRE].
[8] J. Ader, J. Richard, and P. Taxil, *DO NARROW HEAVY MULTI - QUARK STATES EXIST?*, *Phys. Rev. D* **25** (1982) 2370 [InSPIRE].
[9] J. Ballot and J. Richard, *FOUR QUARK STATES IN ADDITIVE POTENTIALS*, *Phys. Lett. B* **123** (1983) 449–451 [InSPIRE].
[10] L. Heller and J. Tjon, *On Bound States of Heavy $Q^2\bar{Q}^2$ Systems*, *Phys. Rev. D* **32** (1985) 755 [InSPIRE].
[11] R. J. Lloyd and J. P. Vary, *All charm tetraquarks*, *Phys. Rev. D* **70** (2004) 014009 [hep-ph/0311179] [InSPIRE].
[12] B. Silvestre-Brac, *Systematics of Q**2 (anti-Q**2) systems with a chromomagnetic interaction*, *Phys. Rev. D* **46** (1992) 2179–2189 [InSPIRE].
[13] B. Silvestre-Brac and C. Semay, *Systematics of $L = 0$ q-2 anti-q-2 systems*, *Z. Phys. C* **57** (1993) 273–282 [InSPIRE].
[14] N. Barnea, J. Vijande, and A. Valcarce, *Four-quark spectroscopy within the hyperspherical formalism*, *Phys. Rev. D* **73** (2006) 054004 [hep-ph/0604010] [InSPIRE].
[15] M. Karliner, S. Nussinov, and J. L. Rosner, *$QQ\bar{Q}\bar{Q}$ states: masses, production, and decays*, *Phys. Rev. D* **95** (2017) 034011 [arXiv:1611.00348] [InSPIRE].
[16] J. Wu, Y.-R. Liu, K. Chen, X. Liu, and S.-L. Zhu, *Heavy-flavored tetraquark states with the $QQ\bar{Q}\bar{Q}$ configuration*, *Phys. Rev. D* **97** (2018) 094015 [arXiv:1605.01134] [InSPIRE].
[17] M. N. Anwar, J. Ferretti, F.-K. Guo, E. Santopinto, and B.-S. Zou, *Spectroscopy and decays of the fully-heavy tetraquarks*, *Eur. Phys. J. C* **78** (2018) 647 [arXiv:1710.02540] [InSPIRE].
[18] J.-M. Richard, A. Valcarce, and J. Vijande, *String dynamics and metastability of all-heavy tetraquarks*, *Phys. Rev. D* **95** (2017) 054019 [arXiv:1703.00783] [InSPIRE].
[19] V. Debastiani and F. Navarra, *A non-relativistic model for the $[cc][\bar{c}\bar{c}]$ tetraquark*, *Chin. Phys. C* **43** (2019) 013105 [arXiv:1706.07553] [InSPIRE].
[20] M.-S. Liu, Q.-F. Lü, X.-H. Zhong, and Q. Zhao, *All-heavy tetraquarks*, *Phys. Rev. D* **100** (2019) 016006 [arXiv:1901.02564] [InSPIRE].
[21] X. Jin, Y. Xue, H. Huang, and J. Ping, *Full-heavy tetraquarks in constituent quark models*, *Eur. Phys. J. C* **80** (2020) 1083 [arXiv:2006.13745] [InSPIRE].
[22] G.-J. Wang, L. Meng, M. Oka, and S.-L. Zhu, *Higher fully charmed tetraquarks: Radial excitations and P-wave states*, *Phys. Rev. D* **104** (2021) 036016 [arXiv:2105.13109] [InSPIRE].
[23] W. Chen, H.-X. Chen, X. Liu, T. Steele, and S.-L. Zhu, *Hunting for exotic doubly hidden-charm/bottom tetraquark states*, *Phys. Lett. B* **773** (2017) 247–251 [arXiv:1605.01647] [InSPIRE].
[24] Z.-G. Wang, *Analysis of the $QQ\bar{Q}\bar{Q}$ tetraquark states with QCD sum rules*, *Eur. Phys. J. C* **77** (2017) 432 [arXiv:1701.04285] [InSPIRE].
[25] Z.-G. Wang, *Tetraquark candidates in the LHCb's di-J/ψ mass spectrum*, *Chin. Phys. C* **44** (2020) 113106 [arXiv:2006.13028] [InSPIRE].
[26] Z.-G. Wang and Z.-Y. Di, *Analysis of the vector and axialvector $QQ\bar{Q}\bar{Q}$ tetraquark states with QCD sum rules*, *Acta Phys. Polon. B* **50** (2019) 1335 [arXiv:1807.08520] [InSPIRE].
[27] R. Albuquerque, S. Narison, A. Rabemananjara, D. Rabetiarivony, and G. Randriamanatrika, *Doubly-hidden scalar heavy molecules and tetraquarks states from QCD at NLO*, *Phys. Rev. D* **102** (2020) 094001 [arXiv:2008.01569] [InSPIRE].
[28] B.-C. Yang, L. Tang, and C.-F. Qiao, *Scalar fully-heavy tetraquark states $QQ'\bar{Q}\bar{Q}'$ in QCD sum rules*, *Eur. Phys. J. C* **81** (2021) 324 [arXiv:2012.04463] [InSPIRE].
[29] J.-R. Zhang, *0^+ fully-charmed tetraquark states*, *Phys. Rev. D* **103** (2021) 014018 [arXiv:2010.07719] [InSPIRE].
[30] W. Heupel, G. Eichmann, and C. S. Fischer, *Tetraquark Bound States in a Bethe-Salpeter Approach*, *Phys. Lett. B* **718** (2012) 545–549 [arXiv:1206.5129] [InSPIRE].
[31] Z.-H. Guo and J. A. Oller, *Insights into the inner structures of the fully charmed tetraquark state $X(6900)$*, *Phys. Rev. D* **103** (2021) 034024 [arXiv:2011.00978] [InSPIRE].
[32] X.-K. Dong, V. Baru, F.-K. Guo, C. Hanhart, and A. Nefediev, *Coupled-Channel Interpretation of the LHCb Double-J/ψ Spectrum and Hints of a New State Near the $J/\psi J/\psi$ Threshold*, *Phys. Rev. Lett.* **126** (2021) 132001 [arXiv:2009.07795] [InSPIRE].
[33] R. Tiwari, D. P. Rathaud, and A. K. Rai, *Spectroscopy of all charm tetraquark states*, [arXiv:2108.04017] [InSPIRE].
[34] C. Hughes, E. Eichten, and C. T. H. Davies, *Searching for beauty-fully bound tetraquarks using lattice nonrelativistic*

QCD, *Phys. Rev. D* **97** (2018) 054505 [arXiv:1710.03236] [InSPIRE].
[35] H.-W. Ke, X. Han, X.-H. Liu, and Y.-L. Shi, *Tetraquark state $X(6900)$ and the interaction between diquark and antidiquark*, *Eur. Phys. J. C* **81** (2021) 427 [arXiv:2103.13140] [InSPIRE].
[36] Z. Zhao, K. Xu, A. Kaewsnod, X. Liu, A. Limphirat, and Y. Yan, *Study of charmoniumlike and fully-charm tetraquark spectroscopy*, *Phys. Rev. D* **103** (2021) 116027 [arXiv:2012.15554] [InSPIRE].
[37] A. V. Berezhnoy, A. V. Luchinsky, and A. A. Novoselov, *Tetraquarks Composed of 4 Heavy Quarks*, *Phys. Rev. D* **86** (2012) 034004 [arXiv:1111.1867] [InSPIRE].
[38] Y. Bai, S. Lu, and J. Osborne, *Beauty-full Tetraquarks*, *Phys. Lett. B* **798** (2019) 134930 [arXiv:1612.00012] [InSPIRE].
[39] M. Karliner, J. L. Rosner, and T. Skwarnicki, *Multiquark States*, *Ann. Rev. Nucl. Part. Sci.* **68** (2018) 17–44 [arXiv:1711.10626] [InSPIRE].
[40] A. Esposito and A. D. Polosa, *A $bb\bar{b}\bar{b}$di-bottomonium at the LHC?*, *Eur. Phys. J. C* **78** (2018) 782 [arXiv:1807.06040] [InSPIRE].
[41] M. A. Bedolla, J. Ferretti, C. D. Roberts, and E. Santopinto, *Spectrum of fully-heavy tetraquarks from a diquark+antidiquark perspective*, *Eur. Phys. J. C* **80** (2020) 1004 [arXiv:1911.00960] [InSPIRE].
[42] P. Lundhammar and T. Ohlsson, *Nonrelativistic model of tetraquarks and predictions for their masses from fits to charmed and bottom meson data*, *Phys. Rev. D* **102** (2020) 054018 [arXiv:2006.09393] [InSPIRE].
[43] R. Zhu, *Fully-heavy tetraquark spectra and production at hadron colliders*, *Nucl. Phys. B* **966** (2021) 115393 [arXiv:2010.09082] [InSPIRE].
[44] M.-S. liu, F.-X. Liu, X.-H. Zhong, and Q. Zhao, *Full-heavy tetraquark states and their evidences in the LHCb di-J/ψ spectrum*, [arXiv:2006.11952] [InSPIRE].
[45] Q.-F. Lü, D.-Y. Chen, and Y.-B. Dong, *Masses of fully heavy tetraquarks $QQ\bar{Q}\bar{Q}$ in an extended relativized quark model*, *Eur. Phys. J. C* **80** (2020) 871 [arXiv:2006.14445] [InSPIRE].
[46] J. F. Giron and R. F. Lebed, *Simple spectrum of $c\bar{c}c\bar{c}$ states in the dynamical diquark model*, *Phys. Rev. D* **102** (2020) 074003 [arXiv:2008.01631] [InSPIRE].
[47] G. Huang, J. Zhao, and P. Zhuang, *Pair structure of heavy tetraquark systems*, *Phys. Rev. D* **103** (2021) 054014 [arXiv:2012.14845] [InSPIRE].
[48] R. N. Faustov, V. O. Galkin, and E. M. Savchenko, *Heavy tetraquarks in the relativistic quark model*, *Universe* **7** (2021) 94 [arXiv:2103.01763] [InSPIRE].
[49] Q. Li, C.-H. Chang, G.-L. Wang, and T. Wang, *Mass spectra and wave functions of $TQQQ^-Q^-$ tetraquarks*, *Phys. Rev. D* **104** (2021) 014018 [arXiv:2104.12372] [InSPIRE].
[50] J. Sonnenschein and D. Weissman, *Deciphering the recently discovered tetraquark candidates around 6.9 GeV*, *Eur. Phys. J. C* **81** (2021) 25 [arXiv:2008.01095] [InSPIRE].
[51] B.-D. Wan and C.-F. Qiao, *Gluonic tetracharm configuration of $X(6900)$*, *Phys. Lett. B* **817** (2021) 136339 [arXiv:2012.00454] [InSPIRE].
[52] Q.-F. Cao, H. Chen, H.-R. Qi, and H.-Q. Zheng, *Some remarks on $X(6900)$*, *Chin. Phys. C* **45** (2021) 103102 [arXiv:2011.04347] [InSPIRE].
[53] M. A. Shifman, A. Vainshtein, and V. I. Zakharov, *QCD and Resonance Physics. Theoretical Foundations*, *Nucl. Phys. B* **147** (1979) 385–447 [InSPIRE].
[54] M. A. Shifman, A. I. Vainshtein, and V. I. Zakharov, *QCD and Resonance Physics: Applications*, *Nucl. Phys. B* **147** (1979) 448–518 [InSPIRE].
[55] P. Colangelo and A. Khodjamirian, *QCD sum rules, a modern perspective*, [hep-ph/0010175] [InSPIRE].
[56] S. Narison, *SVZ sum rules : 30 + 1 years later*, *Nucl. Phys. B Proc. Suppl.* **207-208** (2010) 315–322 [arXiv:1010.1959] [InSPIRE].
[57] S. Narison, *Mini-review on QCD spectral sum rules*, *Nucl. Part. Phys. Proc.* **258-259** (2015) 189–194 [arXiv:1409.8148] [InSPIRE].
[58] R. M. Albuquerque, J. M. Dias, K. P. Khemchandani, A. Martínez Torres, F. S. Navarra, M. Nielsen, and C. M. Zanetti, *QCD sum rules approach to the X, Y and Z states*, *J. Phys. G* **46** (2019) 093002 [arXiv:1812.08207] [InSPIRE].
[59] A. A. Ovchinnikov, A. A. Pivovarov, and L. R. Surguladze, *Baryonic sum rules in the next-to-leading order in alpha-s*, *Int. J. Mod. Phys. A* **6** (1991) 2025–2034 [InSPIRE].
[60] S. Groote, J. G. Korner, and A. A. Pivovarov, *Next-to-Leading Order perturbative QCD corrections to baryon correlators in matter*, *Phys. Rev. D* **78** (2008) 034039 [arXiv:0805.3590] [InSPIRE].
[61] S. Groote, J. G. Korner, and A. A. Pivovarov, *Heavy baryon properties with NLO accuracy in perturbative QCD*, *Eur. Phys. J. C* **58** (2008) 355–382 [arXiv:0807.2148] [InSPIRE].
[62] C.-Y. Wang, C. Meng, Y.-Q. Ma, and K.-T. Chao, *NLO effects for doubly heavy baryons in QCD sum rules*, *Phys. Rev. D* **99** (2019) 014018 [arXiv:1708.04563] [InSPIRE].
[63] R.-H. Wu, Y.-S. Zuo, C. Meng, Y.-Q. Ma, and K.-T. Chao, *NLO effects for Ω_{QQQ} Baryons in QCD Sum Rules*, [arXiv:2104.07384] [InSPIRE].
[64] J. Kublbeck, M. Bohm, and A. Denner, *Feyn Arts: Computer Algebraic Generation of Feynman Graphs and Amplitudes*, *Comput. Phys. Commun.* **60** (1990) 165–180 [InSPIRE].
[65] T. Hahn, *Generating Feynman diagrams and amplitudes with FeynArts 3*, *Comput. Phys. Commun.* **140** (2001) 418–431 [hep-ph/0012260] [InSPIRE].
[66] R. Mertig, M. Bohm, and A. Denner, *FEYN CALC: Computer algebraic calculation of Feynman amplitudes*, *Comput. Phys. Commun.* **64** (1991) 345–359 [InSPIRE].
[67] V. Shtabovenko, R. Mertig, and F. Orellana, *New Developments in FeynCalc 9.0*, *Comput. Phys. Commun.* **207** (2016)

432–444 [arXiv:1601.01167] [InSPIRE].
[68] J. G. Korner, D. Kreimer, and K. Schilcher, *A Practicable gamma(5) scheme in dimensional regularization*, *Z. Phys. C* **54** (1992) 503–512 [InSPIRE].
[69] A. von Manteuffel and C. Studerus, *Reduze 2 - Distributed Feynman Integral Reduction*, [arXiv:1201.4330] [InSPIRE].
[70] A. V. Kotikov, *Differential equations method: New technique for massive Feynman diagrams calculation*, *Phys. Lett. B* **254** (1991) 158–164 [InSPIRE].
[71] Z. Bern, L. J. Dixon, and D. A. Kosower, *Dimensionally regulated one loop integrals*, *Phys. Lett. B* **302** (1993) 299–308 [hep-ph/9212308] [InSPIRE]. [Erratum: Phys.Lett.B 318, 649 (1993)].
[72] E. Remiddi, *Differential equations for Feynman graph amplitudes*, *Nuovo Cim. A* **110** (1997) 1435–1452 [hep-th/9711188] [InSPIRE].
[73] T. Gehrmann and E. Remiddi, *Differential equations for two loop four point functions*, *Nucl. Phys. B* **580** (2000) 485–518 [hep-ph/9912329] [InSPIRE].
[74] X. Liu, Y.-Q. Ma, and C.-Y. Wang, *A Systematic and Efficient Method to Compute Multi-loop Master Integrals*, *Phys. Lett. B* **779** (2018) 353–357 [arXiv:1711.09572] [InSPIRE].
[75] E. Bagan, M. Chabab, and S. Narison, *Baryons with two heavy quarks from QCD spectral sum rules*, *Phys. Lett. B* **306** (1993) 350–356 [InSPIRE].
[76] C. Dominguez, G. Gluckman, and N. Paver, *Mass of the charm quark from QCD sum rules*, *Phys. Lett. B* **333** (1994) 184–189 [hep-ph/9406329] [InSPIRE].
[77] C. Dominguez, L. Hernandez, and K. Schilcher, *Determination of the gluon condensate from data in the charm-quark region*, *JHEP* **07** (2015) 110 [arXiv:1411.4500] [InSPIRE].
[78] S. Aoki *et al.*, *Review of lattice results concerning low-energy particle physics*, *Eur. Phys. J. C* **77** (2017) 112 [arXiv:1607.00299] [InSPIRE].
[79] R. A. Bertlmann, *Heavy Quark - Anti-quark Systems From Exponential Moments in {QCD}*, *Nucl. Phys. B* **204** (1982) 387–412 [InSPIRE].